UNIVERSIDADE FEDERAL DO RIO GRANDE DO SUL
ESCOLA DE ENGENHARIA
PROGRAMA DE PÓS-GRADUAÇÃO EM ENGENHARIA ELÉTRICA

BRUNO HENZ MOSSMANN

TUNING OF RESONANT CONTROLLERS BASED ON THE FREQUENCY RESPONSE

Porto Alegre
2021

BRUNO HENZ MOSSMANN

TUNING OF RESONANT CONTROLLERS BASED ON THE FREQUENCY RESPONSE

Dissertation presented to Programa de Pós-Graduação em Engenharia Elétrica of Universidade Federal do Rio Grande do Sul in partial fulfillment of the requirements for the degree of Master in Electrical Engineering.
Area: Control and Automation

ADVISOR: Prof. Dr. Luís Fernando Alves Pereira

CO-ADVISOR: Prof. Dr. João Manoel Gomes da Silva Junior

Porto Alegre
2021

BRUNO HENZ MOSSMANN

TUNING OF RESONANT CONTROLLERS BASED ON THE FREQUENCY RESPONSE

This dissertation was considered adequate for obtaining the degree of Master in Electrical Engineering and approved in its final form by the Advisor and the Examination Committee.

Advisor: _____
Prof. Dr. Luís Fernando Alves Pereira, UFRGS
Doutor pelo Instituto Tecnológico de Aeronáutica – São José dos Campos, Brasil

Examination Committee:

Prof. Dr. Daniel Sbarbaro, UdeC (Chile)
Doutor pela University of Glasgow – Glasgow, Reino Unido

Prof. Dr. Alexandre Sanfelice Bazanella, UFRGS
Doutor pela Universidade Federal de Santa Catarina – Florianópolis, Brasil

Prof. Dr. Charles Lorenzini, Longhi Engenharia e Automação
Doutor pela Universidade Federal do Rio Grande do Sul – Porto Alegre, Brasil

Coordinator of PPGEE: _____
Prof. Dr. Sérgio Luís Haffner

Porto Alegre, September 2021.

DEDICATÓRIA

Dedico este trabalho aos meus pais, Pedro e Sibila, ao meu irmão, Bernardo, e à minha esposa, Marcela, pelo apoio incansável e compreensão nos momentos de ausência.

AGRADECIMENTOS

De modo especial aos meus pais, Pedro Antonio Mossmann e Sibila Henz Mossmann, por todo o apoio e amor incondicionais dedicados durante toda a minha vida. Ao meu irmão, Bernardo Henz Mossmann, por estar presente e disposto a ajudar. E à minha esposa, Marcela Sousa Mossmann, pelo amor e dedicação e pela compreensão nas vésperas de provas e trabalhos.

Ao Programa de Pós-Graduação em Engenharia Elétrica da UFRGS, PPGEE, pela oportunidade de realizar o mestrado em minha área de pesquisa. Aos Professores do Programa, pelo trabalho e dedicação em contribuir no aprendizado de seus alunos.

Aos Professores Luís Fernando Alves Pereira e João Manoel Gomes da Silva Junior, pela orientação, disponibilidade e auxílio no desenvolvimento deste trabalho.

À Procempa, à Polícia Científica do Paraná e aos meus colegas de trabalho, pelo incentivo e suporte na busca por conhecimento e capacitação.

Aos meus familiares e às pessoas especiais que sempre estiveram presentes e participaram desta conquista. Aos grandes amigos que a UFRGS me deu, em especial ao Maurício Richter e ao Rodrigo Duarte, pelo companheirismo nesta jornada.

Ao CNPq e à CAPES, pela provisão de recursos para o desenvolvimento da pesquisa e para a sua apresentação em periódicos e eventos.

Finalmente, aos colegas pelo auxílio e apoio nas tarefas desenvolvidas durante o curso, meus sinceros agradecimentos.

ABSTRACT

Resonant controllers are introduced to fulfil the increased demand for controllers capable to follow or reject periodic signals with superior performance than conventional PID ones. The main characteristic of these controllers is the infinite gain in the frequency of interest, which can lead to stability problems and makes their tuning more complex. This work presents the computation of resonant controllers parameters based on a frequency response method, using stability margins and sensitivity functions as indicators of performance and stability for the controlled system. In addition, the combination with a phase-lead compensator is proposed to allow better performance in an augmented bandwidth. The method is extended for multiple frequency modes in order to deal with higher harmonic content, resulting in the multi-resonant controller. The proposed method is tested using different classes of processes found in typical control problems in order to illustrate its wide applicability.

Keywords: Resonant controllers, frequency response, periodic signals, phase-lead compensators, proportional resonant controllers, proportional multi-resonant controllers.

RESUMO

Controladores ressonantes são introduzidos para atender à demanda crescente por controladores capazes de seguir ou rejeitar sinais periódicos com desempenho superior ao dos controladores PID convencionais. A principal característica destes controladores é o ganho infinito na frequência de interesse, o que pode levar a problemas de estabilidade e torna o seu projeto e sintonia mais complexos. Este trabalho apresenta um método para a sintonia dos parâmetros de controladores ressonantes baseada em um método de resposta em frequência, usando as margens de estabilidade e as funções sensibilidade como indicadores de desempenho e estabilidade para o sistema controlado. Além disso, a combinação com um compensador de avanço de fase é proposta para possibilitar desempenho superior em uma maior largura de banda. O método é então estendido para múltiplos modos de frequência a fim de considerar sinais de referência ou perturbação com maior conteúdo harmônico, resultando no controlador multirressonante. O método proposto é testado usando diferentes classes de processos encontrados em problemas típicos de controle para demonstrar sua vasta aplicabilidade.

Palavras-chave: controlador ressonante, resposta em frequência, sinais periódicos, compensador de avanço de fase, controlador proporcional ressonante, controlador proporcional multirressonante.

LIST OF FIGURES

LIST OF TABLES

LIST OF ABBREVIATIONS

ABNT	Associação Brasileira de Normas Técnicas
AC	Alternate Current
BIBO	Bounded Input - Bounded Output
DC	Direct Current
IMP	Internal Model Principle
LMI	Linear Matrix Inequality
PID	Proportional-Integral-Derivative
PMR	Proportional Multi-Resonant
PPGEE	Programa de Pós-Graduação em Engenharia Elétrica
PR	Proportional Resonant
RMS	Root Mean Square
THD	Total Harmonic Distortion
UFRGS	Universidade Federal do Rio Grande do Sul
UPS	Uninterruptible Power Supply

LIST OF SYMBOLS

$\sum$	Sum
j	Imaginary unit number $\sqrt{-1}$
k_p	Proportional gain of the controller
k_r	Resonant gain of the controller
ω	Angular frequency variable
ω_r	Fundamental frequency of interest
ω_{mr}	Multiple m of the fundamental frequency
ω_m	Centre frequency of phase-lead compensator, at which the maximum amount of phase is added
ω_u	Ultimate frequency, *i.e.* the frequency for which the phase of the system crosses $-180°$
ϵ	Tolerance value for the steady-state error
M_s	Peak of sensitivity function
M_t	Peak of complementary sensitivity function
M_u	Plant magnitude gain at the ultimate frequency ω_u
M_r	Plant magnitude at the fundamental frequency ω_r
$M_{O\%}$	Maximum percent overshoot
n_s	Settling time in number of cycles
t_s	Settling time
ϕ_{ω_r}	Phase contribution of the controller at frequency ω_r
$\phi_{\omega_{rm}}$	Phase contribution of the controller at frequencies ω_{mr}
ϕ_{ω_m}	Maximum phase contribution of the phase-lead compensator that occurs at frequency ω_m
PM	Phase margin
GM	Gain margin
$S(s)$	Sensitivity function
$T(s)$	Complementary sensitivity function

C_{PR}	PR controller
C_{lead}	Phase-lead Compensator
C_{PMR}	PMR controller
G	Plant or process to be controlled
s	Complex frequency variable
$r(t)$	Reference signal
$y(t)$	Output signal
$u(t)$	Control signal
$d(t)$	Disturbance signal
A	Amplitude of the reference signal

CONTENTS

1 INTRODUCTION

The increasing demand for renewable energy sources and distributed power generation with grid-connected converters leads to new challenges for control system engineers to comply with strict power quality standards. Due to the intermittent nature of renewable sources, energy storage systems are critical in order to allow higher penetration of renewable energy in typical power systems. Moreover, the presence of DC power sources such as photovoltaic, fuel cells and energy storage systems demands efficient and reliable DC/AC power converters (NEJABATKHAH; LI, 2014). Once the power grid networks are typically designed for sinusoidal voltage signals, the devices connecting energy sources to the grid must use controllers that are able to track and reject periodic signals with high harmonic content. For instance, one of the main concerns is the presence of current harmonics in the network, due to the very stringent limits imposed by power quality standards (TIMBUS *et al.*, 2009). Furthermore, as the cables of power systems are not ideal, the voltage drop caused by the inherent resistance of cables leads to distortions of the voltage signal. Nonlinear loads are a major cause of distortion in power grids and in the output of uninterruptible power supplies (UPS). Therefore, controllers must be able to reject these harmonic signals, as well as to track the signal of desired frequency (GRADY; SANTOSO, 2001) (FAROOQ; ZHOU; FARRAG, 2013).

The need of tracking or rejecting sinusoidal and periodic signals also appears in several other practical applications, which include active filters (LASCU *et al.*, 2008)(FUKUDA; YODA, 2001), vibration control (HALIM; MOHEIMANI, 2001)(MOHEIMANI; VAUTIER, 2005), positioning systems (LING *et al.*, 2019)(MAHMOOD; MOHEIMANI; BHIKKAJI, 2008), atomic force microscopy (DAS; POTA; PETERSEN, 2014)(FAIRBAIRN; MOHEIMANI, 2012), induction heating system (NGUYEN *et al.*, 2014), magnetically suspended fly-wheel (SU *et al.*, 2016) and electric vehicles (SALEHIFAR *et al.*, 2014)(SETH; SINGH, 2020).

Although the proportional-integral-derivative (PID) controller has been extensively used in applications with periodic signals due to its simple structure and widespread tuning methods, this type of controller has several limitations in compensating harmonics and tracking periodic signals (SHEN *et al.*, 2010). Thus, the urge for new control techniques

capable of tracking sinusoidal signals while rejecting periodic disturbances with superior performance has become evident. In order to achieve these characteristics, other controllers based on the internal model principle such as the resonant controller and the repetitive controller stand out (SATO *et al.*, 1998) (LORENZINI *et al.*, 2018).

The main characteristic of the so-called resonant controllers is the infinite gain introduced in the frequency of interest, which can lead to stability problems and makes its design and tuning more complex. The proportional resonant (PR) controller can provide zero steady-state error for the tracking or rejection of sinusoidal signals. However, the absence of a prevalent systematic tuning method for the general use of PR controllers restricts its usage. Typically, this type of controller is tuned using trial and error procedures or its parameters are selected based on simulation results, as presented in (TEODORESCU *et al.*, 2006), (TIMBUS *et al.*, 2009), (YEPES *et al.*, 2010), (SHEN *et al.*, 2010) and (WU *et al.*, 2012). Some systematic methods can be found, as presented in (PEREIRA; BAZANELLA, 2015) and (LORENZINI; PEREIRA; BAZANELLA, 2020). Also, different systematic procedures for specific applications can be found, as presented in (BAO *et al.*, 2013) and (LORENZINI *et al.*, 2021), and other tuning approaches use advanced mathematical tools, such as the convex optimization problem subject to linear matrix inequalities (LMI) constraints presented in (PEREIRA *et al.*, 2014), increasing the complexity of controller design.

In this work, the proportional resonant controller topology is considered and a systematic procedure for the computation of the controller parameters based on a frequency response method is proposed. Then, the control strategy is tested using different classes of processes found in typical control problems. The method is extended by the introduction of a phase-lead compensator in the control loop in order to allow better performance in an augmented bandwidth. The proposed method for the PR controller associated with a lead compensator is tested and previous results are compared for different frequencies of interest. In order to improve the response subject to high harmonic content, the method is revised to consider multiple frequency modes, resulting in the proportional multi-resonant (PMR) controller. Finally, the proposed method for the PMR controller is tested for different frequencies of interest.

1.1 Dissertation Objectives

The major aim of this research is to develop an easy to use, systematic procedure for the computation of resonant controllers parameters based on a frequency response method. The main objectives of the study can be summarized as follows:

- To investigate and demonstrate the benefits of combining a phase-lead compensator with resonant controllers.

- To investigate the contribution of multiple frequency modes to the performance of resonant controllers.
- To develop a general, easy to use method based on frequency response characteristics to tune the controllers, using a systematic approach analogous to the classic methods of control theory.

1.2 Publication

Results from this work have been published as listed below:

1. MOSSMANN, B.H.; PEREIRA, L.F.A.; GOMES DA SILVA JR, J.M. "Síntese de Parâmetros de Controladores Proporcionais-Ressonantes através do Método da Resposta em Frequência" (in Portuguese), **Proceedings of the XIV Brazilian Symposium on Intelligent Automation**, 2019 (MOSSMANN; PEREIRA; GOMES DA SILVA JR, 2019).
2. MOSSMANN, B.H.; PEREIRA, L.F.A.; GOMES DA SILVA JR, J.M. "Tuning of Proportional Resonant Controllers Combined with Phase-lead Compensators Based on the Frequency Response", **Journal of Control, Automation and Electrical Systems**, 2021 (MOSSMANN; PEREIRA; GOMES DA SILVA JR, 2021).
3. MOSSMANN, B.H.; PEREIRA, L.F.A.; GOMES DA SILVA JR, J.M. "Tuning of Proportional Multi-Resonant Controllers Combined with Phase-lead Compensators Based on the Frequency Response", [*work in progress*], 2021.

1.3 Dissertation Outline

This dissertation is organized as follows:

· **Chapter 2**: The fundamental concepts used throughout the dissertation are highlighted in this chapter. The general characteristics of resonant controllers are discussed. Performance indices used for the evaluation of results and the classes of processes used for the performance assessment are presented.

· **Chapter 3**: This chapter introduces the PR controller and its parameters. The steps for tuning the PR controller are demonstrated. Simulation results are presented for different classes of processes.

· **Chapter 4**: This chapter considers the combination of a phase-lead compensator to the PR controller, resulting in the PR+Lead compensator. The method is extended for this topology and simulation results are presented for different classes of processes. The disturbance rejection of PR controller and PR+Lead compensator is analysed

and simulation results are presented and compared. A disturbance signal composed by the fundamental and odd harmonics frequencies is considered to evaluate the total harmonic distortion of the output signal.

- **Chapter 5**: This chapter extends the concepts discussed in previous chapters to the case of multiple frequency modes, resulting in the PMR controller. The method is revised for this structure and simulation results are presented for different classes of processes.

- **Chapter 6**: A summary of the research is provided in this chapter along with the conclusions of this study. A discussion about the future directions of the research end the dissertation.

2 FUNDAMENTAL CONCEPTS

In this chapter, the fundamental theoretical background and definitions used throughout the entire dissertation are introduced and the classes of processes considered for the performance assessment of the proposed methods are presented.

2.1 Resonant Controller

The tracking and rejection of periodic signals is an important topic with different practical applications, from electrical power grids to atomic microscopy, as mentioned in the Introduction. One possible approach to determine a suitable controller for working with this type of signal is to consider the internal model principle (IMP).

For a stable closed-loop system as depicted in Figure 1, fundamentally, the IMP states that, if the dynamic structure of the open-loop transfer function contains a model of the dynamics that generate the signals of interest, then asymptotic reference tracking and disturbance rejection with zero steady-state error are achieved.

Figure 1 – Block diagram of the closed-loop system

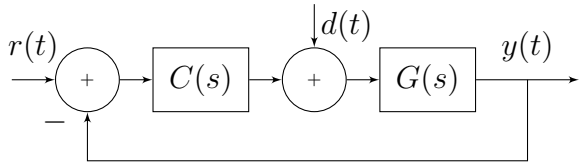

Source: created by the author.

In order to demonstrate the IMP, consider the closed-loop system shown in Figure 1 with the controller $C(s)$, the plant $G(s)$ and the signals $r(t)$, $d(t)$ and $y(t)$ that represent the reference, the disturbance and the output signals respectively. Let $R(s)$, $D(s)$ and $Y(s)$ be the representation of these signals in the frequency domain. The transfer function from the reference to the output $T_r(s)$ and from the disturbance to the output $T_d(s)$ are given by

$$T_r(s) = \frac{Y(s)}{R(s)} = \frac{C(s)G(s)}{1 + C(s)G(s)} \tag{1}$$

$$T_d(s) = \frac{Y(s)}{D(s)} = \frac{G(s)}{1 + C(s)G(s)} \tag{2}$$

Now, consider the particular case of sinusoidal signals of frequency ω_r. If the system is closed-loop stable, the condition for the tracking of the reference signal with zero steady-state error and for the disturbance rejection are as follows

$$|T_r(j\omega_r)| = \left| \frac{C(j\omega_r)G(j\omega_r)}{1 + C(j\omega_r)G(j\omega_r)} \right| = 1 \ , \ \angle T_r(j\omega_r) = 0 \tag{3}$$

$$|T_d(j\omega_r)| = \left| \frac{G(j\omega_r)}{1 + C(j\omega_r)G(j\omega_r)} \right| = 0 \ , \ \angle T_d(j\omega_r) = 0 \tag{4}$$

One can notice that (3) and (4) are verified if $|C(j\omega_r)G(j\omega_r)| = \infty$. Thus, the reference tracking with zero steady-state error and disturbance rejection for sinusoidal signals with a given frequency ω_r are ensured if the controller transfer function introduces an infinite gain at the frequency of the signals to be tracked and rejected. In this particular case, this is true if the controller contains a pair of complex-conjugate poles at frequency ω_r.

For example, PID controllers have a pole at the origin and hence present an infinite peak gain in the open-loop transfer function for constant signals (*i.e.* for zero frequency). Therefore, if the system is closed-loop stable, it allows to track references and reject disturbances of constant nature. Similarly, also based on the IMP, the resonant controller has an infinite peak gain in a given frequency, thus it allows to track sinusoidal references and reject sinusoidal disturbances of that given frequency. Hence, once stability of the closed-loop system is assured, zero steady-state error is achieved. A controller must therefore stabilize the closed-loop system and contain a model of the signals of interest (FRANCIS; WONHAM, 1976) (BENGTSSON, 1977).

In particular, to address the problem of tracking a sinusoidal reference with frequency ω_r, the system must have a pair of imaginary poles in this frequency, i.e., the poles must be located on the imaginary axis at $\pm j\omega_r$. Therefore, in order to guarantee zero steady-state error, the open-loop transfer function of the system must replicate the following term

$$G_r(s) = \frac{1}{s^2 + \omega_r^2} \tag{5}$$

Figure 2 presents the Bode plot for the transfer function (5). It illustrates the infinite resonant peak at frequency ω_r.

The working principle of a resonant control strategy consists in inserting the model given by (5) in the loop transfer function $C(s)G(s)$. Because of the marginally stable poles of the transfer function (5), it can lead to stability problems. The infinite gain and the abrupt decrease in phase make the design and tuning of resonant controllers a challenging effort.

Figure 2 – Bode plot of transfer function $G_r(s)$.

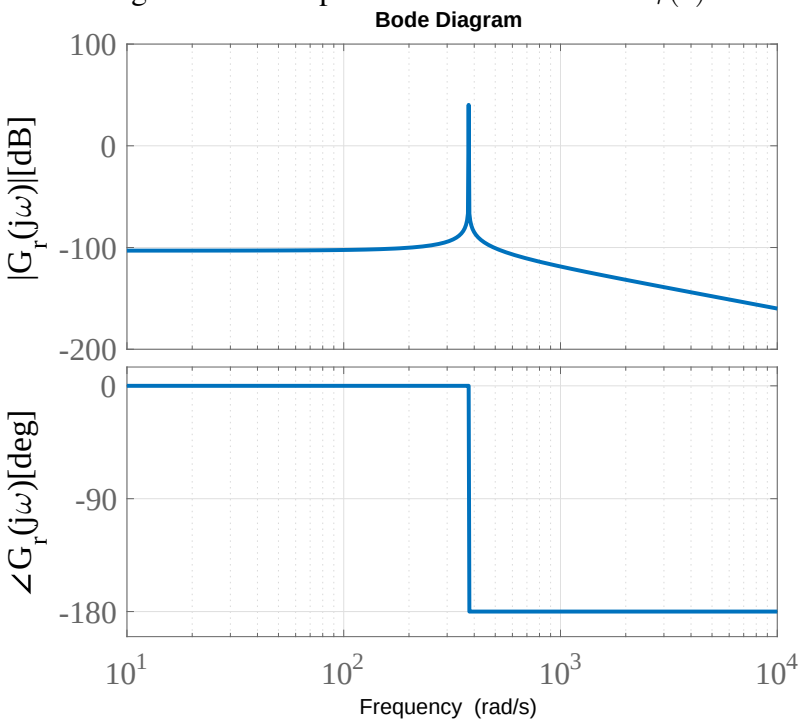

Source: created by the author.

Recall that periodic signals with frequency ω_r can be written as the sum of sinusoidal components known as the Fourier Series (OPPENHEIM; WILLSKY; NAWAB, 1997), given by

$$r(t) = a_0 + \sum_{n=1}^{+\infty}(a_n \cos n\omega_r t + b_n \sin n\omega_r t) \tag{6}$$

The lowest frequency component of the signal is called the fundamental frequency ω_r and its multiples are the so-called harmonics or harmonic frequencies. Thus, in order to deal with generic periodic signals, it is necessary to consider their frequency composition. Following that, the resonant controller can be extended to multiple frequency modes as follows

$$G_{mr}(s) = \frac{1}{s^2 + \omega_r^2} + \frac{1}{s^2 + (2\omega_r)^2} + \frac{1}{s^2 + (3\omega_r)^2} + ... + \frac{1}{s^2 + (N\omega_r)^2} \tag{7}$$

resulting in a multi-resonant controller. Figure 3 illustrates the multiple peaks of resonance of a multi-resonant controller as defined in (7) with $\omega_r = 1\ rad/s$ and its odd multiples up to $N = 11$.

In the next chapters, the application of different resonant controller topologies is discussed. Stability and performance issues are addressed. A systematic method for the tuning and application of this type of controller is proposed, considering general processes for which frequency response characteristics are known or can be measured.

Figure 3 – Bode plot of a multi-resonant controller with $\omega_r = 1\ rad/s$ and its odd multiples up to $N = 11$.

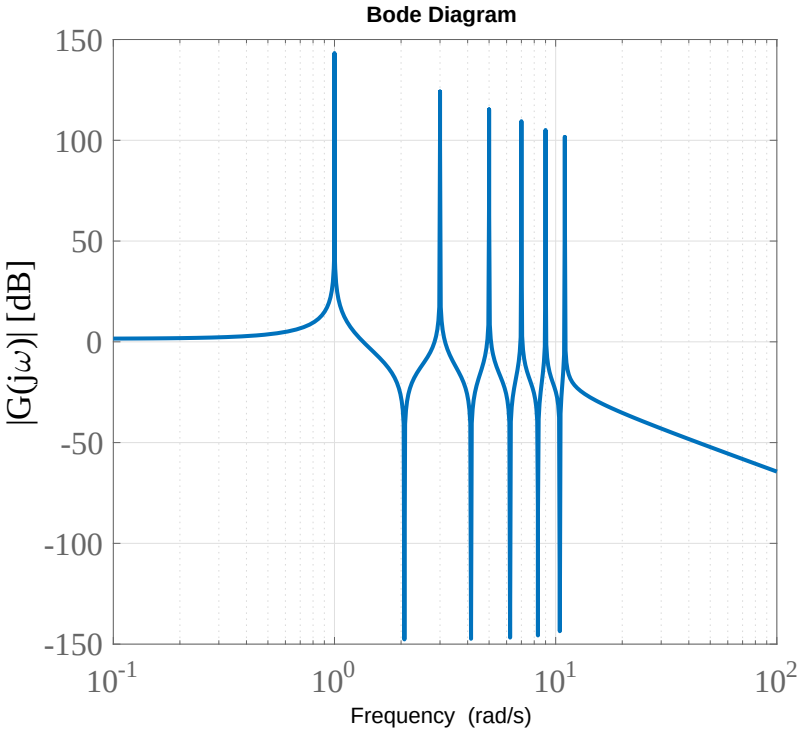

Source: created by the author.

2.2 Performance Indices for Periodic Signals

In order to assess the performance of the controlled system for tracking sinusoidal reference signals in a systematic and standard-compliant way, it is convenient to define criteria compatible with these signals (PEREIRA; BAZANELLA, 2015). A sinusoidal reference signal with frequency ω_r is generically defined as

$$\begin{cases} r(t) = 0 \ , \ \forall t < 0 \\ r(t) = A \sin \omega_r t \ , \ \forall t \geq 0 \end{cases} \tag{8}$$

The maximum overshoot expresses the ratio of maximum peak value of the output signal $y(t)$ in relation to the amplitude of input signal $r(t)$. It is computed as follows

$$M_O = \max \left(\frac{M - A}{A} \ , \ 0 \right) \tag{9}$$

where M is the maximum peak value of the output signal, given by

$$M = \max_t |y(t)| \tag{10}$$

Thus, the percentage of maximum overshoot with respect to the reference amplitude is given by

$$M_{O_\%} = M_O \times 100\% \tag{11}$$

Let $e(t)$ be the tracking error of the system, that expresses the difference between output and input signals. The normalized tracking error in relation to the amplitude A of the reference signal is defined as

$$e_n(t) = \frac{e(t)}{A} \tag{12}$$

The settling time is defined as the smallest time at which the normalized tracking error remains bellow a tolerance value ϵ, that is

$$t_s = \min_{t_1} \ : \ |e_n(t)| < \epsilon \ , \ \forall t > t_1 \tag{13}$$

Typically, the value of ϵ is 2% or 5%. In this work, the settling time t_s is determined with tolerance $\epsilon = 2\%$.

For periodic signals, it is also convenient to represent the settling time as the number of periods of the reference signal before settling. Hence, the number of cycles of the signal elapsed before settling is then given by

$$n_s = \frac{t_s \omega_r}{2\pi} \tag{14}$$

2.3 Stability and Performance Measures

From the knowledge of the frequency response of the plant to be controlled, one seeks to determine the parameters of the controller that deliver satisfactory performance, appropriate stability margins and robustness for the closed-loop system. Consider the closed-loop system structure depicted in Figure 1, where $r(t)$, $d(t)$ and $y(t)$ are the reference, disturbance and output signals, respectively, $G(s)$ and $C(s)$ are the process and controller transfer functions, respectively. The loop transfer function $L(s)$ represents the forward path from the reference $r(t)$ to the output $y(t)$ and is given by

$$L(s) = C(s)G(s) \tag{15}$$

The sensitivity and complementary sensitivity functions provide a good measure of robustness for the system in terms of its stability and tolerance against variations in the process (ASTRÖM; MURRAY, 2010). These functions are respectively given by $S(s)$ and $T(s)$ defined as follows

$$S(s) = \frac{1}{1 + L(s)} \tag{16}$$

$$T(s) = \frac{L(s)}{1 + L(s)} \tag{17}$$

Notice that the relationship between the sensitivity function and the complementary sensitivity function is given by

$$S(s) + T(s) = 1 \tag{18}$$

Examining the peak of the sensitivity function $S(s)$ and of the complementary sensitivity function $T(s)$, given by M_s and M_t respectively, it is possible to deepen the comprehension of the system dynamics provided by the stability margins.

Generally, for a control system with satisfactory performance, the values of M_s and M_t fall between 1 and 2, or more precisely $1.2 < M_s < 2$ and $1 < M_t < 1.5$ (ASTRÖM; MURRAY, 2010) (MORARI; ZAFIRIOU; ZAFIRIOU, 1989).

The effect of the value of M_s in the stability margins of the system can be better understood from the Nyquist plot of the transfer function $L(s)$ as shown in Figure 4. The magnitude diagram of a sensitivity function $S(s)$ for the system with loop function $L(s)$ is shown in Figure 4a. Figure 4b presents the Nyquist plot of the transfer function $L(s)$.

Taking into account that

$$|1 + L(s)| = \frac{1}{|S(s)|} \tag{19}$$

the value M_s is equal to the inverse of the smallest distance from the Nyquist plot of function $L(s)$ to the critical point $-1 + j0$. The magnitude of the sensitivity function has module 1 at frequency ω_{sc}. As depicted in Figure 4, frequencies smaller than ω_{sc} are attenuated by the feedback loop. Frequencies higher than ω_{sc} are amplified by the feedback loop and the highest amplification occurs for frequency ω_{ms}. Decreasing any of the stability margins of the system, either gain or phase margin, leads the Nyquist plot of the function $L(s)$ towards the point $-1 + j0$, yielding a larger value for M_s.

Hence, the peak value of the sensitivity function M_s is a good guide to predict the performance of the system regarding reference tracking and tolerance to disturbances. From the relationship between M_s and stability margins, it is possible to compute estimated values for phase margin (PM) and gain margin (GM) that result in a satisfactory behaviour of the system (MORARI; ZAFIRIOU; ZAFIRIOU, 1989). This relationship is given by

$$GM \geq \frac{M_s}{M_s - 1} \Rightarrow M_s \leq \frac{GM}{GM - 1} \tag{20}$$

$$PM \geq 2 \arcsin\left(\frac{1}{2M_s}\right) \Rightarrow M_s \leq \frac{1}{2 \sin\left(\frac{PM}{2}\right)} \tag{21}$$

As aforementioned, typically the value of M_s must be in the interval $1.2 \leq M_s \leq 2$. From the equations above, assuming $M_s \approx 1.2$ yields $PM \geq 49.25°$ and $GM \geq 15.56dB$.

Figure 4 – Graphical interpretation of the value of M_s.

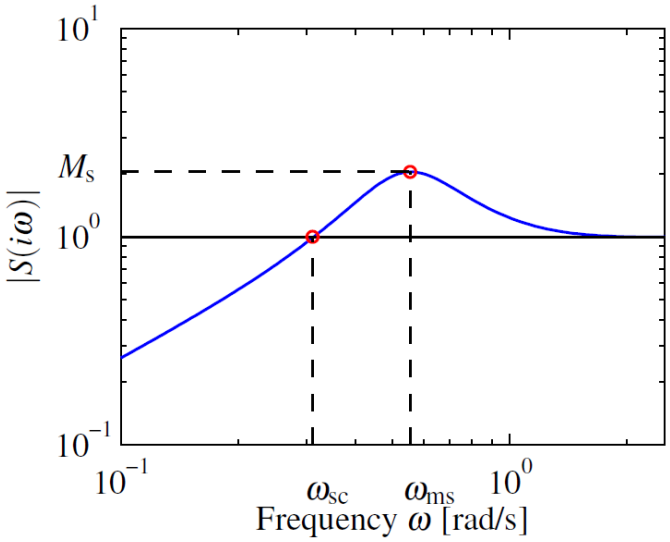

Source: ASTRÖM; MURRAY (2010)

(a)

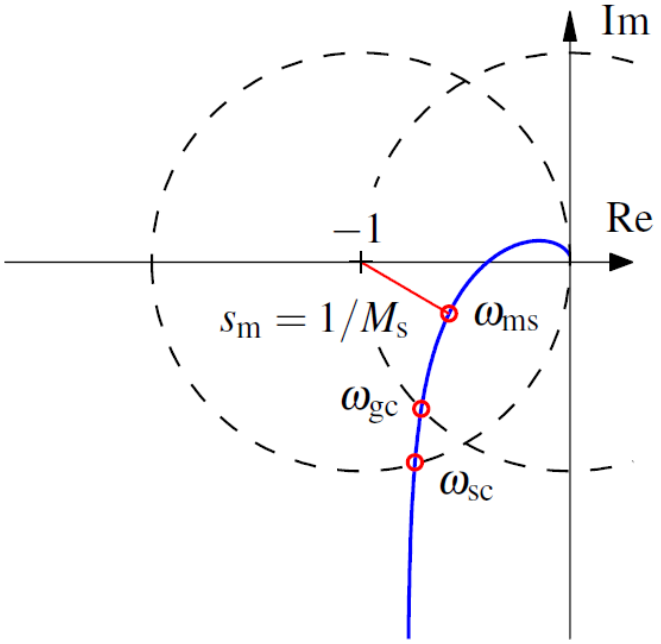

Source: ASTRÖM; MURRAY (2010)

(b)

2.4 Classes of Processes for Performance Assessment

Following, the test batch of processes to assess the proposed method is presented. This test batch represents typical transfer functions with and without ultimate frequency found in control system problems and was selected from (BAZANELLA; PEREIRA; PARRAGA, 2017) and (ÅSTRÖM; HÄGGLUND, 2004).

These selected processes with ultimate frequency, *i.e.* for which the phase of $G(j\omega)$ crosses $-180°$, $G_1(s)$, $G_2(s)$ and $G_3(s)$ are defined as follows

$$G_1(s) = \frac{1}{(s+1)^n} \quad , \quad n = [3 \;\; 4 \;\; 5] \tag{22}$$

$$G_2(s) = \frac{1}{(s+1)((sT)^2 + 1.4Ts + 1))} \quad , \quad T = [0.1 \;\; 0.5 \;\; 1] \tag{23}$$

$$G_3(s) = \frac{1}{(s+1)(1+\alpha s)(1+\alpha^2 s)(1+\alpha^3 s)} \quad , \quad \alpha = [0.1 \;\; 0.9 \;\; 5] \tag{24}$$

Figures 5, 6 and 7 show the Bode plots for processes with ultimate frequency defined in (22), (23) and (24) respectively.

The selected processes without ultimate frequency $G_4(s)$, $G_5(s)$ and $G_6(s)$ are defined as follows

$$G_4(s) = \frac{\alpha}{(s+\alpha)} \quad , \quad \alpha = [0.1 \;\; 0.9 \;\; 5] \tag{25}$$

$$G_5(s) = \frac{\alpha}{(s+1)(s+\alpha)} \quad , \quad \alpha = [0.1 \;\; 0.9 \;\; 5] \tag{26}$$

$$G_6(s) = \frac{1}{s^2 + 2\alpha s + 1} \quad , \quad \alpha = [0.1 \;\; 0.5 \;\; 0.9] \tag{27}$$

Figures 8, 9 and 10 show the Bode plots for processes without ultimate frequency defined in (25), (26) and (27) respectively.

Figure 5 – Bode plots of processes $G_1(s)$.

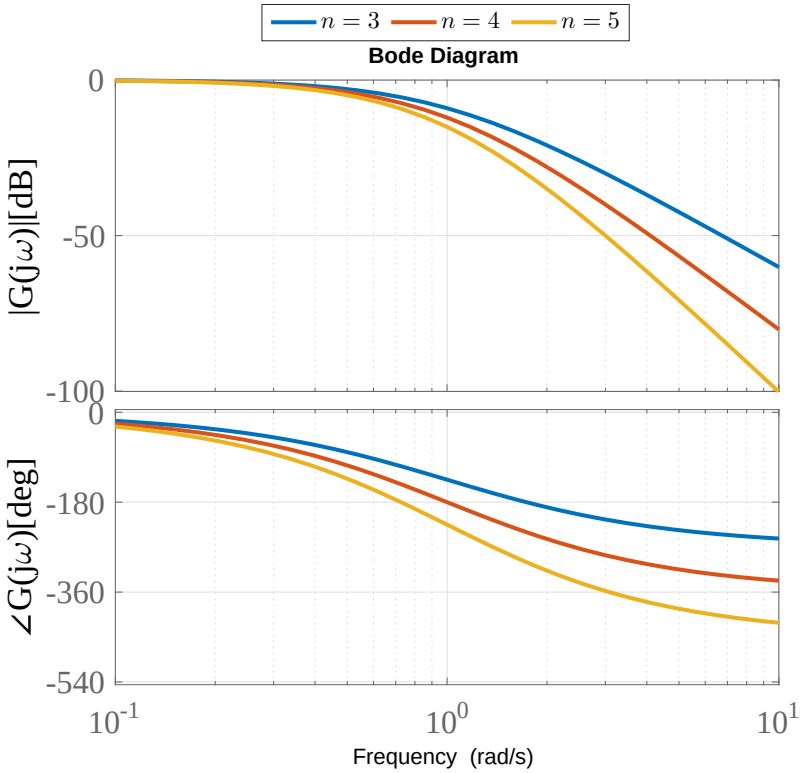

Source: created by the author.

Figure 6 – Bode plots of processes $G_2(s)$.

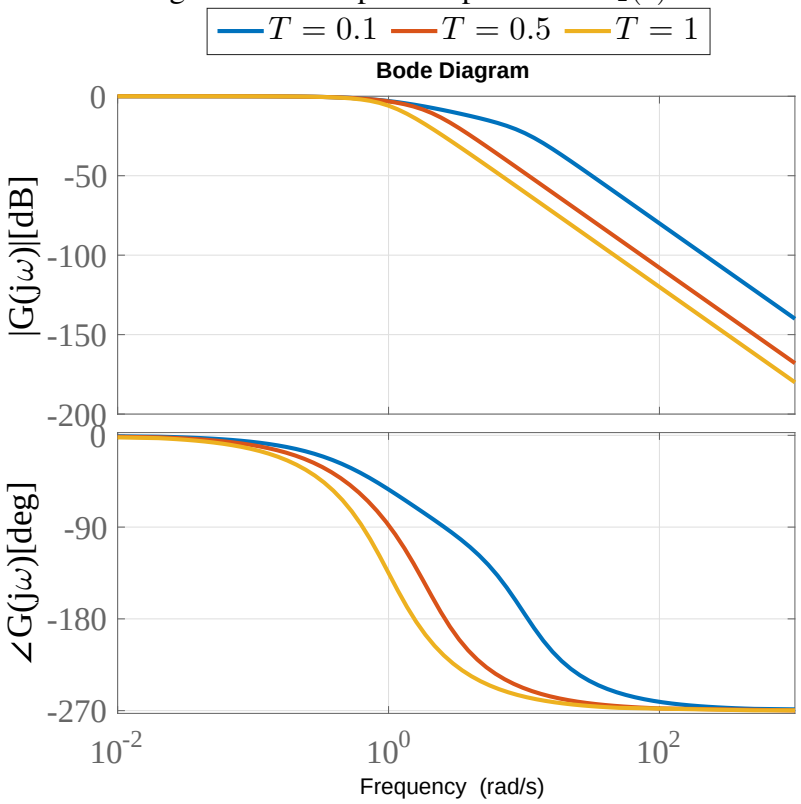

Source: created by the author.

Figure 7 – Bode plots of processes $G_3(s)$.

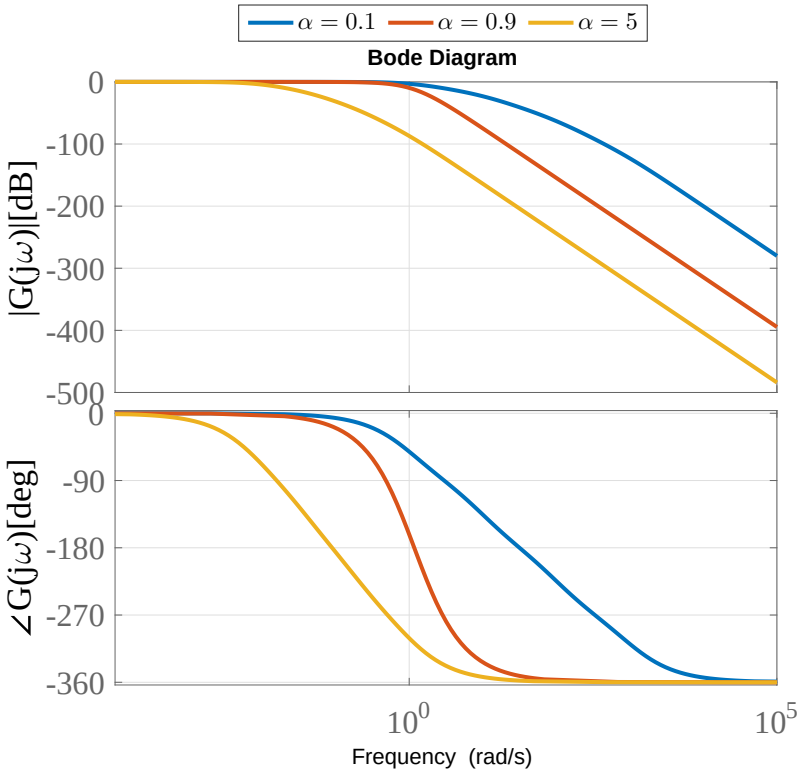

Source: created by the author.

Figure 8 – Bode plots of processes $G_4(s)$.

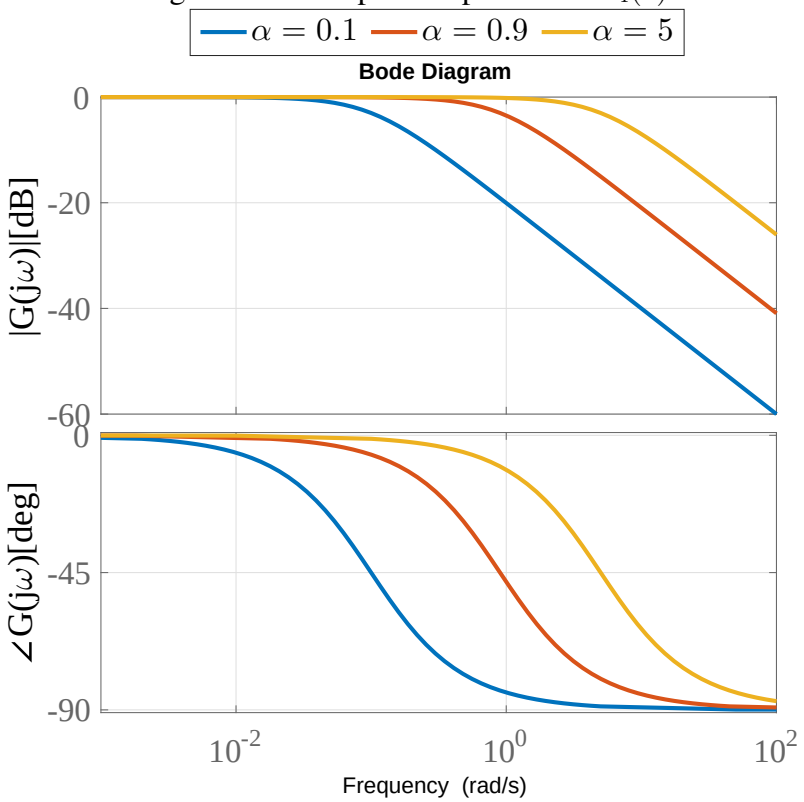

Source: created by the author.

Figure 9 – Bode plots of processes $G_5(s)$.

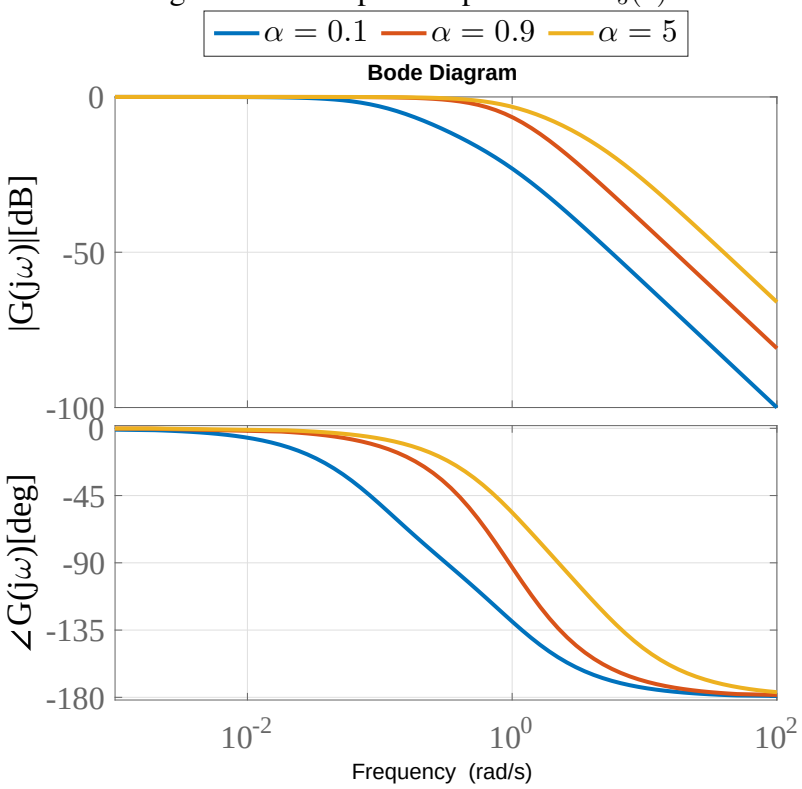

Source: created by the author.

Figure 10 – Bode plots of processes $G_6(s)$.

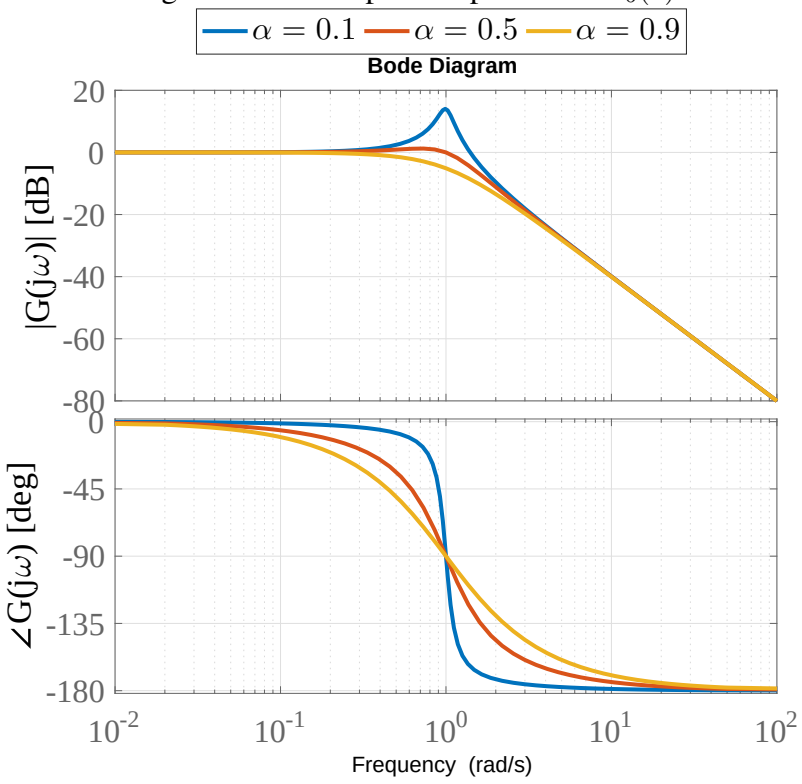

Source: created by the author.

2.5 Chapter Summary

This chapter has presented an overview on resonant controllers and the performance indices for the tracking and rejection of periodic signals. The stability and performance measures considered in the following chapters for the development of the proposed tuning method have been discussed. In addition, the classes of processes used for the performance assessment of the method developed in the next chapters have been introduced.

3 PROPORTIONAL RESONANT CONTROLLER

3.1 Introduction

In the previous chapter, the motivation for the application of resonant controllers to work with periodic signals is discussed based on the IMP. An overview of this type of controller is presented and it follows that to address the problem of tracking a sinusoidal reference with frequency ω_r, the controller must have a pair of imaginary poles in this frequency, *i.e.*, the poles must be located on the imaginary axis in $\pm j\omega_r$. As aforementioned, the infinite resonant peak and the abrupt decrease of phase at frequency ω_r impose challenges to the tuning of the controller parameters aiming at the stabilization and performance requirements for the closed-loop system. In this chapter, the application of this control strategy for the simplest periodic signal, a sinusoidal reference with frequency ω_r, is discussed.

3.2 The Proportional Resonant Structure

Consider the transfer function for the resonant term presented in (5). In order to provide more degrees of freedom and facilitate the closed-loop stabilization, two zeros are inserted in the left half complex plane. The following equation presents the transfer function of the resulting controller (PEREIRA *et al.*, 2014).

$$C_{PR}(s) = \frac{\delta_2 s^2 + \delta_1 s + \delta_0}{s^2 + \omega_r^2} \tag{28}$$

An equivalent structure proposed in this work for the controller (28), which considers explicitly a proportional and a resonant term, is as follows

$$\begin{aligned} C_{PR}(s) &= k_p \left(1 + \frac{s^2 + 2k_{r_1} s + k_{r_2}}{s^2 + \omega_r^2}\right) = \\ &= k_p + \frac{k_p s^2 + 2k_p k_{r_1} s + k_p k_{r_2}}{s^2 + \omega_r^2} \end{aligned} \tag{29}$$

where ω_r is the reference frequency and k_p, k_{r_1} and k_{r_2} are parameters to be tuned.

The resonant part of the controller (29) is given by

$$C_R(s) = \frac{s^2 + 2k_{r_1}s + k_{r_2}}{s^2 + \omega_r^2} \tag{30}$$

Knowledge on the phase contribution associated with zeros of the controller is important to compute the phase margin necessary to ensure the stability of the system. Also, the zeros shall be located in the left half of the s-plane. To analyse the zeros of the resulting PR controller, the equations for $C_{PR}(s)$ given by (29) can be rewritten as follows

$$C_{PR}(s) = \frac{2k_p\left(s^2 + k_{r_1}s + \frac{k_{r_2} + \omega_r^2}{2}\right)}{s^2 + \omega_r^2} \tag{31}$$

Thus, the zeros of $C_{PR}(s)$ are given by

$$\begin{aligned} z_{1_{C_{PR}}} &= \frac{-k_{r_1} + \sqrt{k_{r_1}^2 - 2(\omega_r^2 + k_{r_2})}}{2} \\ z_{2_{C_{PR}}} &= \frac{-k_{r_1} - \sqrt{k_{r_1}^2 - 2(\omega_r^2 + k_{r_2})}}{2} \end{aligned}, \tag{32}$$

It can be noticed that the topology of $C_{PR}(s)$ makes the zeros of the controller independent of k_p. If the zeros are complex numbers, *i.e.* $2(\omega_r^2 + k_{r_2}) > k_{r_1}^2$, their corresponding natural frequency ω_0 is equal to their module and is given by

$$\omega_{0_{C_{PR}}} = \sqrt{\frac{\omega_r^2 + k_{r_2}}{2}} \tag{33}$$

To ensure that the zeros of the controller are placed in the left half complex plane, it is sufficient to have $k_{r_1} > 0$ and $k_{r_2} \geq 0$. From (33), considering $\omega_{0_{C_{PR}}} < \omega_r$, the maximum positive phase contribution of the zeros in the frequency ω_r is obtained with $k_{r_2} = 0$, as this corresponds to the case which frequency $\omega_{0_{C_{PR}}}$ is farthest from frequency ω_r. Thus, from now on, it is assumed $k_{r_2} = 0$. Furthermore, if $k_{r_1}^2 < 2\omega_r^2$, *i.e.* $k_{r_1} < \sqrt{2}\omega_r$, the zeros are complex-conjugate and from (33) yields $\omega_{0_{C_{PR}}} = \frac{\sqrt{2}}{2}\omega_r$ for the topology proposed in (31).

Assume $k_p > 0$. Then the magnitude of the controller (31) frequency response at a given frequency ω is given by

$$|C_{PR}(j\omega)| = \frac{k_p}{|\omega_r^2 - \omega^2|}\sqrt{(\omega_r^2 - 2\omega^2)^2 + 4k_{r_1}^2\omega^2} \tag{34}$$

It can be noticed that for $\omega = 0$ the gain of the controller is k_p, for $\omega = \omega_r$ the gain tends to infinity and for $\omega \gg \omega_r$ the gain tends to $2k_p$.

Moreover, considering $k_{r_1} < \sqrt{2}\,\omega_r$, the phase contribution of the PR controller in a frequency ω is given by

$$\angle C_{PR}(j\omega) = \begin{cases} \arctan\left(\dfrac{2\omega + \sqrt{2\omega_r^2 - k_{r_1}^2}}{k_{r_1}}\right) + \arctan\left(\dfrac{2\omega - \sqrt{2\omega_r^2 - k_{r_1}^2}}{k_{r_1}}\right), \omega < \omega_r \\ -180^\circ + \phi_1(\omega) = \arctan\left(\dfrac{2k_{r_1}\omega}{\omega_r^2 - 2\omega^2}\right) \quad , \quad \omega_r < \omega \end{cases} \tag{35}$$

where $\phi_1(\omega)$ represents the phase of the controller for $\omega < \omega_r$.

Figure 11 presents the Bode plot for $C_{PR}(s)$ with $\omega_r = 0.43\,rad/s$, $k_p = 0.3888$ and different values of k_{r_1}. It illustrates that when choosing a different value for k_{r_1}, the phase of the controller changes whereas its magnitude remains virtually unaffected. Note that as k_{r_1} increases, the damping ratio of the zeros also increases, leading to a smoother phase augmentation for $\omega < \omega_r$. On the other hand, the maximum achieved phase is smaller. In this case, as the phase decreases $180°$ abruptly at the frequency $\omega = \omega_r$, the phase introduced by the controller for $\omega > \omega_r$ tends to be smaller, which can make difficult the stabilization of the closed-loop system or lead to small stability margins depending on the plant characteristics.

In the following sections, it will be shown that the proposed topology for $C_{PR}(s)$ simplifies the tuning process of the PR controller as it makes possible to choose k_p and k_{r_1} independently to fulfill gain and phase requirements of the system, respectively.

Figure 11 – Bode plot of the controller $C_{PR}(s)$ with $\omega_r = 0.43\,rad/s$ and $k_p = 0.3888$ for different values of k_{r_1}.

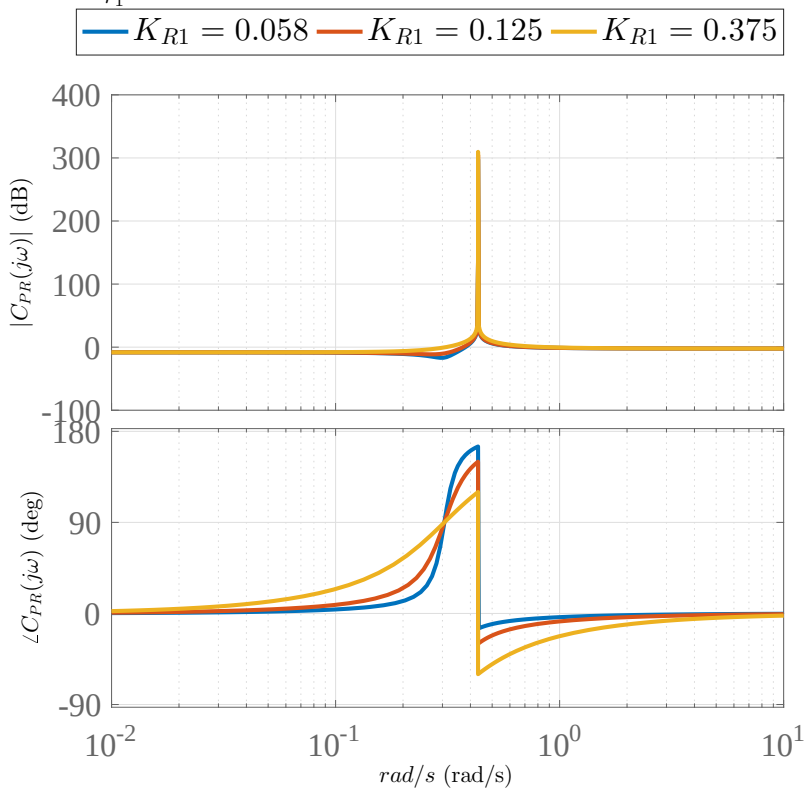

Source: created by the author.

3.3 Tuning of PR Controller

3.3.1 Plants with Ultimate Frequency

This work aims to present a method for the design of PR controllers based on the frequency response, providing satisfactory performance, considering the typical values found for the peak of sensitivity M_s. In particular, in this section the focus is on processes with ultimate frequency, (*i.e.* the phase of $G(j\omega)$ crosses $-180°$), for which it is possible to adjust both phase and gain margins.

Let ω_u be the ultimate frequency of the process (*i.e.* for which its phase crosses $-180°$), and let $M_u = |G(j\omega_u)|$ be the gain of the process at this frequency. The following value of k_p is proposed for the tuning of the controller

$$k_p = \frac{1}{10}\frac{\omega_u^2 - \omega_r^2}{M_u(2\omega_u^2 - \omega_r^2)} \tag{36}$$

Applying the proposed value of k_p to (34), assuming $\omega_r < \omega_u$, and computing $|C_{PR}(j\omega)|$ for the ultimate frequency ω_u yields to

$$|C_{PR}(j\omega_u)| = \frac{1}{10}\frac{\omega_u^2 - \omega_r^2}{M_u(2\omega_u^2 - \omega_r^2)}\frac{\sqrt{(2\omega_u^2 - \omega_r^2)^2 + 4k_{r_1}^2\omega_u^2}}{\omega_u^2 - \omega_r^2} \tag{37}$$

If $4k_{r_1}^2\omega_u^2 \ll (2\omega_u^2 - \omega_r^2)^2$, it follows that

$$|C_{PR}(j\omega_u)| \approx \frac{1}{10M_u} \tag{38}$$

Since $|G(j\omega_u)| = M_u$, it yields that $|C_{PR}(j\omega_u)G(j\omega_u)| \approx \frac{1}{10}$, *i.e.*, the gain margin is approximately $20\ dB$.

On the other hand, from (35), it follows that the minimum phase contribution (*i.e.* the most negative phase contribution) of the controller occurs at the resonant frequency ω_r, where there is a discontinuity, as it can be seen in Figure 11. Let ϕ_{ω_r} be the contribution of phase at frequency $\omega \to \omega_r^+$ required for the controller. Assigning $\omega = \omega_r$ in (35) for $\omega > \omega_r$ to obtain $\angle C(j\omega_r) = \phi_{\omega_r}$ and isolating the parameter k_{r_1} leads to the following expression

$$k_{r_1} = -\frac{\omega_r}{2}\tan(\phi_{\omega_r}) \tag{39}$$

As the minimum phase introduced by the controller occurs at frequency $\omega \to \omega_r^+$, note that (see Fig. 11) for frequencies higher than ω_r, the phase contribution of the controller is larger than ϕ_{ω_r}.

Since the controller introduces an infinite gain at frequency ω_r and gain margin is adjusted nearly at $20\ dB$ by choosing k_p, there must be a frequency ω_c such that $\omega_r < \omega_c < \omega_u$ and $|C_{PR}(j\omega_c)G(j\omega_c)| = 1$. This frequency is the so-called crossover frequency or $0\ dB$ frequency. The phase margin of the system must be adjusted at this frequency.

Because of the very high gain introduced by the controller at frequency ω_r, the choice of k_p to obtain $GM \approx 20dB$ tends to approximate the frequency ω_c towards ω_r.

As previously stated, the controller introduces a minimum phase at frequency $\omega \to \omega_r^+$ and also leads ω_c close to ω_r. Because of such characteristics, it is reasonable to assume the approximation $\omega_c \approx \omega_r$ and that the phase margin of $C_{PR}(j\omega)G(j\omega)$ could be adjusted at frequency ω_r. One can then calculate k_{r_1} using (39) so that $\angle C_{PR}(j\omega_r)G(j\omega_r) \approx -130°$, *i.e.*, $\angle G(j\omega_r) + \phi_{\omega_r} \approx -130°$ or equivalently $\phi_{\omega_r} \approx -130° - \angle G(j\omega_r)$. According to (21), a phase margin of approximately $50°$ corresponds to $M_s \approx 1.2$. Also, as previously stated, the condition to have complex-conjugate zeros is $k_{r_1} < \sqrt{2}\omega_r$. Thus, from (39), $\tan(-\phi_{\omega_r}) < 2\sqrt{2}$ or simply $\phi_{\omega_r} \geq -70.52°$.

Therefore, the choice of k_{r_1} allows to adjust the phase of $C(j\omega)G(j\omega)$ by a procedure virtually independent of its gain, which is adjusted by determining k_p. This feature of the proposed topology simplifies the fine-tuning of the controller.

The method for tuning the PR controller for processes with ultimate frequency proposed in this work can therefore be summarised as follows:

Algorithm:

Step 1. Determine k_p from (36) to adjust the gain margin of the controlled system.

Step 2. From the frequency response of the process, determine the phase contribution that the controller can introduce at frequency ω_r with $\phi_{\omega_r} \approx -130° - \angle G(j\omega_r)$, $\phi_{\omega_r} \geq -70.52°$.

Step 3. Determine k_{r_1} from (39) using the value for ϕ_{ω_r} obtained in the previous step.

In order to evaluate the effectiveness of the tuning method, it is tested for different classes of typical processes with ultimate frequency in Section 3.4.

3.3.2 Plants without Ultimate Frequency

In this section the focus is on processes without ultimate frequency, (*i.e.* the phase of $G(j\omega)$ does not cross $-180°$), for which it is not possible to adjust the gain margin.

Recall from (34) that for $\omega = 0$ the gain of the controller is k_p, for $\omega = \omega_r$ the gain tends to infinity and for $\omega \gg \omega_r$ the gain tends to $2k_p$. Moreover, it can be observed in Figure 12 that at the vicinity of ω_r the gain starts to increase until it peaks to infinity at ω_r, then starts to decrease to $2k_p$.

For a process without ultimate frequency, the gain margin of the system would be infinite. Hence, the proportional gain of the controller can adjust the bandwidth of the system without restriction. Let $M_r = |G(j\omega_r)|$ be the gain of the process at frequency ω_r. The following value of k_p is proposed for the tuning of the controller

Figure 12 – Bode plot of the controller $C_{PR}(s)$ with $\omega_r = 5\,rad/s$ and $k_p = 1$ and $k_{r_1} = 2.5$.

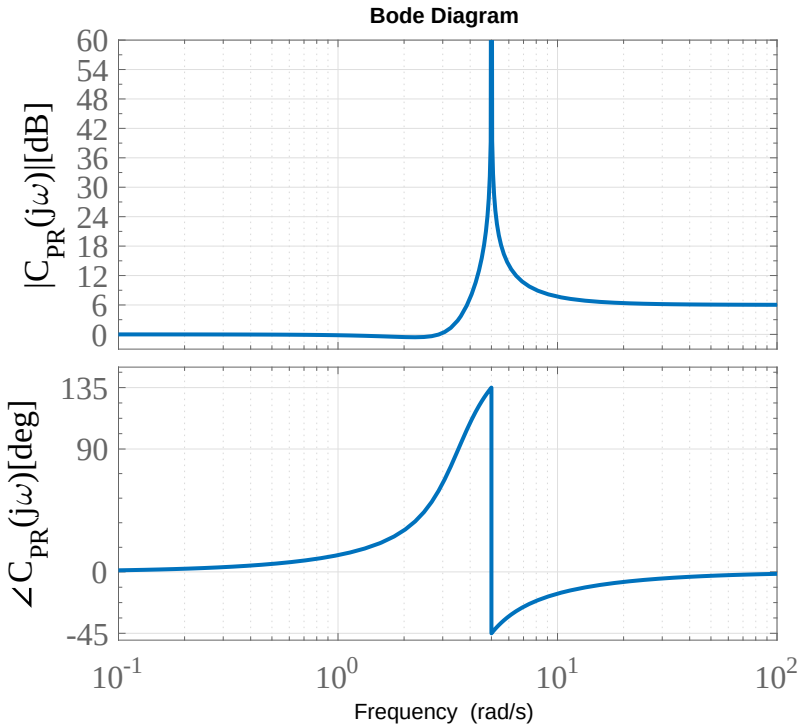

Source: created by the author.

$$k_p = \frac{1}{2M_r} \tag{40}$$

Considering that the controller introduces an infinite gain at frequency ω_r, there must be a frequency ω_c such that $\omega_r < \omega_c$ and $|C_{PR}(j\omega_c)G(j\omega_c)| = 1$. This frequency is the so-called crossover frequency or $0\ dB$ frequency. The phase margin of the system must be adjusted at this frequency. For k_p given by (40), this occurs at the vicinity of ω_r once the gain of the controller rapidly decreases to $2k_p$. Hence, the phase margin can be adjusted at ω_r analogously to the procedure for plants with ultimate frequency from the previous section.

Therefore, following the reasoning from the previous section, k_{r_1} can be adjusted to limit the phase contribution of the controller ϕ_{ω_r} at frequency $\omega \to \omega_r^+$ using the same expression given by (39). Recall that the minimum phase introduced by the controller occurs at frequency $\omega \to \omega_r^+$. For frequencies higher than ω_r, the phase contribution of the controller is larger than ϕ_{ω_r}. However, if the phase of the process at the vicinity of ω_r decreases abruptly, the phase contribution of the controller may compromise the stability of the system if its phase crosses $-180°$, limiting the gain margin that would be infinite otherwise. Thus, one must compute k_{r_1} using (39) so that $\angle C_{PR}(j\omega_r)G(j\omega_r) \approx -130°$, *i.e.*, $\angle G(j\omega_r) + \phi_{\omega_r} \approx -130°$ or equivalently $\phi_{\omega_r} \approx -130° - \angle G(j\omega_r)$. In order to have complex-conjugate zeros, $\phi_{\omega_r} \geq -70.52°$.

For processes with relative degree 2 and with small damping ratio, the phase of the process may decrease too abruptly at the vicinity of ω_r and it is necessary to adopt a stricter limit to the phase contribution of the controller, increasing ϕ_{ω_r}, so that phase and gain margins are within the limits proposed in this work. Phase contribution of the controller at any frequency ω can be verified from (35) to limit ϕ_{ω_r} accordingly.

The method for tuning the PR controller for processes without ultimate frequency proposed in this work can therefore be summarised as follows:

Algorithm:

Step 1. Determine k_p from (40).

Step 2. From the frequency response of the process, determine the phase contribution that the controller can introduce at frequency ω_r with $\phi_{\omega_r} \approx -130^\circ - \angle G(j\omega_r)$, $\phi_{\omega_r} \geq -70.52^\circ$.

Step 3. Determine k_{r_1} from (39) using the value for ϕ_{ω_r} obtained in the previous step.

In order to evaluate the effectiveness of the tuning method, it is tested for different classes of typical processes without ultimate frequency in the next section. In the following tests for processes without ultimate frequency, let ω_{-20dB} represent the frequency at which $|G(j\omega_{-20dB})| = -20dB$, *i.e.* the gain of the process at this frequency is $\frac{1}{10}$.

3.4 Simulation Results for PR Controller

Tables 1 to 3 summarise the results achieved for different ratios between ω_r and ω_u for processes $G_1(s)$, $G_2(s)$ and $G_3(s)$. Tables 4 to 6 summarise the results achieved for different ratios between ω_r and ω_{-20dB} for processes without ultimate frequency $G_4(s)$, $G_5(s)$ and $G_6(s)$. For additional simulation results see Appendix A.1. These tables present the obtained values for settling time n_s, maximum percent overshoot $M_{O_\%}$, peak of sensitivity function M_s, phase margin PM and gain margin GM of the controlled system, as well as the phase of process $G(j\omega)$ at frequency ω_r. Figures 13 to 18 show the output signal normalized with respect to the period of reference signal $r(t)$ for the different values of ω_r. All simulation tests produced a stable response, despite the considerably higher settling time for frequencies ω_r close to the ultimate frequency ω_u.

The parameters k_p and k_{r_1} were computed using the procedure proposed in the previous section. When feasible (*i.e.* in the cases for which $\angle G(j\omega) > -130^\circ$), the parameter k_{r_1} was selected such that the phase of the system $C_{PR}(j\omega)G(j\omega)$ at this frequency would be approximately -130°. In the cases for which $\angle G(j\omega) < -130^\circ$, the phase contribution of the controller was bounded to $\phi_{\omega_r} = -1^\circ$. For processes with relative degree 2 and damping ratio lower than $\frac{\sqrt{2}}{2}$, the phase of the process tends to decrease abruptly, as it is

Table 1 – Tuning parameters and performance indicators for the closed-loop system of $G_1(s)$ with $n = 3$ and different values of ω_r.

ω_r	k_p	k_{r_1}	n_s	$M_{O_\%}$	M_s	GM	PM	$\angle G(j\omega_r)$
$0.1\omega_u$	0.40	0.24	1.22	0%	1.31	$17.7dB$	84.6°	$-29°$
$0.25\omega_u$	0.39	0.37	1.84	1.67%	1.52	$15.8dB$	47.1°	$-70°$
$0.5\omega_u$	0.34	0.03	8.23	3.31%	1.47	$19.5dB$	46.3°	$-123°$
$0.75\omega_u$	0.24	0.01	> 50	35.68%	3.01	$19.7dB$	19.6°	$-157°$
$0.9\omega_u$	0.13	0.01	> 50	71.99%	8.97	$19.2dB$	6.4°	$-172°$

Figure 13 – Closed-loop normalized output signal for process $G_1(s)$ with $n = 3$.

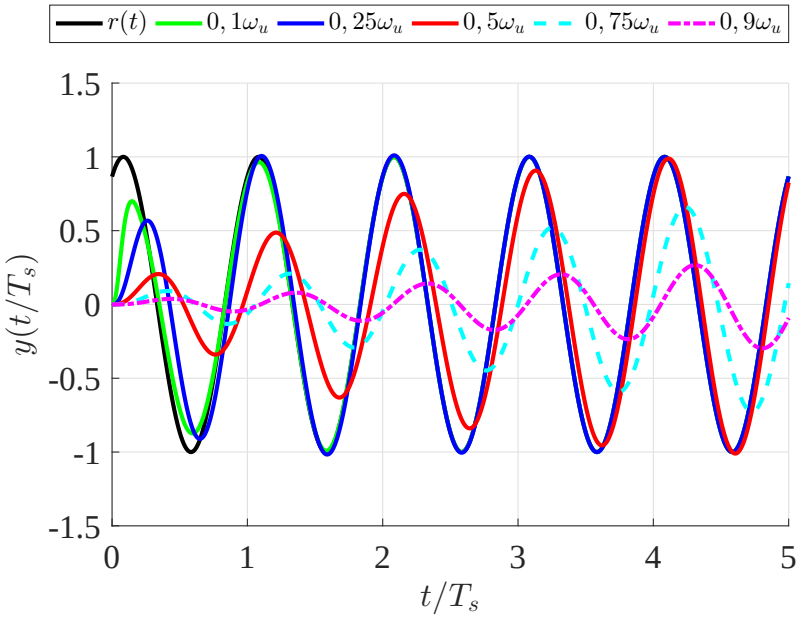

Source: created by the author.

Table 2 – Tuning parameters and performance indicators for the closed-loop system of $G_2(s)$ with $T = 0.1$ and different values of ω_r.

ω_r	k_p	k_{r_1}	n_s	$M_{O_\%}$	M_s	GM	PM	$\angle G(j\omega_r)$
$0.1\omega_u$	0.80	1.47	0.78	0.17%	1.27	$18.2dB$	59.5°	$-55°$
$0.25\omega_u$	0.78	0.77	3.51	0%	1.25	$19dB$	60.4°	$-91°$
$0.5\omega_u$	0.69	0.05	10.67	2.55%	1.39	$20dB$	49°	$-126°$
$0.75\omega_u$	0.49	0.07	> 50	31.91%	2.74	$19.8dB$	21.5°	$-155°$
$0.9\omega_u$	0.26	0.08	> 50	69.03%	7.95	$19.1dB$	7.17°	$-171°$

Figure 14 – Closed-loop normalized output signal for process $G_2(s)$ with $T = 0.1$.

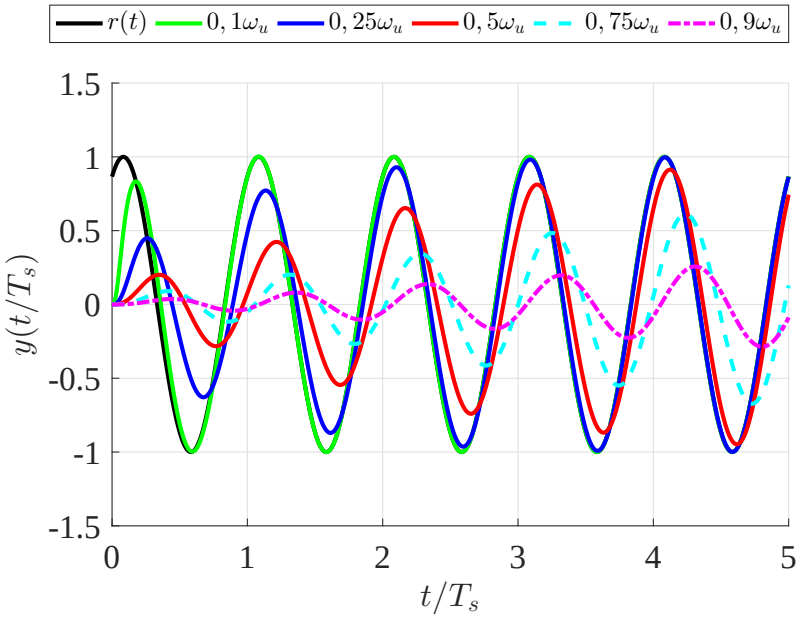

Source: created by the author.

Table 3 – Tuning parameters and performance indicators for the closed-loop system of $G_3(s)$ with $\alpha = 0.1$ and different values of ω_r.

ω_r	k_p	k_{r_1}	n_s	$M_{O_\%}$	M_s	GM	PM	$\angle G(j\omega_r)$
$0.1\omega_u$	5.45	0.91	1.34	10.99%	1.70	$19.2dB$	43.4°	$-92°$
$0.25\omega_u$	5.31	0.07	2.06	1.65%	1.69	$20dB$	40.3°	$-126°$
$0.5\omega_u$	4.70	0.14	16.77	31.17%	2.70	$19.9dB$	22°	$-154°$
$0.75\omega_u$	3.34	0.21	> 50	64.92%	6.65	$19.6dB$	8.66°	$-169°$
$0.9\omega_u$	1.75	0.25	> 50	88.42%	22.48	$18.2dB$	2.55°	$-176°$

Figure 15 – Closed-loop normalized output signal for process $G_3(s)$ with $\alpha = 0.1$.

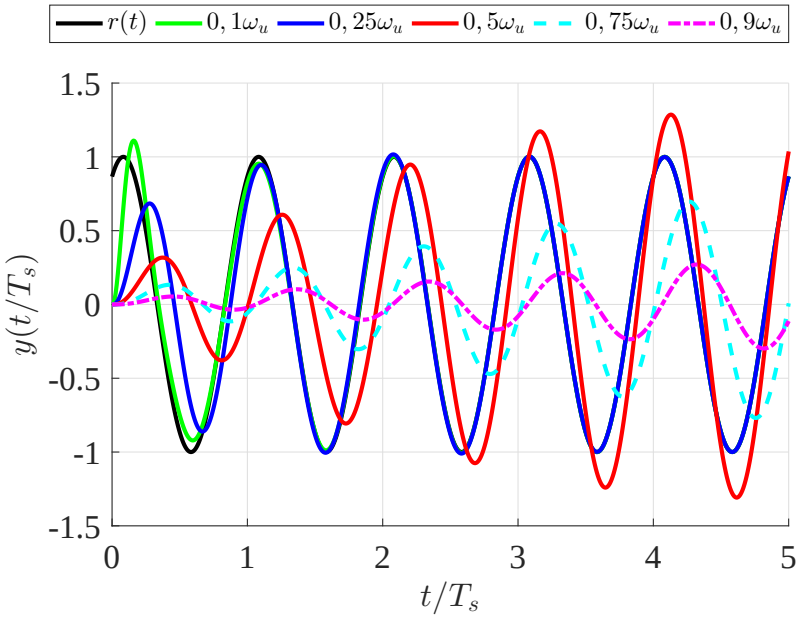

Source: created by the author.

Table 4 – Tuning parameters and performance indicators for the closed-loop system of $G_4(s)$ with $\alpha = 0.1$ and different values of ω_r.

ω_r	k_p	k_{r_1}	n_s	$M_{O_{\%}}$	M_s	GM	PM	$\angle G(j\omega_r)$
$0.1\omega_{-20dB}$	0.71	0.14	0.94	0%	1	∞	77.9°	$-45°$
$0.25\omega_{-20dB}$	1.35	0.22	1.40	0.39%	1	∞	69.6°	$-68.2°$
$0.5\omega_{-20dB}$	2.56	0.31	1.53	0.10%	1	∞	70.6°	$-78.7°$
$0.75\omega_{-20dB}$	3.79	0.40	1.92	0.04%	1	∞	70.8°	$-82.4°$
ω_{-20dB}	5	0.50	1.95	0.03%	1	∞	70.8°	$-84.3°$

Figure 16 – Closed-loop normalized output signal for process $G_4(s)$ with $\alpha = 0.1$.

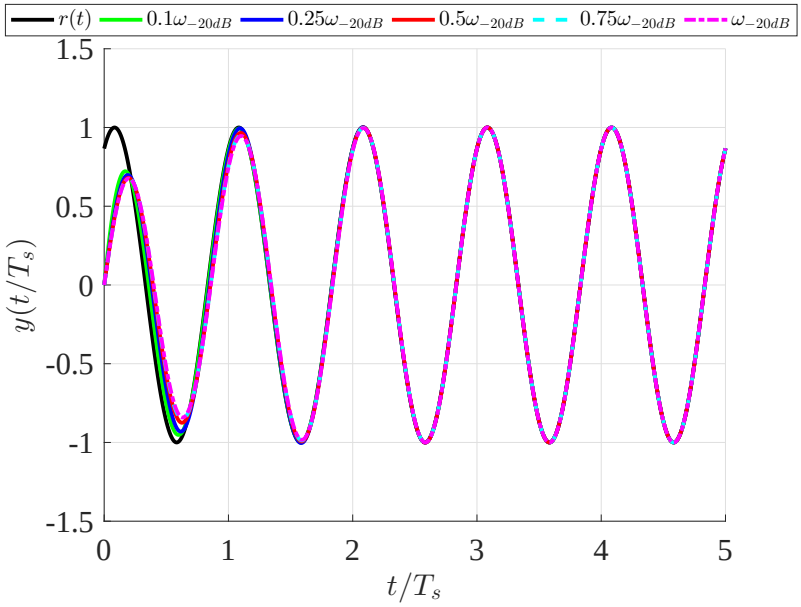

Source: created by the author.

Table 5 – Tuning parameters and performance indicators for the closed-loop system of $G_5(s)$ with $\alpha = 0.1$ and different values of ω_r.

ω_r	k_p	k_{r_1}	n_s	$M_{O_\%}$	M_s	GM	PM	$\angle G(j\omega_r)$
$0.1\omega_{-20dB}$	0.64	0.11	0.67	0%	1.09	∞	77.8°	$-42.4°$
$0.25\omega_{-20dB}$	1.11	0.14	1.42	0.14%	1.18	∞	60.6°	$-73.8°$
$0.5\omega_{-20dB}$	2.16	0.13	1.58	0%	1.30	∞	54.3°	$-96.8°$
$0.75\omega_{-20dB}$	3.42	0.10	1.57	0.01%	1.42	∞	48.4°	$-111°$
ω_{-20dB}	5	0.06	1.45	0.97%	1.54	∞	44°	$-121°$

Figure 17 – Closed-loop normalized output signal for process $G_5(s)$ with $\alpha = 0.1$.

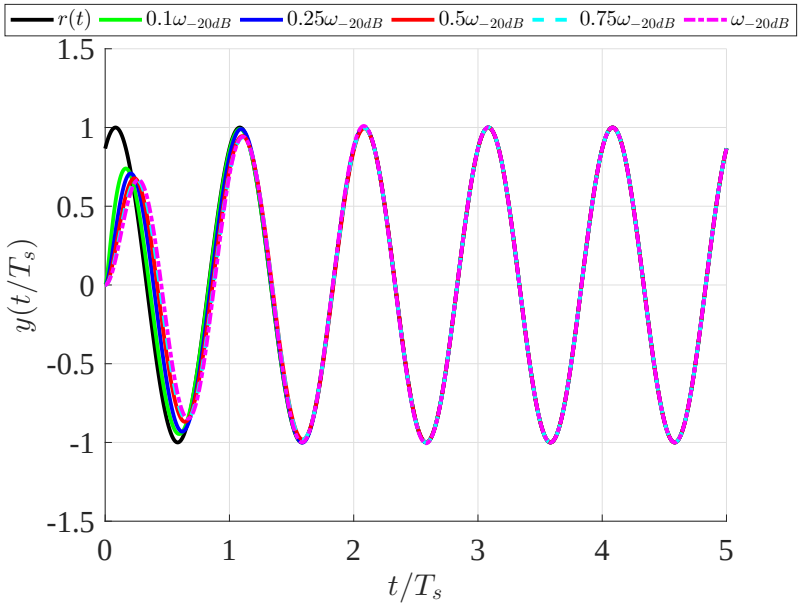

Source: created by the author.

Table 6 – Tuning parameters and performance indicators for the closed-loop system of $G_6(s)$ with $\alpha = 0.1$ and different values of ω_r.

ω_r	k_p	k_{r_1}	n_s	$M_{O_\%}$	M_s	GM	PM	$\angle G(j\omega_r)$
$0.1\omega_{-20dB}$	0.45	0.05	12.83	20.85%	3.98	∞	15.3°	$-4.25°$
$0.25\omega_{-20dB}$	0.18	0.12	10.83	19.97%	3.12	∞	20.4°	$-28°$
$0.5\omega_{-20dB}$	0.89	0.01	22.44	71.86%	8.76	∞	6.5°	$-169°$
$0.75\omega_{-20dB}$	2.62	0.02	36.65	90.79%	16.83	∞	3.4°	$-175°$
ω_{-20dB}	5	0.03	> 50	100.81%	25.25	∞	2.3°	$-176°$

Figure 18 – Closed-loop normalized output signal for process $G_6(s)$ with $\alpha = 0.1$.

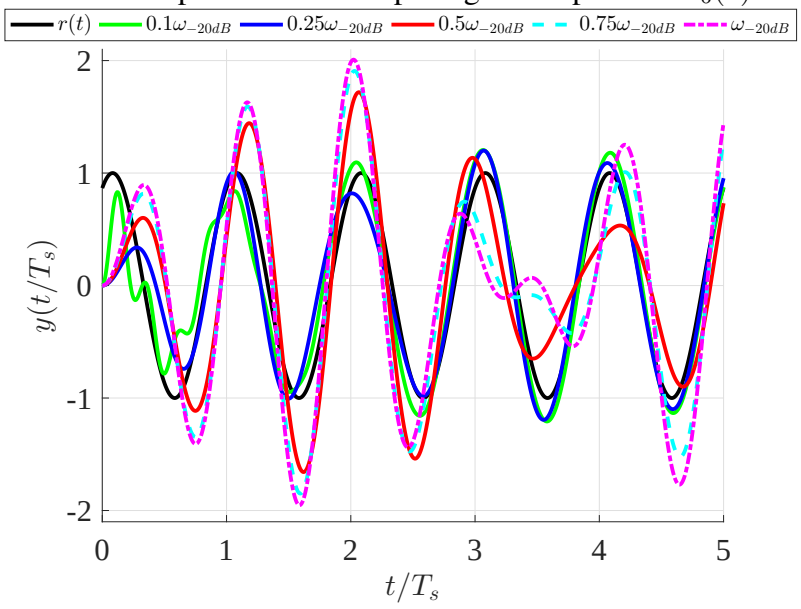

Source: created by the author.

the case for $G_6(s)$ with $\alpha = 0.1$ for instance. In such cases, from the knowledge of the frequency response of the plant and the phase contribution of the controller, the value of ϕ_{ω_r} was increased accordingly in order to avoid crossing -180° of phase.

From the obtained results, it can be noticed that, while the frequency ω_r is such that the phase response of the process at this frequency is higher than -130°, it is possible to choose k_{r_1} to limit the phase of $C_{PR}(j\omega_r)G(j\omega_r)$ to -130°. Thus, the resulting phase margin is higher than 30° and the peak value M_s falls in the desired interval. In such cases, small values for the maximum overshoot and settling time were achieved. In all cases, the adjusted gain margins were as required. On the other hand, as the frequency ω_r increases, the phase margin decreases and the performance of the system degrades considerably. Accordingly, even though it was possible to meet the requirements for the gain margin in all cases, the performance degraded in the cases for which the required phase margin was not achieved and the resulting peak value M_s was not in the desired interval.

3.5 Chapter Summary

This chapter has presented the method for the tuning of PR controllers based on the frequency response characteristics of the plant for processes with and without ultimate frequency. The performance of the method has been assessed for the classes of processes introduced in Chapter 2. The results have demonstrated that when it is possible to meet the requirements for gain and phase margins, the resulting peak value M_s falls in the desired interval and the overall performance is satisfactory. On the other hand, the performance degraded in the cases for which the required phase margin was not achieved and the resulting peak value M_s was not in the desired interval. In the next chapter, the combination of the PR controller with a phase-lead compensator is proposed to overcome these limitations. The results of this chapter have been published in (MOSSMANN; PEREIRA; GOMES DA SILVA JR, 2019).

4 PR+LEAD COMPENSATOR

4.1 Introduction

In the previous chapter, the results have demonstrated that when it is possible to meet the requirements for gain and phase margins, the resulting peak value M_s falls in the desired interval and the overall performance is satisfactory. However, as the frequency ω_r increases, the phase margin decreases and the performance of the system degrades considerably. In these cases, the required phase margin was not achieved and the resulting peak value M_s was not in the desired interval. In order to overcome the limitations of the proposed method to work with higher frequencies ω_r, it is possible to combine the PR controller with a phase-lead compensator.

4.2 Phase-lead Compensator

The phase-lead compensator adds positive phase to the system over a determined frequency range (ASTRÖM; MURRAY, 2010). This class of compensator is generically given by the following transfer function

$$C_{lead}(s) = \frac{s + \dfrac{p}{\alpha}}{s + p} \tag{41}$$

where $\alpha > 1$ and $p > 0$ are real constants to be determined.

The maximum phase contribution of the compensator is given by

$$\phi_m = \arcsin\left(\frac{\alpha - 1}{\alpha + 1}\right) \tag{42}$$

This maximum amount of phase is added at the centre frequency ω_m, which is calculated according to

$$\omega_m = \frac{p}{\sqrt{\alpha}} \tag{43}$$

The Bode plot of a phase-lead compensator designed to have maximum phase contribution $\phi_m = 55^\circ$ at centre frequency $\omega_m = 1.73 rad/s$ is shown in Figure 19. It can

be noticed that this compensator decreases the gain at lower frequencies while increases the phase of the system in a range of frequencies around ω_m. Moreover, one can notice that the compensator structure was selected such that $|C_{lead}(j\omega)| = 1$ for $\omega \to \infty$. As this type of compensator is a high pass filter, in practice, usually it should provide up to $60°$ of maximum phase contribution (MESSNER *et al.*, 2007).

Figure 19 – Bode plot of phase-lead compensator $C_{lead}(s)$ with maximum phase contribution $\phi_m = 55°$ at frequency $\omega_m = 1.73 rad/s$.

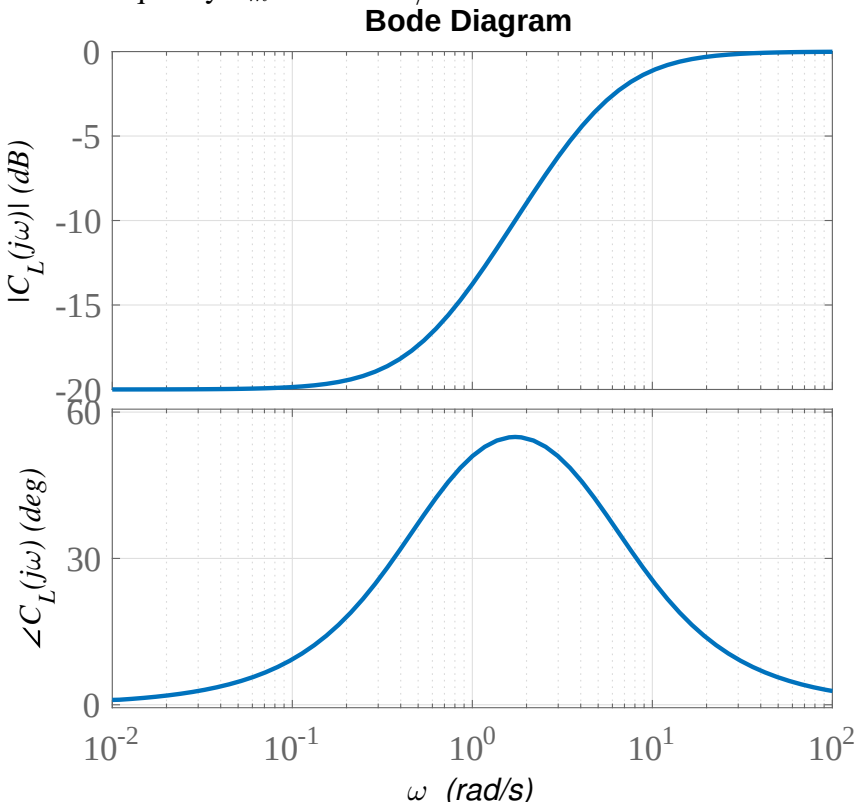

Source: created by the author.

Taking advantage of the features of phase-lead compensator, it may be convenient to tune such compensator for maximum contribution at the ultimate frequency of the process ω_u. As stated in Chapter 3, the proposed method for the tuning of PR controller leads to satisfactory results for frequencies of interest ω_r such that $C_{PR}(j\omega_r)G(j\omega_r)$ has its phase higher than $-130°$. Thus, to achieve suitable results for frequencies ω_r closer to the ultimate frequency ω_u, it is reasonable to consider a lead compensator designed to add approximately $55°$ of phase at frequency ω_u.

From (42), the corresponding value of α to get a maximum contribution $\phi_m \approx 55°$ is $\alpha = 10$. Then, it follows from (43) that the value of p to make $\omega_m = \omega_u$ is calculated by

$$p = \sqrt{\alpha}\,\omega_u = \sqrt{10}\,\omega_u \tag{44}$$

4.3 Tuning of PR+Lead Compensator

4.3.1 Plants with Ultimate Frequency

The method proposed in Chapter 3 for the PR controller must have its parameters updated to work with the pre-compensated plant $C_{lead}(s)G(s)$. Let ω_{uc} be the ultimate frequency of the compensated plant (*i.e.* the frequency such that $\angle C_{lead}(j\omega)G(j\omega) = -180°$), and let $M_{uc} = |C_{lead}(j\omega_{uc})G(j\omega_{uc})|$ be the gain of the pre-compensated plant at this frequency. Thus, following the reasoning made in Section 3.3, the value of k_p is revised to

$$k_{p_c} = \frac{1}{10}\frac{\omega_{uc}^2 - \omega_r^2}{M_{uc}(2\omega_{uc}^2 - \omega_r^2)} \tag{45}$$

As stated in Section 3.3.1, for frequencies higher than ω_r the phase introduced by the PR controller is larger than ϕ_{ω_r}. The parameter k_{r_1} has the same formulation from (39), whereas the value of ϕ_{ω_r} must now consider the phase of the pre-compensated system, so that $\angle C_{PR}(j\omega_r)C_{lead}(j\omega_r)G(j\omega_r) \approx -130°$.

Figure 20 illustrates the association of the PR controller with a phase-lead compensator by comparing the Bode plot of $C(s)G_3(s)$ for $\omega_r = 0.5\omega_u$ with and without the pre-compensation. One can notice that the gain margin is nearly unaffected, whereas the phase margin is considerably increased with the phase-lead compensator.

The method for tuning the PR+lead compensator for processes with ultimate frequency proposed in this work can therefore be summarised as follows:

Algorithm:

Step 1. Design the phase-lead compensator with $\alpha = 10$ and p given by (44).

Step 2. Determine k_{p_c} from (45).

Step 3. From the frequency response of the pre-compensated system, determine the phase contribution that the controller can introduce at frequency ω_r with $\phi_{\omega_r} \approx -130° - \angle C_{lead}(j\omega_r)G(j\omega_r)$, $\phi_{\omega_r} \geq -70.52°$, such that the phase of $C_{PR}(j\omega_r)C_{lead}(j\omega_r)G(j\omega_r)$ at this frequency is approximately $-130°$.

Step 4. Determine k_{r_1} from (39) using the value for ϕ_{ω_r} obtained in the previous step.

In order to evaluate the effectiveness of the tuning method, it is tested for different classes of typical processes with ultimate frequency in Section 4.4.

4.3.2 Plants without Ultimate Frequency

For plants without ultimate frequency, a phase-lead compensator can be used to increase the phase of processes of relative degree 2 at higher frequencies, such that it is possible

Figure 20 – Bode plot of $C_{PR}(s)G_3(s)$ and $C_{PR+lead}(s)G_3(s)$ with $\phi_m = 55°$ at frequency ω_u for $\omega_r = 0.5\omega_u$.

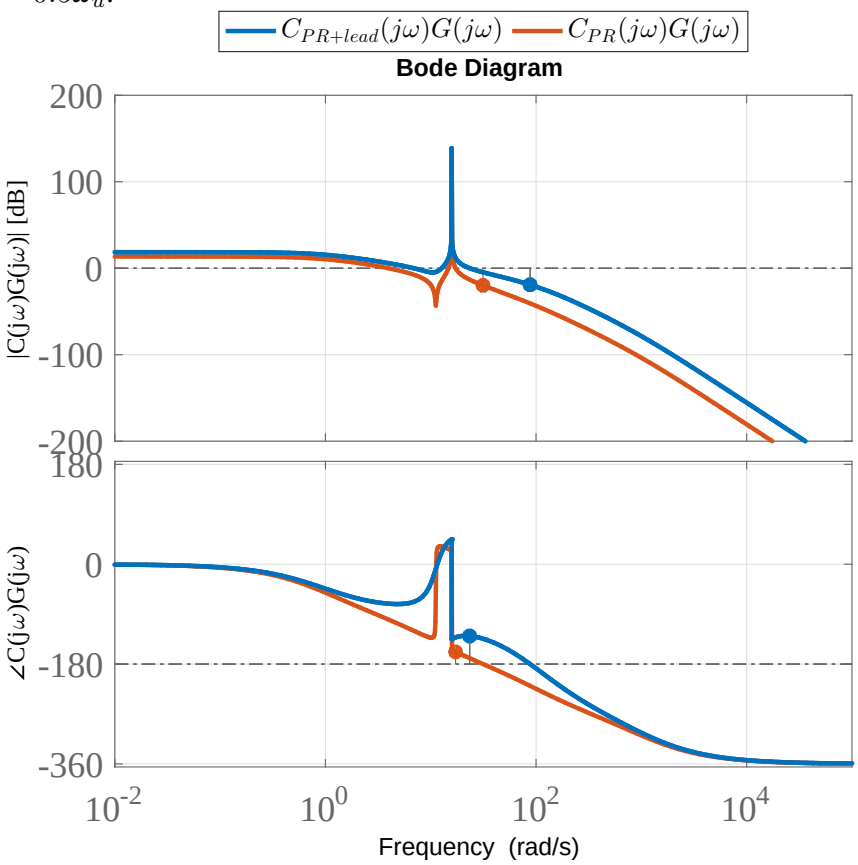

Source: created by the author.

to obtain $\angle C_{PR}(j\omega_r)C_{lead}(j\omega_r)G(j\omega_r) \approx -130°$. In the simulations of the following section, a phase-lead compensator was designed to have its maximum contribution at frequency $\omega_m = \omega_{-20dB}$ of processes $G_5(s)$ and $G_6(s)$, *i.e.* at the frequency for which the gain of the process is $\frac{1}{10}$. Processes with relative degree 1, such as those of class $G_4(s)$ for example, have phase higher than $-90°$ and therefore the combination with a phase-lead compensator is not considered for this type of process.

The value of k_p has the same formulation from (40), whereas the value of M_r must now consider the gain of the pre-compensated system $C_{lead}(j\omega_r)G(j\omega_r)$ at frequency ω_r.

As stated in section 3.3.2, for frequencies higher than ω_r the phase introduced by the PR controller is larger than ϕ_{ω_r}. The parameter k_{r_1} has the same formulation from (39), whereas the value of ϕ_{ω_r} must now consider the phase of the pre-compensated system, so that $\angle C_{PR}(j\omega_r)C_{lead}(j\omega_r)G(j\omega_r) \approx -130°$.

The method for tuning the PR+lead compensator for processes without ultimate frequency proposed in this work can therefore be summarised as follows:

Algorithm:

Step 1. Design the phase-lead compensator with $\alpha = 10$ and $p = \sqrt{\alpha}\,\omega_{-20dB}$.

Step 2. Determine k_p from (40).

Step 3. From the frequency response of the pre-compensated system, determine the phase contribution that the controller can introduce at frequency ω_r with $\phi_{\omega_r} \approx -130^\circ - \angle C_{lead}(j\omega_r)G(j\omega_r)$, $\phi_{\omega_r} \geq -70.52^\circ$, such that the phase of $C_{PR}(j\omega_r)C_{lead}(j\omega_r)G(j\omega_r)$ at this frequency is approximately -130°.

Step 4. Determine k_{r_1} from (39) using the value for ϕ_{ω_r} obtained in the previous step.

In order to evaluate the effectiveness of the tuning method, it is tested for different classes of typical processes without ultimate frequency in the next section.

4.4 Simulation Results for PR+Lead Compensator

To allow a comparison between the controllers proposed in this work for tracking sinusoidal reference signals, the PR+Lead compensator controller is tested using the same plants and criteria defined in the simulations for the PR controller in section 3.4. Also, analogous tables and plots are presented to demonstrate the simulation results.

Tables 7 to 9 summarise the results achieved for different ratios between ω_r and ω_u for processes $G_1(s)$, $G_2(s)$ and $G_3(s)$. Tables 10 to 11 summarise the results achieved for different ratios between ω_r and ω_{-20dB} for processes $G_5(s)$ and $G_6(s)$. For additional simulation results see Appendix A.2. These tables present the obtained values for settling time n_s, maximum percent overshoot $M_{O_\%}$, peak of sensitivity function M_s, phase margin PM and gain margin GM of the final controlled system, as well as the original phase margin of process $G(j\omega)$ at the frequency of interest. Figures 21 to 25 show the output signal normalized in relation to the period of reference signal $r(t)$ for the different values of ω_r. All simulation tests produced a stable response.

Table 7 – Tuning parameters and performance indicators for the closed-loop system of $G_1(s)$ with $n = 3$ and different values of ω_r for PR+lead compensator.

ω_r	k_p	k_{r_1}	n_s	$M_{O_\%}$	M_s	GM	PM	$\angle G(j\omega_r)$
$0.5\omega_u$	5.34	0.43	1.66	0%	1.47	$17.7dB$	54.8°	-123°
$0.75\omega_u$	5.16	0.17	3.02	0%	1.43	$19.1dB$	52.9°	-157°
$0.9\omega_u$	5.00	0.07	4.37	1.01%	1.45	$19.7dB$	49.3°	-172°
ω_u	4.88	0.08	6.59	4.62%	1.56	$19.6dB$	43.1°	-180°

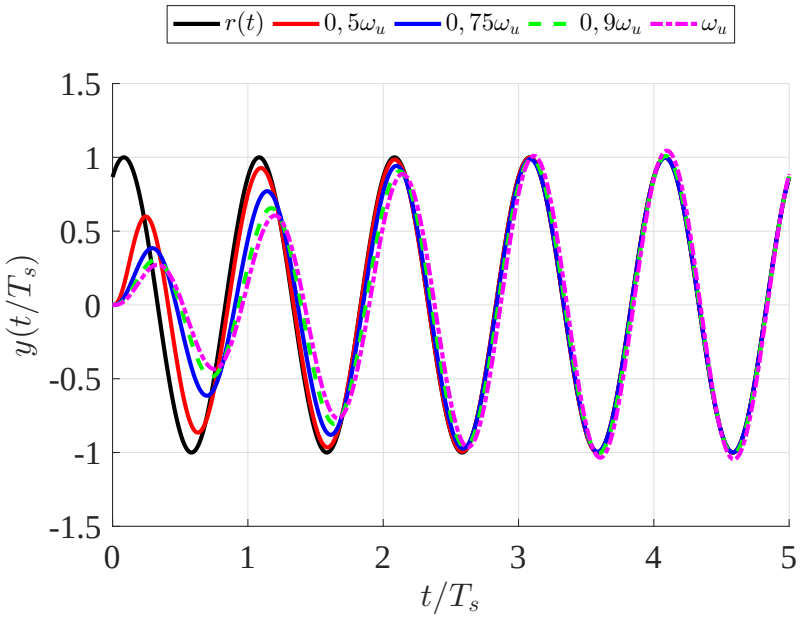

Figure 21 – Closed-loop normalized output signal for process $G_1(s)$ with $n = 3$, for PR+lead compensator.

Table 8 – Tuning parameters and performance indicators for the closed-loop system of $G_2(s)$ with $T = 0.1$ and different values of ω_r for PR+lead compensator.

ω_r	k_p	k_{r_1}	n_s	$M_{O_\%}$	M_s	GM	PM	$\angle G(j\omega_r)$
$0.5\omega_u$	9.34	2.68	2.56	0%	1.40	$17.5dB$	59.5°	$-126°$
$0.75\omega_u$	8.94	2.34	4.22	2.58%	1.55	$17.6dB$	44.4°	$-156°$
$0.9\omega_u$	8.60	1.29	6.18	4.46%	1.58	$18.6dB$	42.7°	$-171°$
ω_u	8.32	0.47	8.07	4.98%	1.57	$19.5dB$	42.9°	$-180°$

Figure 22 – Closed-loop normalized output signal for process $G_2(s)$ with $T = 0.1$, for PR+lead compensator.

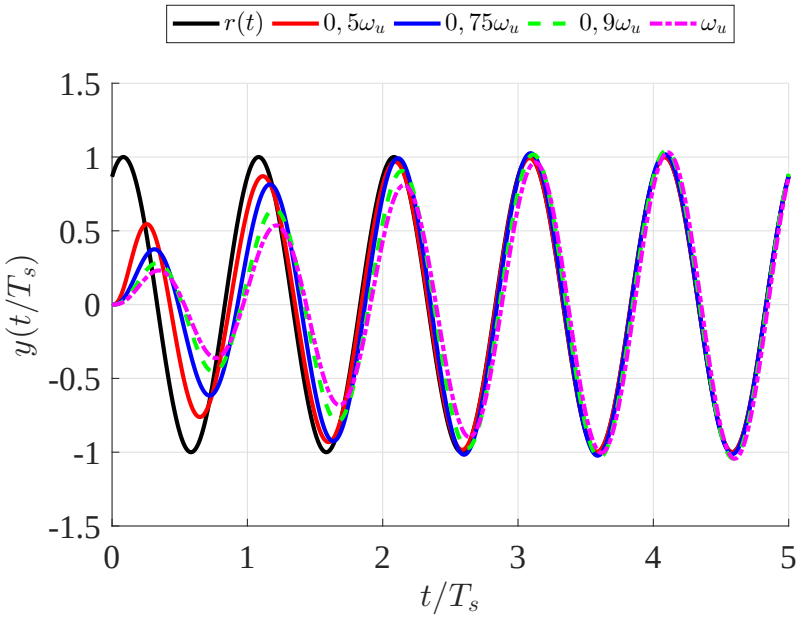

Source: created by the author.

Table 9 – Tuning parameters and performance indicators for the closed-loop system of $G_3(s)$ with $\alpha = 0.1$ and different values of ω_r for PR+lead compensator.

ω_r	k_p	k_{r_1}	n_s	$M_{O_\%}$	M_s	GM	PM	$\angle G(j\omega_r)$
$0.5\omega_u$	84.62	4.56	1.54	0%	1.38	$19.1dB$	50.6°	$-154°$
$0.75\omega_u$	82.96	3.18	2.91	0.83%	1.42	$19.4dB$	48.3°	$-169°$
$0.9\omega_u$	81.60	1.24	3.88	0.87%	1.40	$19.7dB$	49.4°	$-176°$
ω_u	80.54	1.38	4.80	2.50%	1.46	$19.7dB$	46°	$-180°$

Table 10 – Tuning parameters and performance indicators for the closed-loop system of $G_5(s)$ with $\alpha = 0.9$ and different values of ω_r for PR+lead compensator.

ω_r	k_p	k_{r_1}	n_s	$M_{O_\%}$	M_s	GM	PM	$\angle G(j\omega_r)$
$0.5\omega_{-20dB}$	8.79	1.59	0.95	0.88%	1.18	∞	59°	$-112°$
$0.75\omega_{-20dB}$	12.13	1.32	1.49	0.03%	1.20	∞	60°	$-132°$
ω_{-20dB}	15.81	1.23	1.56	0%	1.25	∞	57.5°	$-143°$

Figure 23 – Closed-loop normalized output signal for process $G_3(s)$ with $\alpha = 0.1$, for PR+lead compensator.

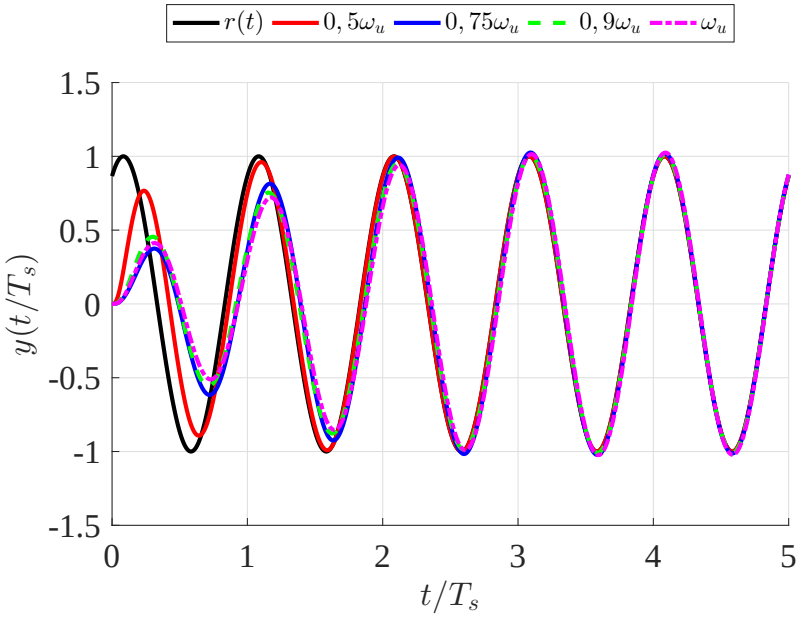

Source: created by the author.

Figure 24 – Closed-loop normalized output signal for process $G_5(s)$ with $\alpha = 0.9$, for PR+lead compensator.

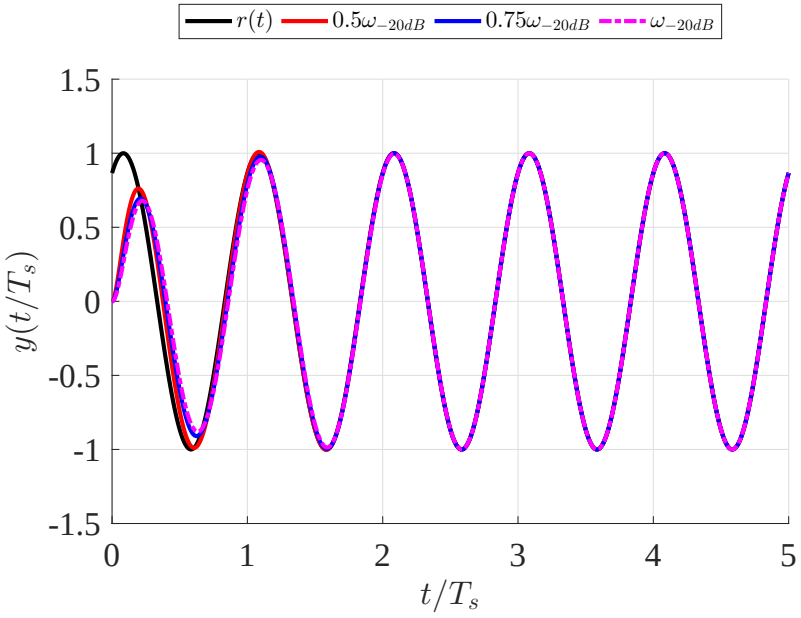

Source: created by the author.

Table 11 – Tuning parameters and performance indicators for the closed-loop system of $G_6(s)$ with $\alpha = 0.1$ and different values of ω_r for PR+lead compensator.

ω_r	k_p	k_{r_1}	n_s	$M_{O_\%}$	M_s	GM	PM	$\angle G(j\omega_r)$
$0.1\omega_{-20dB}$	4.26	0.46	1.53	1.36%	1.41	∞	43.5°	$-4.25°$
$0.25\omega_{-20dB}$	1.35	0.72	4.40	10.83%	2.01	∞	30°	$-28°$
$0.5\omega_{-20dB}$	4.83	0.13	3.28	3.64%	1.21	∞	54.3°	$-169°$
$0.75\omega_{-20dB}$	10.45	0.20	2.91	3.52%	1.24	∞	54.1°	$-175°$
ω_{-20dB}	15.81	0.26	2.38	2.86%	1.31	∞	51.7°	$-176°$

Figure 25 – Closed-loop normalized output signal for process $G_6(s)$ with $\alpha = 0.1$, for PR+lead compensator.

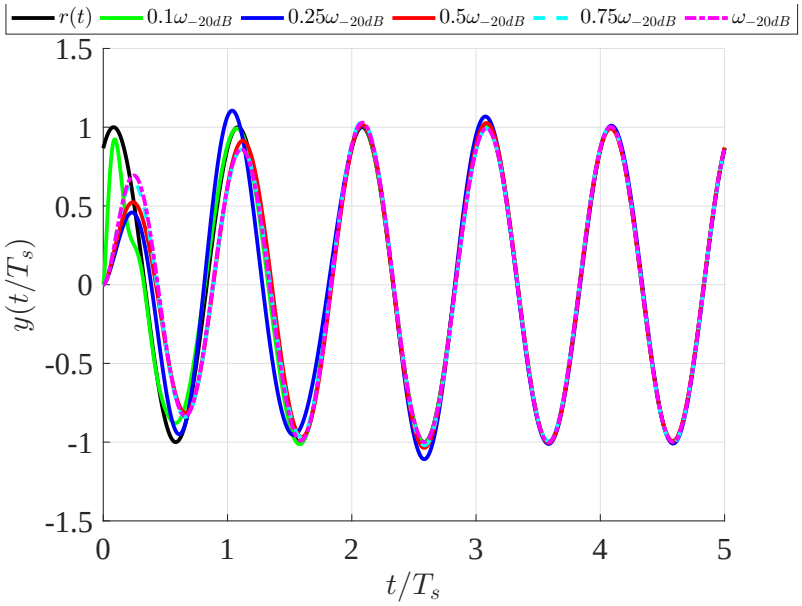

Source: created by the author.

The parameters k_{p_c} and k_{r_1} were computed by the procedure described in the previous section. Comparing the obtained results with those presented in section 3.4, one can notice that the introduction of the phase-lead compensator considerably improved the performance of the system for higher frequencies. For the range of frequencies tested, the resulting phase margins are higher than 30° and the peak value M_s falls in the desired interval. Hence, suitable values for the maximum overshoot and settling time were achieved.

4.5 Disturbance Rejection Analysis

In order to evaluate the performance of the proposed method for the closed-loop system shown in the block diagram of Figure 1 subject to a disturbance composed by the fundamental frequency ω_r and its harmonic frequencies, this section explores the effects of this type of disturbance in terms of the percent of Total Harmonic Distortion ($THD_\%$) (IEEE, 1992) observed in the output of the system. Let $d(t)$ represent a disturbance signal with half of the amplitude A of reference signal $r(t)$ and composed by frequency ω_r and its odd-multiples up to the 11^{th} component, given by

$$d(t) = \frac{A}{2}\left(0.3337\cos\left(\omega_r t\right) + 0.287\cos\left(3\omega_r t\right) + 0.2076\cos\left(5\omega_r t\right) + \right.$$
$$\left. +0.1181\cos(7\omega_r t) + 0.0414\cos(9\omega_r t) + 0.0122\cos(11\omega_r t)\right) \quad (46)$$

This signal is constructed to emulate, for instance, the type of distortion caused by typical nonlinear devices connected to power systems, such as the switched mode power supplies commonly used in many electronic devices, for which the input circuit is a single-phase bridge rectifier with a capacitive filter (RODRÍGUEZ *et al.*, 2005). Figure 26 presents the normalized reference and disturbance signals.

Tables 12, 13 and 14 summarise the results achieved for different ratios between ω_r and ω_u. These tables present the obtained values for settling time n_s, maximum percent overshoot $M_{O_\%}$ and percent of total harmonic distortion $THD_\%$ of the final controlled system with PR controller and PR+Lead compensator. Values for the peak of sensitivity function M_s, phase margin PM and gain margin GM of the final controlled system, and the original phase margin of process $G(j\omega)$ at the frequency of interest are the same of those in the previous sections for the corresponding design method and frequency ratio, thus were omitted.

Comparing the obtained results with those presented in the Sections 3.4 and 4.4, one can notice that the values for settling time n_s and maximum percent overshoot $M_{O\%}$ with higher frequencies ω_r are similar for the corresponding design method and frequency ratio, in spite of the presence of a disturbance. Note that, although the controller was not designed to reject components of higher frequency, the system acts as a low-pass filter, significantly reducing the distortion caused by higher harmonic frequencies. For frequencies ω_r given by lower ratios of ω_u, this characteristic was less evident and the

Table 12 – Performance indicators for the closed-loop system of $G_1(s)$ with $n = 3$ and different values of ω_r subject to disturbance $d(t)$

	PR			PR+Lead		
ω_r	n_s	$M_{O_\%}$	$THD_\%$	n_s	$M_{O_\%}$	$THD_\%$
$0.1\omega_u$	–	16.33%	11.68%	–	8.59%	6.55%
$0.25\omega_u$	–	6.89%	4.14%	–	4.65%	3.85%
$0.5\omega_u$	8.72	3.69%	0.70%	2.08	0.00%	0.87%
$0.75\omega_u$	> 50	36.90%	0.23%	3.05	0.00%	0.25%
$0.9\omega_u$	> 50	73.52%	0.13%	4.36	0.94%	0.14%
ω_u				6.22	4.66%	0.10%

Table 13 – Performance indicators for the closed-loop system of $G_2(s)$ with $T = 0.1$ and different values of ω_r subject to disturbance $d(t)$

	PR			PR+Lead		
ω_r	n_s	$M_{O_\%}$	$THD_\%$	n_s	$M_{O_\%}$	$THD_\%$
$0.1\omega_u$	–	8.66%	5.77%	–	4.29%	3.50%
$0.25\omega_u$	–	1.44%	1.84%	–	2.03%	1.78%
$0.5\omega_u$	10.72	2.56%	0.34%	2.57	0.00%	0.41%
$0.75\omega_u$	> 50	32.13%	0.10%	4.24	2.61%	0.11%
$0.9\omega_u$	> 50	69.19%	0.06%	6.18	4.51%	0.06%
ω_u				7.69	5.02%	0.05%

Figure 26 – Normalized signals $r(t)$ and $d(t)$.

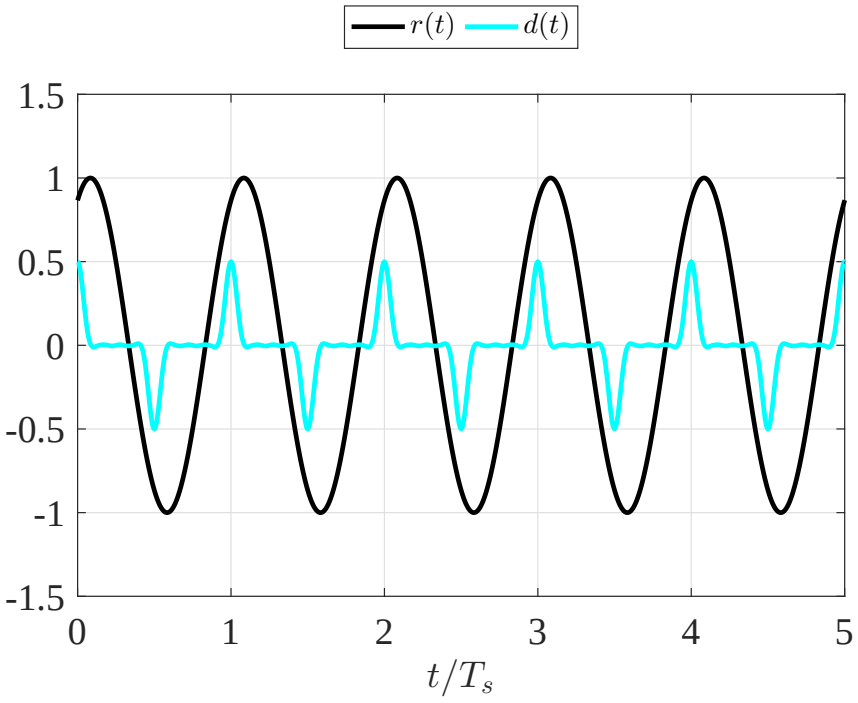

Source: created by the author.

Figure 27 – Comparison of normalized output signals of process $G_1(s)$ with $n = 3$ subject to disturbance $d(t)$ for $\omega_r = 0.1\omega_u$ using PR and PR+lead controllers.

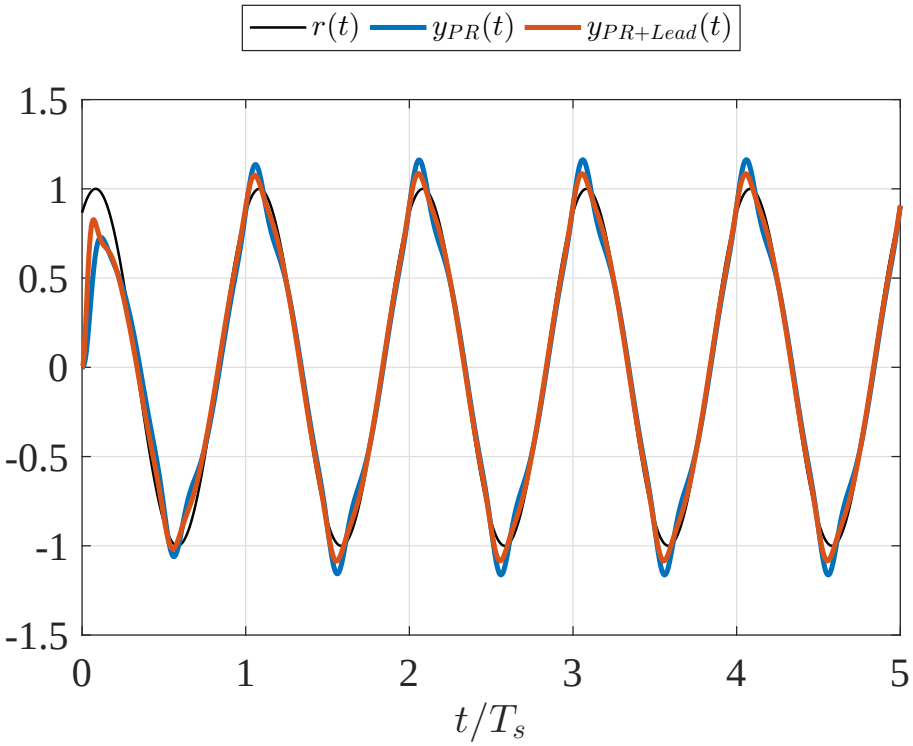

Source: created by the author.

distortion caused by the disturbance has restrained the output error from settling below the tolerance value $\epsilon < 2\%$. These cases are represented by "$-$" in the corresponding cells for

Figure 28 – Comparison of normalized output signals of process $G_2(s)$ with $T = 0.1$ subject to disturbance $d(t)$ for $\omega_r = 0.1\omega_u$ using PR and PR+lead controllers.

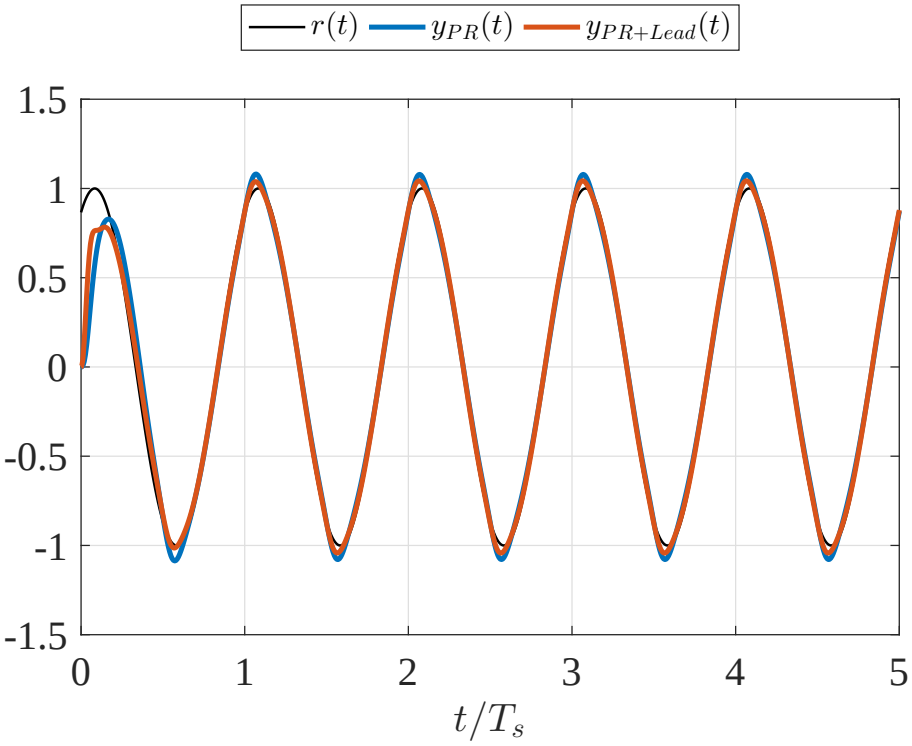

Source: created by the author.

Table 14 – Performance indicators for the closed-loop system of $G_3(s)$ with $\alpha = 0.1$ and different values of ω_r subject to disturbance $d(t)$

	PR			PR+Lead		
ω_r	n_s	$M_{O_\%}$	$THD_\%$	n_s	$M_{O_\%}$	$THD_\%$
$0.1\omega_u$	–	11.68%	1.72%	0.52	2.37%	0.66%
$0.25\omega_u$	2.06	1.67%	0.28%	1.24	0.39%	0.28%
$0.5\omega_u$	17.19	31.39%	0.06%	1.54	0.00%	0.08%
$0.75\omega_u$	> 50	65.17%	0.02%	2.91	0.82%	0.03%
$0.9\omega_u$	> 50	88.42%	0.02%	3.88	0.86%	0.02%
ω_u				4.80	2.50%	0.01%

the settling time n_s. The design method for the PR+Lead compensator resulted in better performance indices in comparison with the PR controller responses. Figures 27, 28 and 29 present the output of each system for frequency ratio $\omega_r = 0.1\omega_u$ to illustrate the effect of higher levels of THD in the output waveform.

Figure 29 – Comparison of normalized output signals of process $G_3(s)$ with $\alpha = 0.1$ subject to disturbance $d(t)$ for $\omega_r = 0.1\omega_u$ using PR and PR+lead controllers.

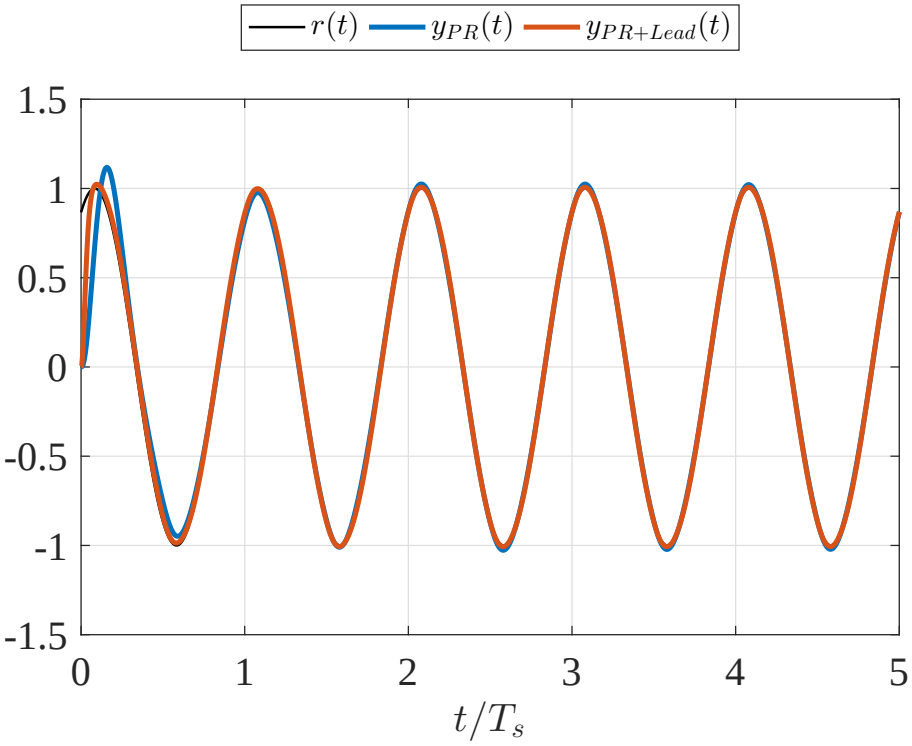

Source: created by the author.

4.6 Chapter Summary

This chapter has considered the combination of the PR controller with a phase-lead compensator in order to allow better performance in an augmented bandwidth. The method has been revised to deal with this new structure for processes with and without ultimate frequency. The performance of the proposed method has been assessed for the classes of processes introduced in Chapter 2. The overall performance of the system for higher frequencies has greatly improved when compared with the results obtained in Chapter 3.

Finally, this chapter has analysed the performance of the proposed method for the PR controller and the PR+Lead compensator with respect to harmonic disturbance rejection. The results for each method have been compared and some concluding remarks based on these results end the chapter. Despite the improvement of performance presented by the PR+Lead compensator, in many cases the harmonic content of the disturbance has restrained the output error from settling below its tolerance value. In the next chapter, the controller topology is extended to multiple peaks of resonance, in order to obtain reference tracking and disturbance rejection of a wider range of periodic signals. The results of this chapter have been published in (MOSSMANN; PEREIRA; GOMES DA SILVA JR, 2021).

5 PMR CONTROLLER

5.1 Introduction

In this chapter, the PR controller is extended to multiple peaks of resonance, in order to obtain reference tracking and disturbance rejection of a wider range of periodic signals. For signals with higher harmonic composition, a controller with multiple modes of resonance can achieve better performance in reference tracking and disturbance rejection. The resulting controller is a Proportional Multi-Resonant controller (PMR) (ABU-RUB; MALINOWSKI; AL-HADDAD, 2014).

5.2 The Proportional Multi-Resonant Structure

Recall the resonant part of the controller given by (30) in Chapter 3. It can be expressed for each harmonic m as follows

$$C_{R_m}(s) = \frac{s^2 + 2k_{r_{1m}}s + k_{r_{2m}}}{s^2 + (m\omega_r)^2} \ , \ m = 1, 2, 3, 4, ..., N \tag{47}$$

The PR controller can be extended for multiple modes of resonance by inserting the corresponding resonant part of each frequency mode in the loop transfer function. This extension can be arranged in series or in parallel connection. For the series connection, the PMR controller can be expressed as follows

$$C_{PMR_s}(s) = k_{pmr}\left(1 + C_{R_1}\right)\ C_{R_2}\ ...\ C_{R_N} \tag{48}$$

For the parallel connection, the PMR controller can be expressed as follows

$$C_{PMR_p}(s) = k_{pmr}\left(1 + C_{R_1} + C_{R_2} + ... + C_{R_N}\right) \tag{49}$$

Figure 30 presents the Bode plot for series and parallel topologies of $C_{PMR}(j\omega)$ with $k_{pmr} = 1$, $\omega_r = 1\ rad/s$, $\phi_{\omega_{r1}} = -30°$, $\phi_{\omega_{rm}} = -5°$ and odd harmonic frequency modes up to $N = 11$. Notice the peaks of resonance at each frequency mode $m\omega_r$ and the phase contribution of the PMR controller. Starting from the knowledge and assumptions

Figure 30 – Bode plot of series and parallel topologies of PMR controller $C_{PMR}(j\omega)$ with $k_{pmr} = 1$, $\omega_r = 1\ rad/s$, $\phi_{\omega_{r1}} = -30°$, $\phi_{\omega_{rm}} = -5°$ and odd harmonic frequency modes up to $N = 11$.

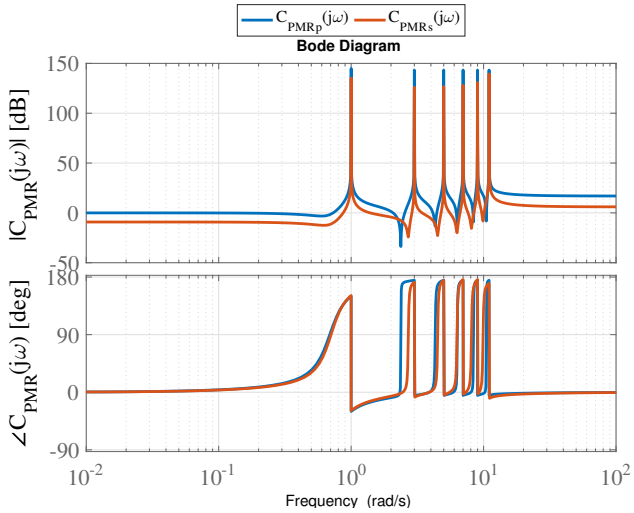

Source: created by the author.

developed in previous chapters, a systematic method for the tuning and application of the PMR controller is proposed in this chapter.

Following the reasoning presented in Chapter 4, a phase-lead compensator can be used to increase the system bandwidth and/or to improve the phase margin of the system. Figure 31 illustrates the resulting controller with series structure. Figure 32 illustrates the resulting controller with parallel structure.

Figure 31 – Block diagram of the series topology of the PMR controller.

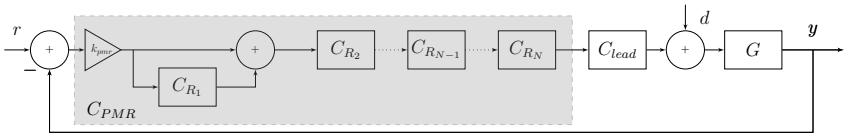

Source: created by the author.

Figure 32 – Block diagram of the parallel topology of the PMR controller.

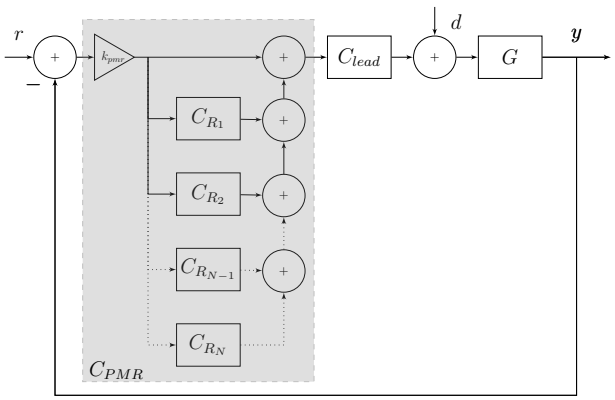

Source: created by the author.

In the next sections, based on an extension of the reasoning performed in Chapters 3 and 4, a systematic procedure for the computation of the parameters of each topology of the PMR controller is proposed.

5.3 Tuning of PMR Controller

Consider that the PMR controller not necessarily has to deal with all frequency modes from the fundamental frequency ω_r up to $N\omega_r$. Hence, let $\mathcal{H} = \{1,\ \dots\ , N\}$ be a set of integers whose elements represent the frequency modes present in the PMR controller. Let N_o be the total number of elements in $\mathcal{H}$ and N be the highest element in the set. For example, the set $\mathcal{H} = \{1, 3, 7, 11\}$ has $N = 11$ and $N_o = 4$.

5.3.1 Series Topology

In this section, the procedure for the computation of parameters for the series topology of the PMR controller is proposed. In the series topology, the resulting controller is the product of each harmonic frequency mode transfer function. Thus, considering the resonant mode of each harmonic $m \geq 2$ given by (47), the magnitude contribution of each mode is given by

$$|C_{R_m}(j\omega)| = \frac{\sqrt{k_{r_{2m}}^2 + 2(2k_{r_{1m}}^2 - k_{r_{2m}})\omega^2 + \omega^4}}{|(m\omega_r)^2 - \omega^2|}\ ,\ m \geq 2,\ m \in \mathcal{H} \tag{50}$$

Notice that for $\omega = 0$ the gain contribution of each mode is $\frac{k_{r_{2m}}}{(m\omega_r)^2}$, for $\omega = m\omega_r$ the gain tends to infinity and for $\omega \gg \omega_r$ the gain tends to 1.

Moreover, the phase contribution of each mode in a frequency $\omega > m\omega_r$ is given by

$$\angle C_{R_m}(j\omega) = \arctan\left(\frac{2k_{r_{1m}}\omega}{k_{r_{2m}} - \omega^2}\right)\ ,\ m \geq 2,\ m \in \mathcal{H} \tag{51}$$

In order to adjust the gain contribution of each mode, let $k_{r_{2m}}$ be given by

$$k_{r_{2m}} = \beta(m\omega_r)^2\ ,\ m \geq 2,\ m \in \mathcal{H}\ \text{ and }\ 0 < \beta < 1 \tag{52}$$

Thus, from (50) with $\omega = 0$, $|C_{R_m}(0)| = \beta$.

Let $\phi_{\omega_{rm}}$ be the contribution of phase at frequency $\omega \rightarrow m\omega_r^+$ required for the corresponding mode. Assigning $\omega = m\omega_r$ and $k_{r_{2m}} = \beta(m\omega_r)^2$ in (51) to obtain $\angle C_{R_m}(jm\omega_r) = \phi_{\omega_{rm}}$ and isolating the parameter $k_{r_{1m}}$ leads to the following expression

$$k_{r_{1m}} = -\frac{m\omega_r(1-\beta)}{2}\tan(\phi_{\omega_{rm}})\ ,\ m \geq 2,\ m \in \mathcal{H} \tag{53}$$

From (47), for each frequency mode the corresponding zeros are given by

$$\begin{aligned} z_{1_{C_{R_m}}} &= -k_{r_{1m}} + \sqrt{k_{r_{1m}}^2 - k_{r_{2m}}} \ , \\ z_{2_{C_{R_m}}} &= -k_{r_{1m}} - \sqrt{k_{r_{1m}}^2 - k_{r_{2m}}} \end{aligned} \tag{54}$$

If $k_{r_{1m}}^2 < k_{r_{2m}}$, *i.e.* $k_{r_{1m}} < \sqrt{k_{r_{2m}}}$, the zeros are complex-conjugate and their corresponding natural frequency $\omega_{0_{C_{R_m}}}$ is equal to their module. From (47) and considering $k_{r_{2m}} = \beta(m\omega_r)^2$ and $k_{r_{1m}}$ as defined in (53), this frequency is given by

$$\omega_{0_{C_{R_m}}} = \sqrt{k_{r_{2m}}} = m\omega_r\sqrt{\beta} \ , \ m \geq 2, \ m \in \mathcal{H} \tag{55}$$

To ensure that the zeros of the controller are placed in the left half complex plane, it is sufficient to have $k_{r_{1m}} > 0$ and $k_{r_{2m}} \geq 0$. Let γ represent the ratio between the natural frequency of the zeros given by (54) and frequency mode $m\omega_r$. Thus,

$$\gamma = \frac{\omega_{0_{C_{R_m}}}}{m\omega_r} = \sqrt{\beta} \tag{56}$$

Therefore, the parameter β determines the gain contribution of each frequency mode at lower frequencies and the ratio determined by γ. Thus, there is a compromise between the gain at lower frequencies and the natural frequency of the zeros. Considering $0 < \beta < 1$, if β is close to 1 the natural frequency of the zeros $\omega_{0_{C_{R_m}}}$ is located almost at the same frequency of its corresponding poles $m\omega_r$ and the resonant effect deteriorates. Also, if β is closer to 1 it results in a neutral gain contribution at lower frequencies. Thus, heuristically, it is reasonable to propose $\beta = 0.81$, which yields to $\gamma = 0.9$.

From the formulation developed for the fundamental frequency in the previous Chapters and considering that usually this frequency presents the highest energy in the spectrum of the signal, the tuning of the parameters k_{pmr} and $k_{r_{11}}$ follows the same procedure proposed in Chapter 4 for plants with and without ultimate frequency accordingly. It is reasonable to make $k_{r_{11}} < \omega_r$ and hence from (39), assume $\phi_{\omega_r} \geq -63.43°$.

The total phase contribution of the series topology of the PMR controller corresponds to the sum of the phase contribution of each frequency mode. Therefore, the phase contribution at each frequency mode $m\omega_r$ corresponds to the value of $\phi_{\omega_{rm}}$ plus the sum of a residual phase contribution from every other frequency mode. Intermediate frequency modes $m \geq 2 \in \mathcal{H}$ perceive negative residual phase contribution from lower modes and positive residual phase contribution from higher modes. For the highest frequency mode, only negative residual phase from lower modes is perceived. These observations can be noticed in Figure 30 for the series topology of the PMR controller, where the phase contribution at the highest frequency mode is lower than for the intermediate frequency modes.

The value of $k_{r_{1m}}$ must be computed from (53) to limit the phase contribution of the controller, $\phi_{\omega_{rm}}$, at each harmonic frequency. Recall that the relationship between the peak of the sensitivity function M_s and the phase margin PM given by (21), from which

it follows that if $M_s \approx 2$ the phase margin should be greater than $28.96°$. Based on this relationship and considering the infinite peak gain that occurs at each harmonic component found in $C_{PMR}(s)$, it is reasonable to have $k_{r_{1m}}$ such that the phase of the pre-compensated system $\angle C_{lead}(jN\omega_r)G(jN\omega_r)$ at the highest harmonic can be larger than $-145°$, *i.e.*, at this point there is at least $35°$ above the critical phase $-180°$ and it is possible to satisfy $PM \geq 28.96°$. Thus, the value for $k_{r_{1m}}$ is chosen to limit the phase contribution of each frequency mode, $\phi_{\omega_{rm}}$ and the negative residual phase contribution between frequency modes. Hence, it is reasonable to choose $\phi_{\omega_{rm}} = -5°$ at each harmonic frequency $m\omega_r$ for $m \geq 2 \in \mathcal{H}$.

The method for tuning the series topology of PMR controller proposed in this work can therefore be summarised as follows:

Algorithm:

Step 1. Design the PR+lead compensator for the fundamental frequency ω_r using the method proposed in Chapter 4, assuming $\phi_{\omega_r} \geq -63.43°$.

Step 2. Determine $k_{r_{2m}} = \beta(m\omega_r)^2$ with $\beta = 0.81$ for each $m \geq 2$, $m \in \mathcal{H}$.

Step 3. Determine $k_{r_{1m}}$ from (53) with $\beta = 0.81$ and $\phi_{\omega_{rm}} = -5°$ for each $m \geq 2$, $m \in \mathcal{H}$.

In order to evaluate the effectiveness of the tuning method, it is tested for different classes of typical processes with and without ultimate frequency in Section 5.4.

5.3.2 Parallel Topology

In this section, the procedure for the computation of parameters for the parallel topology of the PMR controller is proposed. Notice that the expression for this topology in (49) can be rearranged as follows

$$C_{PMR_p}(s) = k_{pmr}\left(\frac{1}{N_o} + C_{R_1}\right) + k_{pmr}\left(\frac{1}{N_o} + C_{R_2}\right) + ... + k_{pmr}\left(\frac{1}{N_o} + C_{R_N}\right) \quad (57)$$

where N_o is the total number of multiple frequency modes $m\omega_r$ in the PMR controller.

This is equivalent to a sum of PR controllers as presented in Chapter 3. Assigning the corresponding structure from (47) to each term and considering $k_{r_{2m}} = 0$, this equation can be rearranged as follows

$$C_{PMR_p}(s) = \sum_{m\in\mathcal{H}}\left(\frac{(N_o+1)k_{pmr}s^2 + 2N_o k_{pmr}k_{r_{1m}}s + k_{pmr}(m\omega_r)^2}{N_o(s^2 + (m\omega_r)^2)}\right) \quad (58)$$

Notice from (58) that for $\omega = 0$ the gain of the controller is k_{pmr}, for $\omega = m\omega_r$ the gain tends to infinity and for $\omega \gg \omega_r$ the gain tends to $(N_o + 1)k_{pmr}$. Applying the least common multiple in (58) and rearranging its terms, it can be expressed as follows

$$C_{PMR_p}(s) = \frac{k_{pmr}}{N_o} \prod_{n\in\mathcal{H}} \frac{1}{s^2+(n\omega_r)^2} \sum_{m\in\mathcal{H}} \left(\left((N_o+1)s^2 + 2N_o k_{r_{1_m}} s + (m\omega_r)^2\right) \prod_{\substack{n\in\mathcal{H} \\ n\neq m}} \left(s^2+(n\omega_r)^2\right) \right) \tag{59}$$

From (59), it can be noticed that at each frequency mode $m\omega_r$ the product $\prod \left(s^2+(n\omega_r)^2\right)$ makes the numerator equals to zero for every $n \neq m$. Hence, at any frequency $m\omega_r$ the only term that is not null is its corresponding term from (57) given by

$$C_{PMR_p}(s \approx mj\omega_r) = k_{pmr}\left(\frac{1}{N_o} + C_{R_m}\right) = \frac{k_{pmr}}{N_o}\left(\frac{(N_o+1)s^2 + 2N_o k_{r_{1_m}} s + (m\omega_r)^2}{s^2+(m\omega_r)^2}\right) \tag{60}$$

which is similar to the PR controller presented in Chapter 3.

5.3.2.1 Plants with Ultimate Frequency

In this section, the procedure for the computation of parameters for the parallel topology of the PMR controller for processes with ultimate frequency is proposed. The procedure for the PR+lead compensator should have its parameters revised to work with the compensated system $C_{lead}(s)G(s)$ and multiple modes of resonance. Recall that ω_{uc} is the ultimate frequency of the pre-compensated system, for which its phase crosses $-180°$, and $M_{uc} = |C_{lead}(j\omega_{uc})G(j\omega_{uc})|$ is the gain of the system at this frequency. Following similar reasoning as presented in Chapter 4, the value of k_p must be revised to adjust the gain margin.

As previously stated, with the parallel topology, for $\omega \gg \omega_r$ the gain tends to $(N_o + 1)k_{pmr}$. In order to limit the gain introduced by the PMR controller at high frequencies, it is reasonable to consider a factor κ in the denominator, with $1 \leq \kappa \leq (N_o + 1)$. Hence, the value of k_p is revised to

$$k_{pmr} = \frac{1}{10\kappa} \frac{\omega_{uc}^2 - \omega_r^2}{M_{uc}(2\omega_{uc}^2 - \omega_r^2)} \tag{61}$$

Recall that in Chapters 3 and 4, $\kappa = 1$ and $N_o = 1$ and the gain tends to $2k_p$ for $\omega \gg \omega_r$, as expected. If $\kappa = 1$, k_{pmr} has the same formulation from previous chapters and the gain at high frequencies can become too high. On the other hand, if $\kappa = (N_o + 1)$ the gain at low frequencies, which tends to k_{pmr}, can be too low and the system response can potentially become too slow. Thus, considering that $N_o \leq 9$ must be sufficient for most applications, it is reasonable to adjust $\kappa = 2$. Fine adjustments can be made iteratively if needed.

Let $\phi_{\omega_{rm}}$ be the phase contribution of the controller at frequency $\omega \to m\omega_r^+$ required for the controller at each frequency $m\omega_r$. Following similar reasoning presented in Chapter 3 to obtain (39), the value proposed for $k_{r_{1_m}}$ is given by

$$k_{r_{1_m}} = -\frac{m\omega_r}{2}\tan(\phi_{\omega_{rm}}) \ , \ m \in \mathcal{H} \tag{62}$$

Analogously to the procedure proposed in Section 5.3.1, the value of $k_{r_{11}}$ is computed from (62) for the phase of $C_{PMR}(j\omega_r)C_{lead}(j\omega_r)G(j\omega_r)$ at this frequency to be approximately $-130°$. As previously stated, the condition to have complex-conjugate zeros is $k_{r_{11}} < \sqrt{2}\omega_r$ and from (62), $\phi_{\omega_r} \geq -70.52°$. It is reasonable to make $k_{r_{11}} < \omega_r$ and hence from (62), $\phi_{\omega_r} \geq -63.43°$.

Following the reasoning presented in Section 5.3.1, the value of $k_{r_{1_m}}$ must be computed from (62) to limit the phase contribution of the controller, $\phi_{\omega_{rm}}$, at each harmonic frequency. Thus, the value for $k_{r_{1_m}}$ is chosen to limit the phase contribution of the controller, $\phi_{\omega_{rm}}$, to $-5°$ at each harmonic frequency $m\omega_r$ for $m \geq 2$.

The method for tuning the PMR controller for processes with ultimate frequency proposed in this work can therefore be summarised as follows:

Algorithm:

Step 1. Design the phase-lead compensator with $\alpha = 10$ and p given by (44).

Step 2. Determine k_{pmr} from (61).

Step 3. From the frequency response of the pre-compensated system, determine the phase contribution that the controller can introduce at frequency ω_r with $\phi_{\omega_{r1}} \approx -130° - \angle C_{lead}(j\omega_r)G(j\omega_r)$, $\phi_{\omega_{r1}} \geq -63.43°$, such that the phase of $C_{PMR}(j\omega_r)C_{lead}(j\omega_r)G(j\omega_r)$ at this frequency is approximately $-130°$.

Step 4. Determine $k_{r_{11}}$ from (62) using the value for $\phi_{\omega_{r1}}$ obtained in the previous step.

Step 5. Determine $k_{r_{1_m}}$ from (62) with $\phi_{\omega_{rm}} = -5°$ for each $m \geq 2$, $m \in \mathcal{H}$.

In order to evaluate the effectiveness of the tuning method, it is tested for different classes of typical processes with ultimate frequency in Section 5.4.

5.3.2.2 Plants without Ultimate Frequency

In this section, the procedure for the computation of parameters for the parallel topology of the PMR controller for processes without ultimate frequency is proposed. Analogously to the procedure for plants with ultimate frequency, a factor κ is considered in order to reduce the high frequency gain introduced by the PMR controller. The value of k_p is revised to

$$k_{pmr} = \frac{1}{2\kappa M_r} \tag{63}$$

As previously stated, considering that $N_o \leq 9$ must be sufficient for most applications, it is reasonable to adjust $\kappa = 2$ and fine adjustments can be made iteratively if needed.

Following the reasoning from the previous section, $k_{r_{1_m}}$ can be adjusted to limit the phase contribution of the controller $\phi_{\omega_{rm}}$ at frequencies $\omega \to m\omega_r^+$ using the same expression given by (62). One must compute $k_{r_{11}}$ using (62) so that $\angle C_{PMR}(j\omega_r)C_{lead}(j\omega_r)G(j\omega_r) \approx -130°$, *i.e.*, $\angle C_{lead}(j\omega_r)G(j\omega_r) + \phi_{\omega_{r1}} \approx -130°$ or equivalently $\phi_{\omega_{r1}} \approx -130° - \angle C_{lead}(j\omega_r)G(j\omega_r)$. As described in the previous section, in order to have $k_{r_{11}} < \omega_r$, then $\phi_{\omega_r} \geq -63.43°$.

As stated in Chapter 3, if the phase of the process at the vicinity of ω_r decreases abruptly, the phase contribution of the controller may compromise the stability of the system if its phase crosses $-180°$, limiting the gain margin that would be infinite otherwise. For processes with relative degree 2 and with small damping ratio, the phase of the process may decrease too abruptly at the vicinity of ω_r and it is necessary to adopt a stricter limit to the phase contribution of the controller, increasing $\phi_{\omega_{r1}}$ so that phase and gain margins are within the limits proposed in this work.

The method for tuning the PMR controller for processes without ultimate frequency proposed in this work can therefore be summarised as follows:

Algorithm:

Step 1. For processes with relative degree 2, design the phase-lead compensator with $\alpha = 10$ and $p = \sqrt{\alpha}\ \omega_{-20dB}$.

Step 2. Determine k_{pmr} from (63).

Step 3. From the frequency response of the pre-compensated system, determine the phase contribution that the controller can introduce at frequency ω_r with $\phi_{\omega_{r1}} \approx -130° - \angle C_{lead}(j\omega_r)G(j\omega_r)$, $\phi_{\omega_{r1}} \geq -63.43°$, such that the phase of $C_{PMR}(j\omega_r)C_{lead}(j\omega_r)G(j\omega_r)$ at this frequency is approximately $-130°$.

Step 4. Determine $k_{r_{11}}$ from (62) using the value for $\phi_{\omega_{r1}}$ obtained in the previous step.

Step 5. Determine $k_{r_{1_m}}$ from (62) with $\phi_{\omega_{rm}} = -5°$ for each $m \geq 2$, $m \in \mathcal{H}$.

In order to evaluate the effectiveness of the tuning method, it is tested for different classes of typical processes without ultimate frequency in the next section.

5.4 Simulation Results for PMR Controller

Let $d(t)$ represent the disturbance with frequency content composed by the odd multiples of ω_r. This signal is bounded to the same maximum amplitude A of the reference signal $r(t)$ and its equation for the odd multiple integers of the fundamental frequency ω_r is as follows:

· For $N = 11$ and $\mathcal{H} = \{1, 3, 5, 7, 9, 11\}$, the signal $d(t)$ is given by

$$d(t) = A\left(\frac{1}{2}\sin\left(3\omega_r t + \frac{\pi}{6}\right) + \frac{4}{20}\sin\left(5\omega_r t + \frac{\pi}{4}\right) + \frac{3}{20}\sin(7\omega_r t) + \frac{2}{20}\sin(9\omega_r t) + \frac{1}{20}\sin(11\omega_r t)\right) \tag{64}$$

· For $N = 9$ and $\mathcal{H} = \{1, 3, 5, 7, 9\}$, the signal $d(t)$ is given by

$$d(t) = A\left(\frac{1}{2}\sin\left(3\omega_r t + \frac{\pi}{6}\right) + \frac{4}{20}\sin\left(5\omega_r t + \frac{\pi}{4}\right) + \frac{3}{20}\sin(7\omega_r t) + \frac{3}{20}\sin(9\omega_r t)\right) \tag{65}$$

· For $N = 7$ and $\mathcal{H} = \{1, 3, 5, 7\}$, the signal $d(t)$ is given by

$$d(t) = A\left(\frac{1}{2}\sin\left(3\omega_r t + \frac{\pi}{6}\right) + \frac{4}{20}\sin\left(5\omega_r t + \frac{\pi}{4}\right) + \frac{6}{20}\sin(7\omega_r t)\right) \tag{66}$$

· For $N = 5$ and $\mathcal{H} = \{1, 3, 5\}$, the signal $d(t)$ is given by

$$d(t) = A\left(\frac{1}{2}\sin\left(3\omega_r t + \frac{\pi}{6}\right) + \frac{1}{2}\sin\left(5\omega_r t + \frac{\pi}{4}\right)\right) \tag{67}$$

· For $N = 3$ and $\mathcal{H} = \{1, 3\}$, the signal $d(t)$ is given by

$$d(t) = A\sin\left(3\omega_r t + \frac{\pi}{6}\right) \tag{68}$$

Figure 33 presents the normalized disturbance and reference signals considering $\mathcal{H} = \{1, 3, 5, 7, 9, 11\}$.

Figure 33 – Normalized signals $r(t)$ and $d(t)$ considering $\mathcal{H} = \{1, 3, 5, 7, 9, 11\}$.

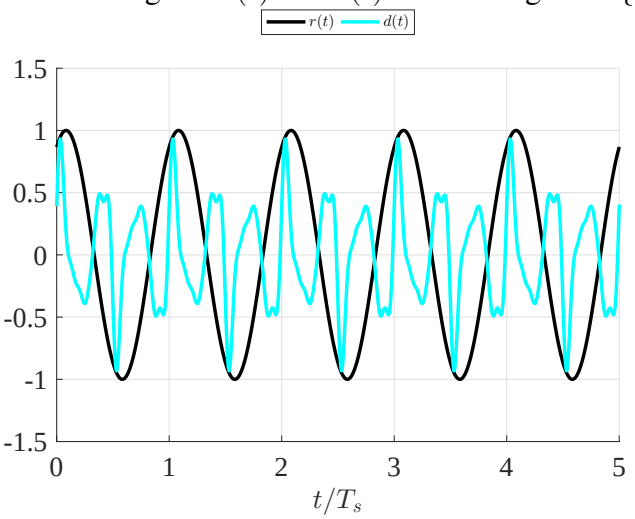

Source: created by the author.

In order to assess the performance of the proposed method for the systems shown in Figures 31 and 32 subject to the disturbance defined by (64) to (68), the PMR controller is tested using the same plants and criteria defined in Chapter 2. Also, analogous tables and plots are presented to demonstrate the simulation results. For the class of processes $G_4(s)$,

ω_r is such that $|C_{lead}(jN\omega_r)G(jN\omega_r)| = -20dB$ in each case. For all other classes of processes, ω_r is such that $\angle C_{lead}(jN\omega_r)G(jN\omega_r) = -145°$ in each case and it is possible to obtain a phase margin of $28.96°$. In every test, $d(t)$ is bounded to the same maximum amplitude A of the reference signal $r(t)$ and N is the same of the PMR controller.

5.4.1 Series Topology Simulation Results

In order to illustrate the application of the method for the series topology of the PMR controller, consider the process $G_1(s)$ with $n = 3$ for which $\omega_u = 1.73\ rad/s$. To improve the bandwidth of the process, begin by designing the phase-lead compensator with p given by (44). Thus, $p = \sqrt{10}\ \omega_u = 5.47$. Figure 34 presents the Bode plot for the pre-compensated system $C_{lead}(s)G_1(s)$, for which $\omega_{uc} = 3.88\ rad/s$ and $M_{uc} = -40.8\ dB$.

Figure 34 – Bode plots of the pre-compensated system $C_{lead}(s)G_1(s)$ with $n = 3$, for which $\omega_{uc} = 3.88\ rad/s$ and $M_{uc} = -40.8\ dB$, and of the system $C_{PMR_s}(s)C_{lead}(s)G_1(s)$.

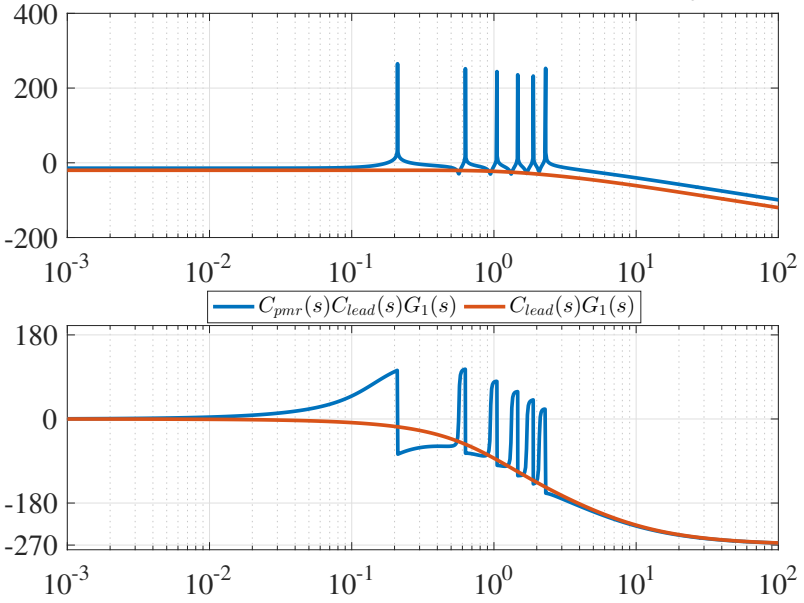

Source: created by the author.

Recall that the disturbance signal is composed by the odd multiple integers of the fundamental frequency ω_r up to N. For testing purposes, consider the case for which frequency ω_r is such that $\angle C_{lead}(jN\omega_r)G(jN\omega_r) = -145°$ and therefore it is challenging, though possible, to obtain a phase margin greater than $28.96°$. Otherwise, if $\angle C_{lead}(jN\omega_r)G(jN\omega_r) < -145°$, then the phase should be compensated in order to make it possible to accomplish the required phase margin. For the pre-compensated system $C_{lead}(s)G_1(s)$ shown in Figure 34, $\angle C_{lead}(jN\omega_r)G(jN\omega_r) = -145°$ corresponds to $\omega_r \approx \frac{2.27}{N}\ rad/s$, *e.g.* for $N = 11$ then $\omega_r = 0.21\ rad/s$ and for $N = 9$ then $\omega_r = 0.25\ rad/s$.

Now, given $\omega_r = 0.21\ rad/s$, consider the case with $N = 11$. The corresponding set of harmonic frequencies is $\mathcal{H} = \{1, 3, 5, 7, 9, 11\}$ and $N_o = 6$. From the frequency response

of the pre-compensated system shown in Figure 34, then $\angle C_{lead}(j11\omega_r)G(j11\omega_r) = -145°$. The phase of the pre-compensated system at frequency ω_r is $\angle C_{lead}(j\omega_r)G(j\omega_r) = -16.8°$.

Hence, for $\omega_r = 0.21rad/s$, k_{pmr} is computed from (45) as follows

$$k_{pmr} = \frac{1}{10}\frac{\omega_{uc}^2 - \omega_r^2}{M_{uc}(2\omega_{uc}^2 - \omega_r^2)} = 5.47 \tag{69}$$

The phase contribution that the controller can introduce at the fundamental frequency ω_r is given by $\phi_{\omega_r} \approx -130° - \angle C_{lead}(j\omega_r)G(j\omega_r) = -130° + 16.8° = -113.2°$ with $\phi_{\omega_r} \geq -63.43°$. Hence, assuming $\phi_{\omega_r} = -60°$, $k_{r_{11}}$ is computed from (39) as follows

$$k_{r_{11}} = -\frac{\omega_r}{2}\tan(\phi_{\omega_r}) = -\frac{0.21}{2}\tan(-60°) = 0.18 \tag{70}$$

The parameters $k_{r_{1m}}$ and $k_{r_{2m}}$ are given by (53) and (52), respectively. Assuming $\beta = 0.81$ and $\phi_{\omega_{rm}} = -5°$, the obtained values are presented in Table 15.

Table 15 – Tuning parameters $k_{r_{1m}}$ and $k_{r_{2m}}$ for the process $G_1(s)$ with $n = 3$ and the series topology of PMR controller with frequency modes up to $N = 11$.

m	3	5	7	9	11
$k_{r_{1m}}$	0.0052	0.0087	0.0122	0.0157	0.0192
$k_{r_{2m}}$	0.32	0.89	1.75	2.89	4.32

The results achieved for process $G_1(s)$ with the controller designed with these parameters are summarised in the line for $\omega_r = 0.21rad/s$ and $N = 11$ of Table 16. Figure 34 presents the Bode plot of the system $C_{PMR_s}(s)C_{lead}(s)G_1(s)$. The output signal normalized in relation to the period of reference signal $r(t)$ for this case is shown in Figure 35. Also, the root mean square (RMS) value of the output signal, $y_{RMS}(t)$, and the portion of the output signal due to the disturbance are shown in this figure. The same procedure is repeated accordingly for every case of each different process and the results are presented bellow.

Tables 16 to 18 summarise the results achieved for processes $G_1(s)$, $G_2(s)$ and $G_3(s)$ with reference signal $r(t)$ subject to disturbance $d(t)$ composed by harmonic components odd multiples of the fundamental frequency ω_r up to N as described from (64) to (68). Tables 19 to 21 summarise the results achieved for processes $G_4(s)$, $G_5(s)$ and $G_6(s)$. The tables present the obtained values for settling time n_s, maximum percent overshoot $M_{O_\%}$, peak of sensitivity function M_s, phase margin PM and gain margin GM of the final controlled system. Figures 35 to 40 show the output signal normalized in relation to the

period of reference signal $r(t)$ for the system subject to a disturbance $d(t)$ with harmonic content up to the 11^{th} multiple of ω_r given by (64) (*i.e.* with the harmonic content up to the 11^{th} multiple of ω_r), the root mean square (RMS) value of the output signal, $y_{RMS}(t)$, and the portion of the output signal due to the disturbance, $y_d(t)$.

Table 16 – Tuning parameters and performance indicators for the closed-loop system of $G_1(s)$ with $n = 3$ and odd multiples of ω_r up to N for the series topology of the PMR controller.

ω_r	N	k_{pmr}	$k_{r_{11}}$	n_s	$M_{O_{\%}}$	M_s	GM	PM
$0.76\ rad/s$	3	5.37	0.66	9.53	7.05%	4.71	$14.2dB$	12.3°
$0.45\ rad/s$	5	5.44	0.39	3.39	0.57%	3.07	$16.1dB$	19.1°
$0.32\ rad/s$	7	5.46	0.28	3.34	0%	2.77	$16.5dB$	21.2°
$0.25\ rad/s$	9	5.47	0.22	4.39	0%	2.75	$16.4dB$	21.4°
$0.21\ rad/s$	11	5.47	0.18	5.90	0.01%	3.00	$16.1dB$	19.6°

Figure 35 – Closed-loop normalized output signal for process $G_1(s)$ with $n = 3$, for the series topology of the PMR controller with odd multiples of ω_r up to 11.

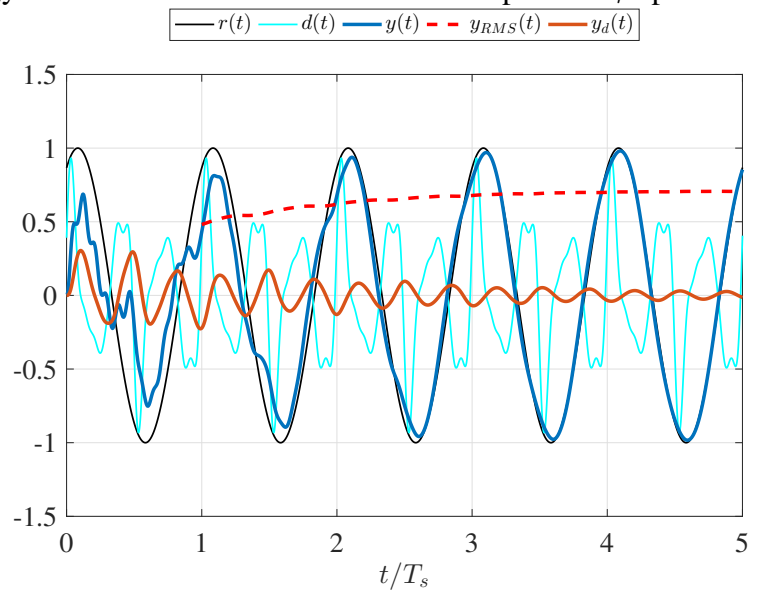

Source: created by the author.

Table 17 – Tuning parameters and performance indicators for the closed-loop system of $G_2(s)$ with $T = 0.1$ and odd multiples of ω_r up to N for the series topology of the PMR controller.

ω_r	N	k_{pmr}	$k_{r_{11}}$	n_s	$M_{O_{\%}}$	M_s	GM	PM
$4.50\ rad/s$	3	9.43	3.74	8.74	6.35%	4.62	$13.9dB$	12.5°
$2.70\ rad/s$	5	9.56	2.34	3.89	0.67%	3.28	$15.6dB$	17.8°
$1.93\ rad/s$	7	9.60	1.67	3.03	0.54%	2.99	$15.9dB$	19.6°
$1.50\ rad/s$	9	9.61	1.30	3.52	0.11%	2.92	$15.9dB$	20.1°
$1.23\ rad/s$	11	9.62	1.06	4.53	0.14%	2.97	$15.7dB$	19.8°

Figure 36 – Closed-loop normalized output signal for process $G_2(s)$ with $T = 0.1$, for the series topology of the PMR controller with odd multiples of ω_r up to 11.

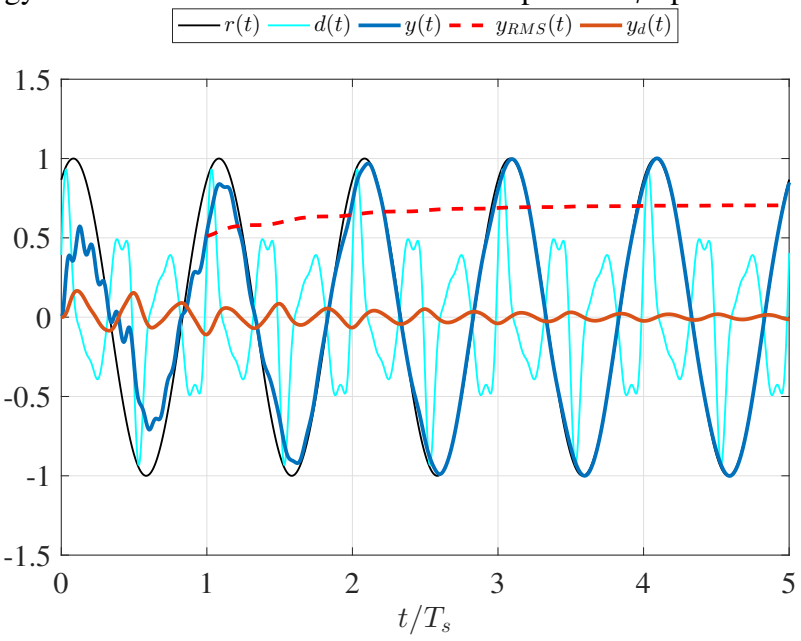

Source: created by the author.

Table 18 – Tuning parameters and performance indicators for the closed-loop system of $G_3(s)$ with $\alpha = 0.1$ and odd multiples of ω_r up to N for the series topology of the PMR controller.

ω_r	N	k_{pmr}	$k_{r_{11}}$	n_s	$M_{O_{\%}}$	M_s	GM	PM
16.72 rad/s	3	84.46	3.55	4.04	3.06%	2.34	18.4dB	25.4°
10.03 rad/s	5	85.38	3.26	2.92	1.52%	2.37	18.1dB	25°
7.16 rad/s	7	85.64	3.00	2.90	0.85%	2.42	17.9dB	24.5°
5.57 rad/s	9	85.74	2.60	2.45	1.87%	2.47	17.6dB	24.1°
4.56 rad/s	11	85.79	2.44	2.94	1.79%	2.52	17.3dB	23.3°

Figure 37 – Closed-loop normalized output signal for process $G_3(s)$ with $\alpha = 0.1$, for the series topology of the PMR controller with odd multiples of ω_r up to 11.

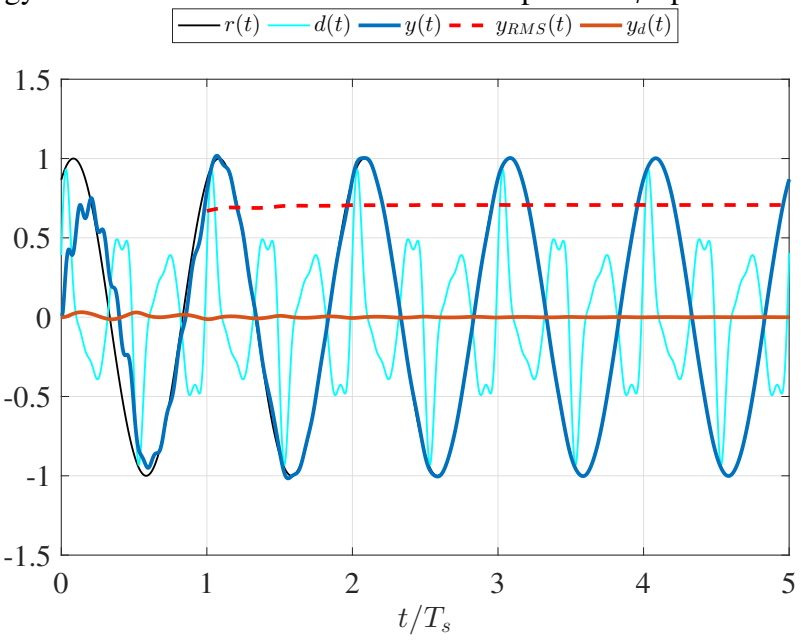

Source: created by the author.

Table 19 – Tuning parameters and performance indicators for the closed-loop system of $G_4(s)$ with $\alpha = 0.1$ and odd multiples of ω_r up to N for the series topology of the PMR controller.

ω_r	N	k_{pmr}	$k_{r_{11}}$	n_s	$M_{O_{\%}}$	M_s	GM	PM
$0.33\ rad/s$	3	1.73	0.25	3.13	5.21%	1	∞	77.7°
$0.2\ rad/s$	5	1.12	0.17	3.96	5.03%	1	∞	81.1°
$0.14\ rad/s$	7	0.87	0.12	4.98	4.07%	1	∞	82.5°
$0.11\ rad/s$	9	0.75	0.10	6.48	3.84%	1	∞	83.8°
$0.09\ rad/s$	11	0.67	0.08	7.99	3.83%	1	∞	84°

Figure 38 – Closed-loop normalized output signal for process $G_4(s)$ with $\alpha = 0.1$, for the series topology of the PMR controller with odd multiples of ω_r up to 11.

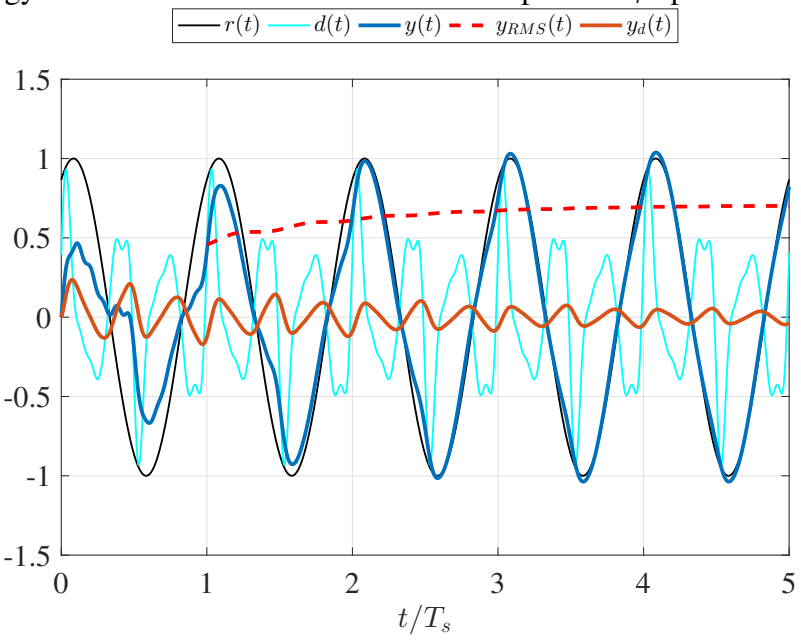

Source: created by the author.

Table 20 – Tuning parameters and performance indicators for the closed-loop system of $G_5(s)$ with $\alpha = 0.1$ and odd multiples of ω_r up to N for the series topology of the PMR controller.

ω_r	N	k_{pmr}	$k_{r_{11}}$	n_s	$M_{O_\%}$	M_s	GM	PM
1.69 rad/s	3	29.10	0.51	4.73	3.93%	2.39	∞	24.7°
1.01 rad/s	5	18.36	0.69	5.05	5.52%	2.66	∞	22°
0.72 rad/s	7	15.10	0.63	4.94	2.41%	2.65	∞	22.1°
0.56 rad/s	9	13.46	0.49	4.95	0.71%	2.56	∞	22.8°
0.46 rad/s	11	12.42	0.40	5.46	0.08%	2.56	∞	22.9°

Figure 39 – Closed-loop normalized output signal for process $G_5(s)$ with $\alpha = 0.1$, for the series topology of the PMR controller with odd multiples of ω_r up to 11.

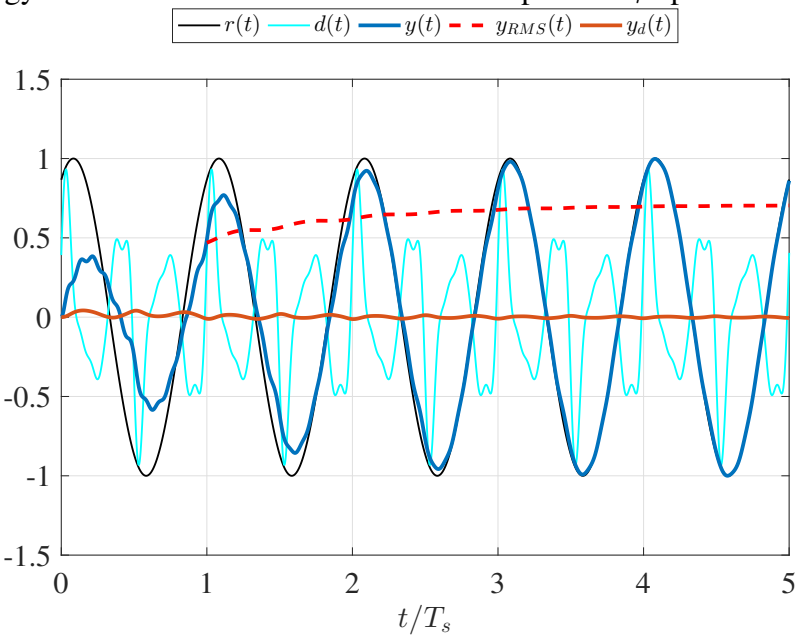

Source: created by the author.

Table 21 – Tuning parameters and performance indicators for the closed-loop system of $G_6(s)$ with $\alpha = 0.1$ and odd multiples of ω_r up to N for the series topology of the PMR controller.

ω_r	N	k_{pmr}	$k_{r_{11}}$	n_s	$M_{O_{\%}}$	M_s	GM	PM
$4.33\ rad/s$	3	22.59	0.27	3.92	4.19%	2.04	∞	29.4°
$2.60\ rad/s$	5	11.07	0.21	5.56	4.09%	2.08	∞	28.7°
$1.86\ rad/s$	7	6.22	0.15	5.47	4.24%	2.13	∞	28°
$1.44\ rad/s$	9	3.30	0.14	8.90	4.36%	2.16	∞	27.3°
$1.18\ rad/s$	11	1.51	0.26	20.51	6.84%	2.29	∞	25.7°

Figure 40 – Closed-loop normalized output signal for process $G_6(s)$ with $\alpha = 0.1$, for the series topology of the PMR controller with odd multiples of ω_r up to 11.

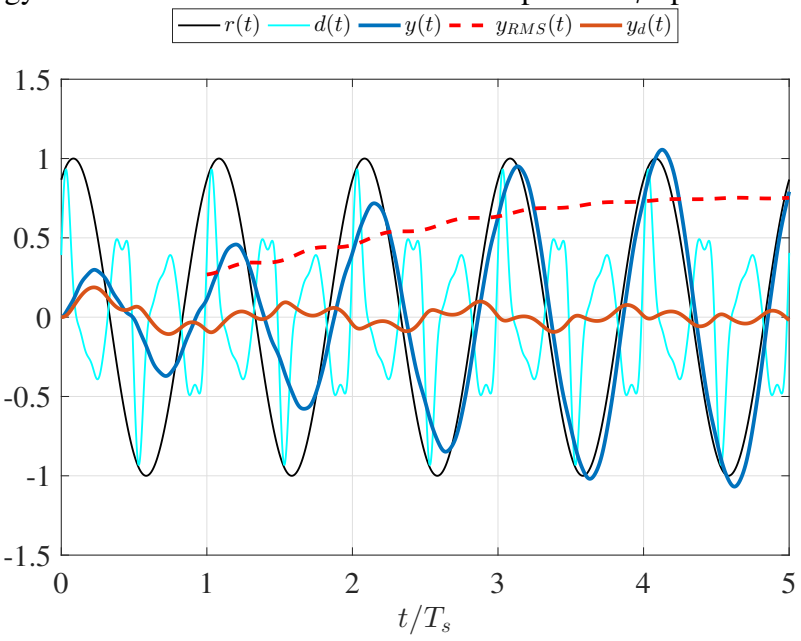

Source: created by the author.

The parameters k_{pmr} and $k_{r_{11}}$ for the fundamental frequency were determined using the same procedure proposed in Chapter 4 for plants with and without ultimate frequency. Parameters $k_{r_{1m}}$ and $k_{r_{2m}}$ were determined by (53) and (52) respectively, considering $\phi_{\omega_{rm}} = -5°$ and $\beta = 0.81$.

From the results shown in Tables 16 to 21, for the range of frequencies tested, it can be observed that the resulting phase margins are close to the value of $28.96°$ and the gain margin is higher than $15\ dB$ in most cases. This corresponds to the high limit for the peak value M_s, which falls nearly into the desired interval in most cases. However, in some cases it can be observed that the peak value M_s is higher than the proposed interval. Hence, suitable values for the maximum overshoot and settling time were achieved for most cases. In Figures 35 to 40, it can be observed that in all cases the signal $y_d(t)$ tends to zero and the signal $y_{RMS}(t)$ rapidly converges to its steady-state value. In the next section, these results are compared with those for the parallel topology of the PMR controller.

5.4.2 Parallel Topology Simulation Results

In order to illustrate the application of the method for the parallel topology of the PMR controller, consider again the process $G_1(s)$ with $n = 3$ for which $\omega_u = 1.73\ rad/s$. To improve the bandwidth of the process, begin by designing the phase-lead compensator with p given by (44). Thus, $p = \sqrt{10}\ \omega_u = 5.47$. Recall that for the pre-compensated system $C_{lead}(s)G_1(s)$, $\omega_{uc} = 3.88\ rad/s$ and $M_{uc} = -40.8\ dB$.

Figure 41 – Bode plots of the pre-compensated system $C_{lead}(s)G_1(s)$ with $n = 3$, for which $\omega_{uc} = 3.88\ rad/s$ and $M_{uc} = -40.8\ dB$, and of the system $C_{PMR_p}(s)C_{lead}(s)G_1(s)$.

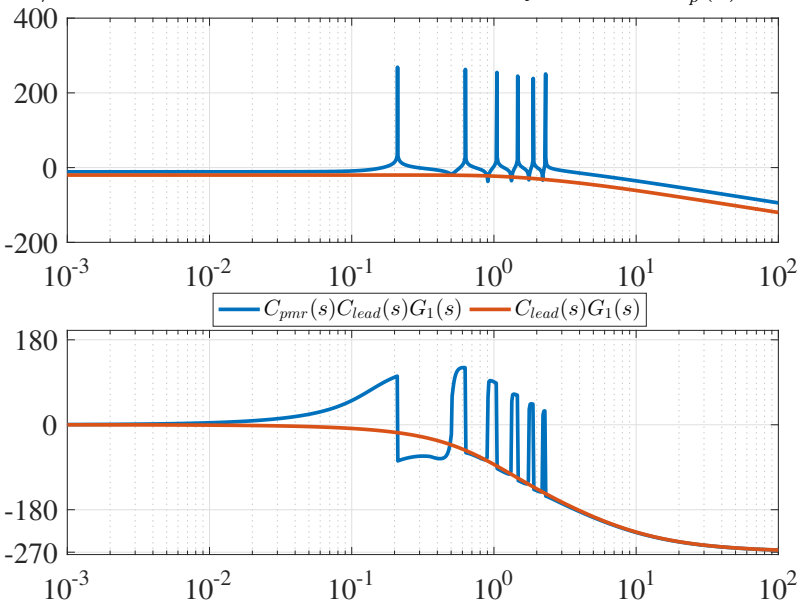

Source: created by the author.

Now, given $\omega_r = 0.21\ rad/s$, consider the case with $N = 11$. The corresponding set of harmonic frequencies is $\mathcal{H} = \{1, 3, 5, 7, 9, 11\}$and $N_o = 6$. From the frequency response

of the pre-compensated system shown in Figure 41, then $\angle C_{lead}(j11\omega_r)G(j11\omega_r) = -145°$. The phase of the pre-compensated system at frequency ω_r is $\angle C_{lead}(j\omega_r)G(j\omega_r) = -16.8°$.

Hence, assuming $\kappa = 2$, k_{pmr} is computed from (61) as follows

$$k_{pmr} = \frac{1}{10\kappa} \frac{\omega_{uc}^2 - \omega_r^2}{M_{uc}(2\omega_{uc}^2 - \omega_r^2)} = 2.74 \tag{71}$$

The phase contribution that the controller can introduce at the fundamental frequency ω_r is given by $\phi_{\omega_{r_1}} \approx -130° - \angle C_{lead}(j\omega_r)G(j\omega_r) = -130° + 16.8° = -113.2°$ with $\phi_{\omega_{r_1}} \geq -63.43°$. Hence, assuming $\phi_{\omega_{r_1}} = -60°$, $k_{r_{11}}$ is computed from (62) as follows

$$k_{r_{11}} = -\frac{m\omega_r}{2}\tan(\phi_{\omega_{rm}}) = -\frac{0.21}{2}\tan(-60°) = 0.18 \tag{72}$$

The parameters $k_{r_{1m}}$ for $m \geq 2$ are also given by (62). Assuming $\phi_{\omega_{rm}} = -5°$ for each $m \geq 2 \in \mathcal{H}$, the obtained values are presented in Table 22.

Table 22 – Tuning parameters $k_{r_{1m}}$ for the process $G_1(s)$ with $n = 3$ and the parallel topology of PMR controller with frequency modes up to $N = 11$.

m	3	5	7	9	11
$k_{r_{1m}}$	0.0276	0.0459	0.0643	0.0827	0.1010

The results achieved for process $G_1(s)$ with the controller designed with these parameters are summarised in the line for $\omega_r = 0.21rad/s$ and $N = 11$ of Table 23. Figure 41 presents the Bode plot of the system $C_{PMR_p}(s)C_{lead}(s)G_1(s)$. The output signal normalized in relation to the period of reference signal $r(t)$ for this case is shown in Figure 42. Also, the root mean square (RMS) value of the output signal, $y_{RMS}(t)$, and the portion of the output signal due to the disturbance are shown in this plot. The same procedure is repeated accordingly for every case of each different process and the results are presented bellow.

Tables 23 to 25 summarise the results achieved for processes $G_1(s)$, $G_2(s)$ and $G_3(s)$ with reference signal $r(t)$ subject to disturbance $d(t)$ composed by harmonic components odd multiples of the fundamental frequency ω_r up to N. Tables 26 to 28 summarise the results achieved for processes $G_4(s)$, $G_5(s)$ and $G_6(s)$. For additional simulation results see Appendix A.3. The tables present the obtained values for settling time n_s, maximum percent overshoot $M_{O_\%}$, peak of sensitivity function M_s, phase margin PM and gain margin GM of the final controlled system. Figures 42 to 47 show the output signal normalized in relation to the period of reference signal $r(t)$ for the system subject to a disturbance $d(t)$ with harmonic content up to the 11^{th} multiple of ω_r, the root mean square

(RMS) value of the output signal $y_{RMS}(t)$ and the portion of the output signal due to the disturbance $y_d(t)$.

Table 23 – Tuning parameters and performance indicators for the closed-loop system of $G_1(s)$ with $n = 3$ and odd multiples of ω_r up to N for the parallel topology of the PMR controller.

ω_r	N	k_{pmr}	$k_{r_{11}}$	n_s	$M_{O_{\%}}$	M_s	GM	PM
$0.76\ rad/s$	3	2.69	0.66	4.08	5.06%	2.35	$18.3dB$	25.8°
$0.45\ rad/s$	5	2.72	0.39	2.79	0.09%	2.21	$17.2dB$	27.4°
$0.32\ rad/s$	7	2.73	0.28	2.73	0.03%	2.19	$15.8dB$	27.9°
$0.25\ rad/s$	9	2.74	0.22	2.77	0.24%	2.23	$14.4dB$	27.4°
$0.21\ rad/s$	11	2.74	0.18	3.26	0.87%	2.40	$13.0dB$	25.5°

Figure 42 – Closed-loop normalized output signal for process $G_1(s)$ with $n = 3$, for the parallel topology of the PMR controller with odd multiples of ω_r up to 11.

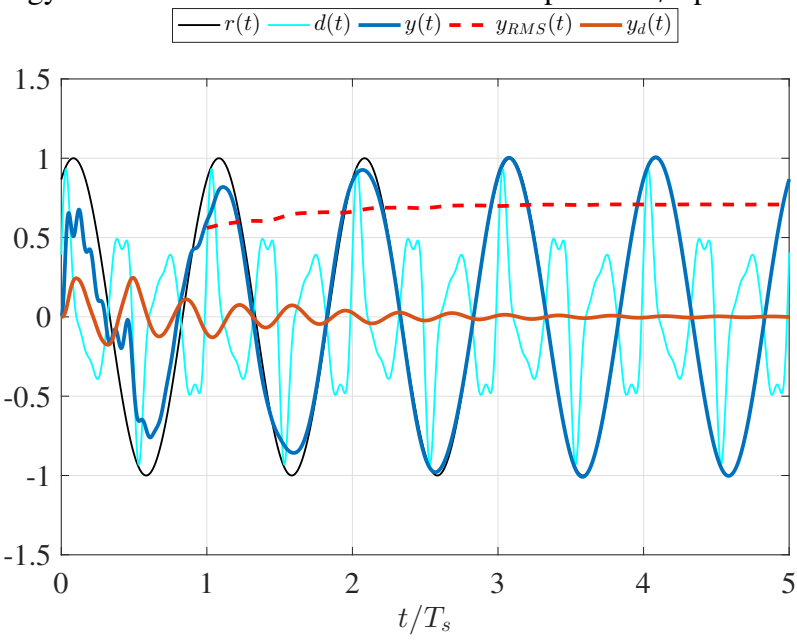

Source: created by the author.

Table 24 – Tuning parameters and performance indicators for the closed-loop system of $G_2(s)$ with $T = 0.1$ and odd multiples of ω_r up to N for the parallel topology of the PMR controller.

ω_r	N	k_{pmr}	$k_{r_{11}}$	n_s	$M_{O_{\%}}$	M_s	GM	PM
$4.50\ rad/s$	3	4.71	3.74	5.04	4.27%	2.36	$18.0dB$	25.6°
$2.70\ rad/s$	5	4.78	2.34	3.41	0.26%	2.30	$16.9dB$	26.3°
$1.93\ rad/s$	7	4.80	1.67	2.57	0%	2.30	$15.4dB$	26.4°
$1.50\ rad/s$	9	4.81	1.30	2.55	0%	2.32	$14.1dB$	26.3°
$1.23\ rad/s$	11	4.81	1.06	2.12	0.01%	2.37	$12.9dB$	25.9°

Figure 43 – Closed-loop normalized output signal for process $G_2(s)$ with $T = 0.1$, for the parallel topology of the PMR controller with odd multiples of ω_r up to 11.

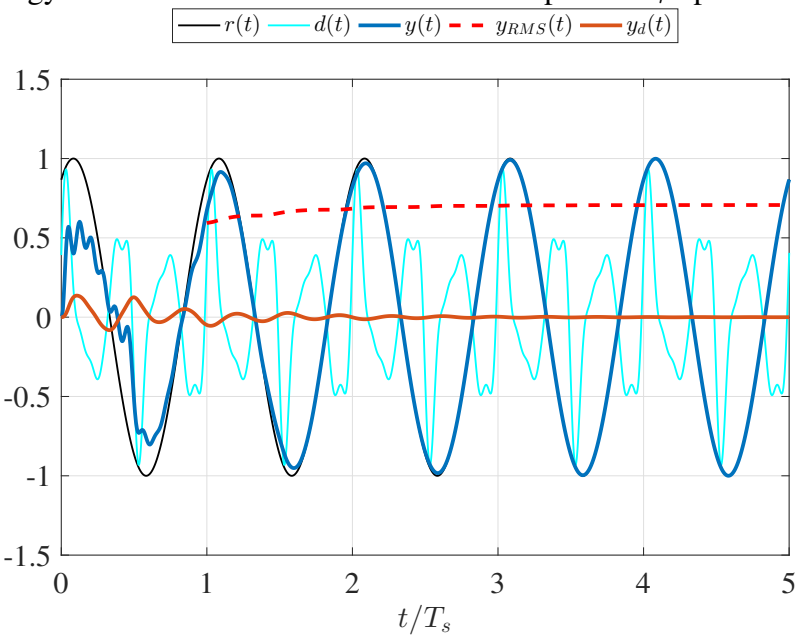

Source: created by the author.

Table 25 – Tuning parameters and performance indicators for the closed-loop system of $G_3(s)$ with $\alpha = 0.1$ and odd multiples of ω_r up to N for the parallel topology of the PMR controller.

ω_r	N	k_{pmr}	$k_{r_{11}}$	n_s	$M_{O_{\%}}$	M_s	GM	PM
16.72 rad/s	3	42.23	3.55	5.31	2.03%	2.13	20.6dB	28.3°
10.03 rad/s	5	42.69	3.26	2.89	0.13%	2.13	18.2dB	28.4°
7.16 rad/s	7	42.82	3.00	1.93	0.14%	2.12	16.4dB	28.3°
5.57 rad/s	9	42.87	2.60	1.45	0.56%	2.16	14.8dB	28.2°
4.56 rad/s	11	42.90	2.44	1.07	5.56%	2.20	13.5dB	27.8°

Figure 44 – Closed-loop normalized output signal for process $G_3(s)$ with $\alpha = 0.1$, for the parallel topology of the PMR controller with odd multiples of ω_r up to 11.

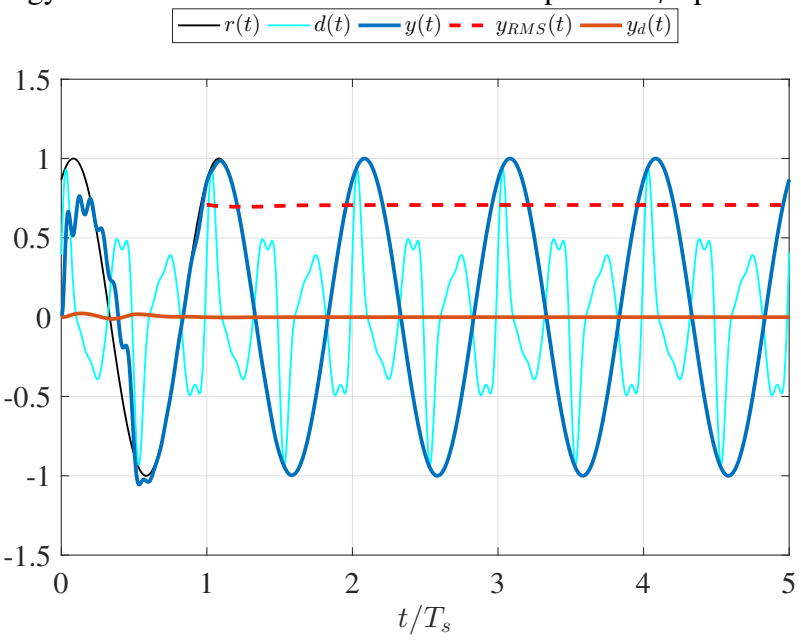

Source: created by the author.

Table 26 – Tuning parameters and performance indicators for the closed-loop system of $G_4(s)$ with $\alpha = 0.1$ and odd multiples of ω_r up to N for the parallel topology of the PMR controller.

ω_r	N	k_{pmr}	$k_{r_{11}}$	n_s	$M_{O_\%}$	M_s	GM	PM
$0.33\ rad/s$	3	0.87	0.25	3.68	3.03%	1.08	∞	89.1°
$0.2\ rad/s$	5	0.56	0.17	3.13	2.80%	1.07	∞	90.3°
$0.14\ rad/s$	7	0.44	0.12	3.01	0.80%	1.08	∞	90.8°
$0.11\ rad/s$	9	0.37	0.10	3.03	0%	1.09	∞	91°
$0.09\ rad/s$	11	0.34	0.08	3.04	0%	1.11	∞	91.1°

Figure 45 – Closed-loop normalized output signal for process $G_4(s)$ with $\alpha = 0.1$, for the parallel topology of the PMR controller with odd multiples of ω_r up to 11.

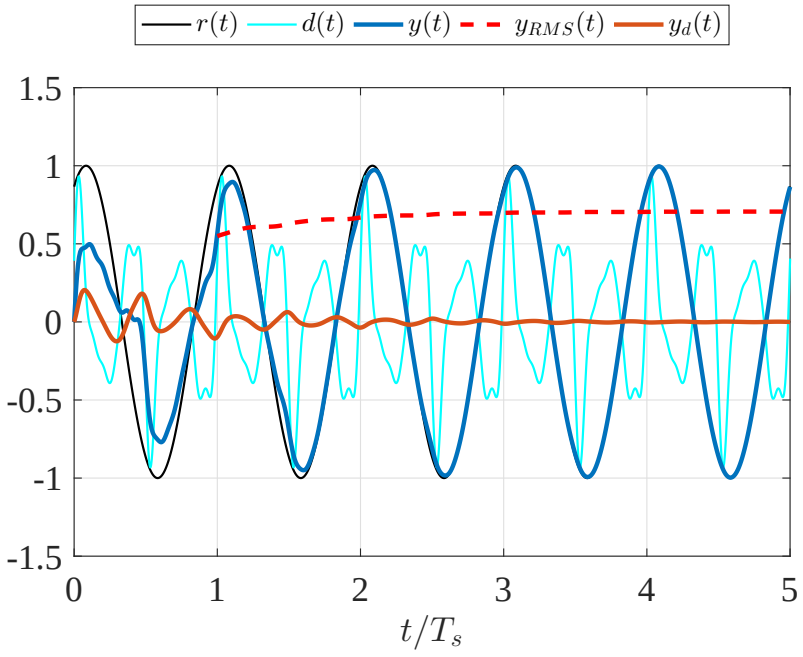

Source: created by the author.

Table 27 – Tuning parameters and performance indicators for the closed-loop system of $G_5(s)$ with $\alpha = 0.1$ and odd multiples of ω_r up to N for the parallel topology of the PMR controller.

ω_r	N	k_{pmr}	$k_{r_{11}}$	n_s	$M_{O_\%}$	M_s	GM	PM
1.69 rad/s	3	14.55	0.51	5.08	4.36%	2.03	∞	29.6°
1.01 rad/s	5	9.18	0.69	4.06	4.97%	2.00	∞	30°
0.72 rad/s	7	7.55	0.63	3.05	1.72%	1.99	∞	30.1°
0.56 rad/s	9	6.73	0.49	2.97	0.21%	1.98	∞	30.3°
0.46 rad/s	11	6.21	0.40	2.97	0.27%	1.97	∞	30.4°

Figure 46 – Closed-loop normalized output signal for process $G_5(s)$ with $\alpha = 0.1$, for the parallel topology of the PMR controller with odd multiples of ω_r up to 11.

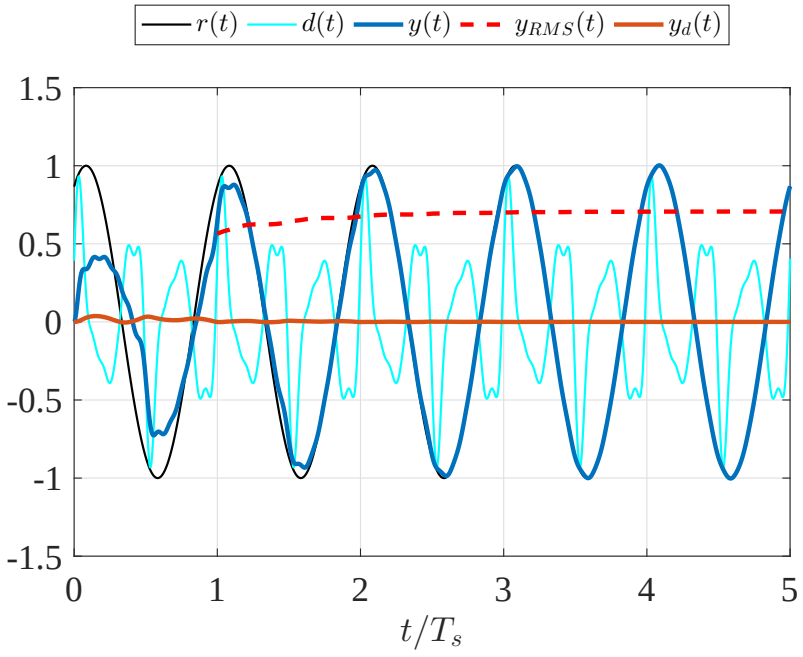

Source: created by the author.

Table 28 – Tuning parameters and performance indicators for the closed-loop system of $G_6(s)$ with $\alpha = 0.1$ and odd multiples of ω_r up to N for the parallel topology of the PMR controller.

ω_r	N	k_{pmr}	$k_{r_{11}}$	n_s	$M_{O_\%}$	M_s	GM	PM
$4.33\ rad/s$	3	11.30	0.27	5.56	4.37%	2.00	∞	30°
$2.60\ rad/s$	5	5.53	0.21	5.58	4.44%	1.99	∞	30.2°
$1.86\ rad/s$	7	3.11	0.15	7.03	4.54%	1.98	∞	30.3°
$1.44\ rad/s$	9	1.65	0.14	7.04	4.69%	1.98	∞	30.3°
$1.18\ rad/s$	11	0.76	0.26	10.48	12.97%	1.99	∞	30.2°

Figure 47 – Closed-loop normalized output signal for process $G_6(s)$ with $\alpha = 0.1$, for the parallel topology of the PMR controller with odd multiples of ω_r up to 11.

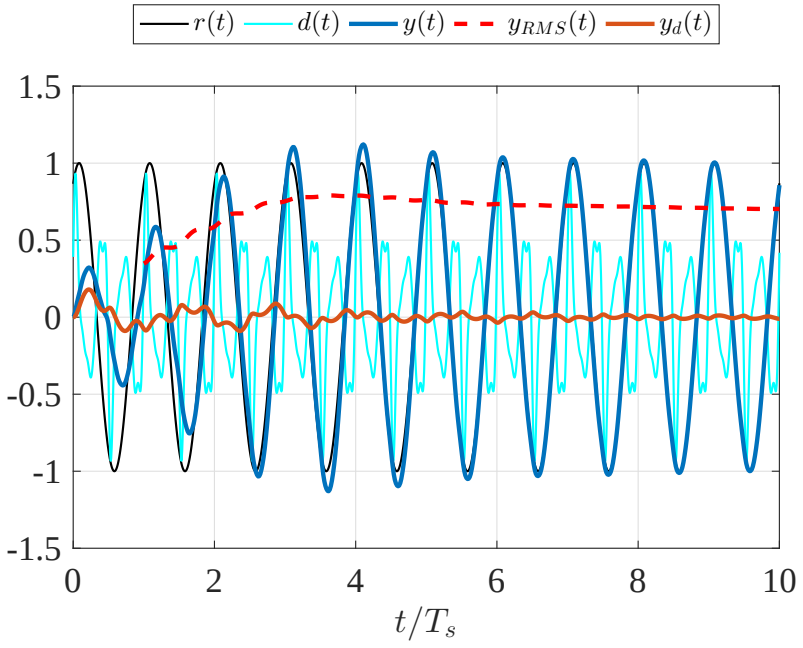

Source: created by the author.

The parameter k_{pmr} was determined by (61) for processes $G_1(s)$, $G_2(s)$ and $G_3(s)$ and by (63) for processes $G_4(s)$, $G_5(s)$ and $G_6(s)$ considering $\kappa = 2$. The parameter $k_{r_{11}}$ was computed using (39) to limit phase contribution of the controller at frequency ω_r such that the phase of the system $C_{PMR}(j\omega)C_{lead}(j\omega)G(j\omega)$ at this frequency would be approximately $-130°$. Parameters $k_{r_{11}}$ for $m \geq 2$ were determined by (62) considering $\phi_{\omega_{rm}} = -5°$.

From the results shown in Tables 23 to 28, for the range of frequencies tested, it can be observed that the resulting phase margins are close to the value of $28.96°$ corresponding to the high limit for the peak value M_s, which falls nearly into the desired interval. Hence, suitable values for the maximum overshoot and settling time were achieved. In Figures 42 to 47, it can be observed that in all cases the signal $y_d(t)$ tends to zero and the signal $y_{RMS}(t)$ rapidly converges to its steady-state value.

Comparing the obtained results with those presented in Subsection 5.4.1, one can notice that for the parallel topology of the PMR controller the results for the gain and phase margins are more consistent and the values of M_s are lower than those for the series topology of the PMR controller for the same processes. This is due to the fact that for the parallel topology, the transfer function of the controller at each frequency $m\omega_r$ is reduced to its corresponding term shown in (60), which is similar to the structure thoroughly discussed in previous chapters and to which analogous reasoning applies. On the other hand, with the series topology, the phase contribution of the controller at the highest harmonic frequency depends also on a sum of residual phase contribution from previous modes. This characteristic can degrade the phase margin of the system and prevent the peak value M_s from falling into the desired interval. Moreover, for the series topology more parameters need to be computed. Hence, for further analysis in the next Sections, only the method for the parallel topology of the PMR controller is considered.

5.5 Disturbance Rejection Analysis with PMR controller

This section aims to evaluate the effects of a harmonic disturbance in terms of the percent of Total Harmonic Distortion ($THD_{\%}$) (IEEE, 1992) observed in the output of the system with the parallel topology of the PMR controller. Now, consider $d(t)$ given in (46) with the same amplitude A of reference signal $r(t)$. Figure 48 presents the normalized disturbance and reference signals.

Tables 29 to 31 summarise the results achieved for different orders of the PMR controller. For additional simulation results see Appendix A.4. For each process, the fundamental frequency ω_r is selected such that the phase of the pre-compensated system is equal to $-145°$ at the 11^{th} harmonic frequency and it is possible to obtain a phase margin of $28.96°$. These tables present the obtained values for settling time n_s, maximum percent overshoot $M_{O_{\%}}$ and percent of total harmonic distortion $THD_{\%}$ of the final controlled

Figure 48 – Normalized signals $r(t)$ and $d(t)$.

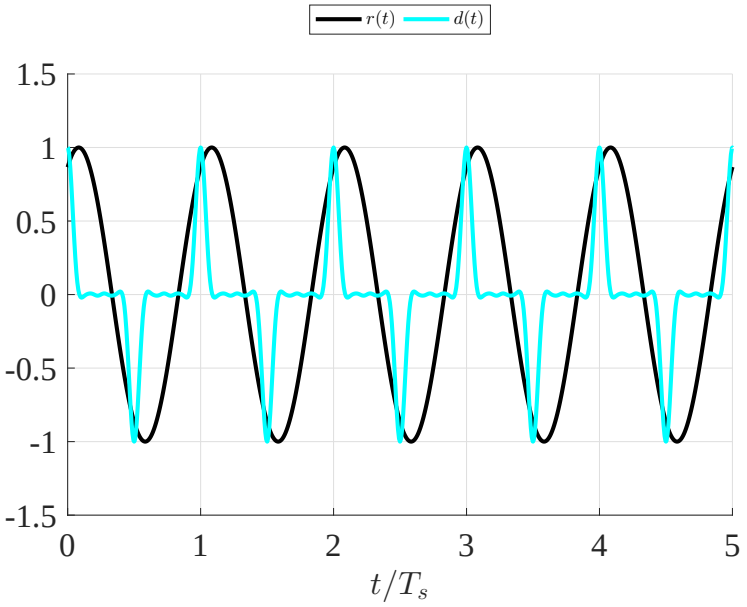

Source: created by the author.

system. Figures 49 to 51 show the output signal normalized in relation to the period of reference signal $r(t)$ for the system subject to a disturbance with harmonic content up to the 11^{th} multiple of ω_r and different orders of the PMR controller.

Table 29 – Performance indicators for the closed-loop system of $G_1(s)$ with $n = 3$ and different orders of the PMR controller subject to disturbance $d(t)$

N	k_{pmr}	$k_{r_{11}}$	n_s	$M_{O_{\%}}$	M_s	GM	PM	$THD_{\%}$
1	2.74	0.18	–	22.65%	1.15	25.2dB	118°	15.36%
3	2.74	0.18	–	8.64%	1.49	21.8dB	102°	6.40%
5	2.74	0.18	–	2.40%	1.49	19.2dB	73.2°	2.38%
7	2.74	0.18	3.13	1.44%	1.48	17dB	53.5°	0.63%
9	2.74	0.18	2.98	1.90%	1.75	15.1dB	38.6°	0.14%
11	2.74	0.18	2.98	3.31%	2.31	13.1dB	26.6°	0%

Figure 49 – Comparison of normalized output signals of process $G_1(s)$ with $n = 3$ subject to disturbance $d(t)$ for PMR controller with odd multiples of ω_r up to m.

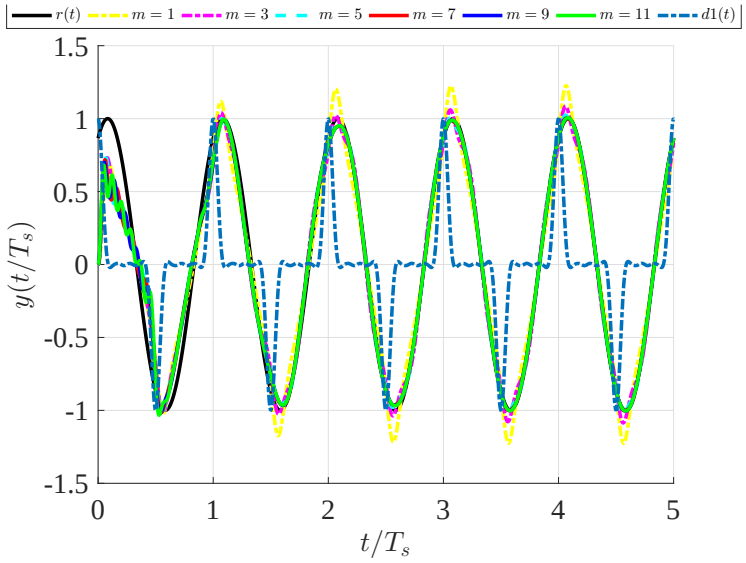

Source: created by the author.

Table 30 – Performance indicators for the closed-loop system of $G_2(s)$ with $T = 0.1$ and different orders of the PMR controller subject to disturbance $d(t)$

N	k_{pmr}	$k_{r_{11}}$	n_s	$M_{O_\%}$	M_s	GM	PM	$THD_\%$
1	4.81	1.06	–	10.4%	1.13	25.1dB	91.4°	7.36%
3	4.81	1.06	–	3.45%	1.22	21.8dB	103°	3.05%
5	4.81	1.06	2.99	0.49%	1.31	19.1dB	81.8°	1.18%
7	4.81	1.06	2.53	0%	1.46	16.9dB	58.7°	0.33%
9	4.81	1.06	2.53	0%	1.72	14.9dB	40.3°	0.07%
11	4.81	1.06	2.52	0.01%	2.37	12.9dB	25.9°	0%

Figure 50 – Comparison of normalized output signals of process $G_2(s)$ with $T = 0.1$ subject to disturbance $d(t)$ for PMR controller with odd multiples of ω_r up to m.

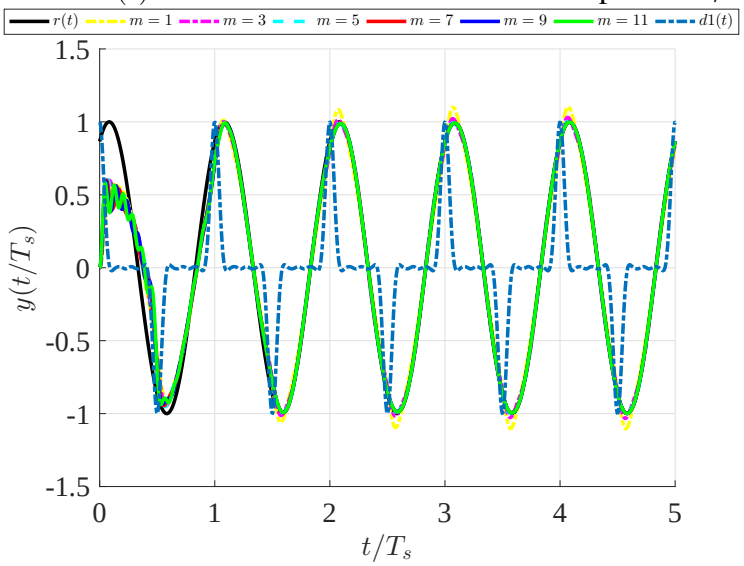

Source: created by the author.

Table 31 – Performance indicators for the closed-loop system of $G_3(s)$ with $\alpha = 0.1$ and different orders of the PMR controller subject to disturbance $d(t)$

N	k_{pmr}	$k_{r_{11}}$	n_s	$M_{O_\%}$	M_s	GM	PM	$THD_\%$
1	42.9	2.44	1.49	1.71%	1.16	25.6dB	68.5°	1.35%
3	42.9	2.44	1.49	7.32%	1.24	22.1dB	65.8°	0.42%
5	42.9	2.44	1.04	9.82%	1.34	19.4dB	56.1°	0.14%
7	42.9	2.44	1.04	9.97%	1.49	17.3dB	46.2°	0.03%
9	42.9	2.44	1.07	9.42%	1.75	15.3dB	36.8°	0.01%
11	42.9	2.44	1.07	8.96%	2.19	13.5dB	28°	0%

From the results presented, one can notice how the order of the PMR controller affects the resulting $THD_\%$ in the output. For lower orders of the PMR controller, for which not all harmonic components are considered by the controller, the distortion caused by the disturbance could restrain the output error from settling below the tolerance value $\epsilon < 2\%$. These cases are represented by "$-$" in the corresponding cells for the settling time n_s.

Figure 51 – Comparison of normalized output signals of process $G_3(s)$ with $\alpha = 0.1$ subject to disturbance $d(t)$ for PMR controller with odd multiples of ω_r up to m.

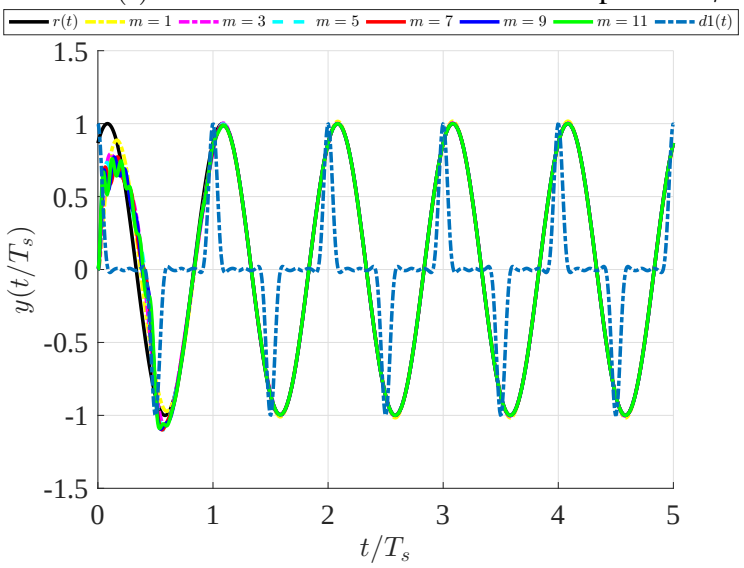

Source: created by the author.

5.6 Chapter Summary

This chapter has extended the method for the tuning of PR+Lead compensator with multiple modes of resonance for processes with and without ultimate frequency using series and parallel connections of the resonant modes. The new structures have been presented and discussed. The performance of the proposed method has been assessed for the classes of processes introduced in Chapter 2 for both series and parallel topologies. The results for the parallel topology of the PMR controller have shown more consistent values for the gain and phase margins and lower values for M_s with all classes of processes tested. The method has been evaluated with respect to harmonic disturbance rejection and the resulting total harmonic distortion. As expected, the results demonstrated that the $THD_{\%}$ in the output decreases as the order of the PMR controller increases, then it is able to deal with more harmonic frequency modes of the disturbance signal. The performance of the system in terms of the $THD_{\%}$ has greatly improved when compared with the results obtained in Section 4.5, even when considering a disturbance signal with the same amplitude of the reference signal.

6 CONCLUSION

This work proposed a systematic approach to determine the parameters of resonant controllers based on the knowledge of the plant frequency response, similar to the frequency response method for phase-lead and lag compensators. This approach enables to suitably employ the resonant controllers for reference tracking or disturbance rejection of periodic signals. The procedure allows to compute the controller parameters based on the process frequency response characteristics and tune each of them through a virtually independent process. In order to use the method, the knowledge of magnitude and phase at a limited number of points of the process frequency response suffice, essentially at the reference frequency ω_r, at its multiple harmonic modes $m\omega_r$ and at the ultimate frequency ω_u. The method presented differs from other techniques found in the control literature as it introduces a systematic methodology to compute the controller parameters with low computational effort, analogous to the classic methods of control theory for the tuning of phase lead-lag compensators, for instance.

Considering the stability margins and peak of sensitivity functions as indicators of closed-loop system performance, expressions for computation of the PR controller tuning parameters were developed. Via simple mathematical operations, it is possible to directly obtain a suitable set of parameters k_p and k_{r_1} to adjust the phase and gain margins virtually independently. Simulations with classes of processes found in typical control system problems shown that the method accomplished satisfactory results for frequencies of interest ω_r such that phase margin of the controlled system was higher than 30°. For the plants in the test batch this was achieved if the phase of the process at frequency ω_r was higher than -130° and one could choose k_{r_1} such that $C_{PR}(j\omega_r)G(j\omega_r) > -130^\circ$.

In order to improve the performance in an augmented bandwidth, the combination of the PR controller with a phase-lead compensator was proposed. The initial method was revised to obtain a new set of parameters that match the needs for the pre-compensated system. New simulations were carried out for the test batch and the obtained results were compared with those of the previous section. It was shown that the method accomplished satisfactory results for higher frequencies of interest ω_r, up to the ultimate frequency of the plants ω_u. The performance was greatly improved when compared to the results obtained

with a standard PR controller.

The performance of the method has been analysed regarding harmonic disturbance rejection in terms of the percent of total harmonic distortion in the output. The results for the PR controller and the PR+lead compensator were compared and the performance of the PR+lead compensator surpasses that of PR controller for the performance indices criteria analysed. However, as expected, the distortion of the output signal accentuates for disturbance signals with high harmonic content.

Finally, in order to cope with reference tracking and/or disturbance rejection of periodic signals with high harmonic content, the method has been extended to consider controllers with multiple peaks of resonance. The structure of the PR controller was revisited and series and parallel connections of resonant modes were considered. Expressions for computation of the PMR controller tuning parameters were developed for both series and parallel topologies. New simulations were carried out for the test batch. The results for the parallel topology of the PMR controller have shown more consistent values for the gain and phase margins and lower values for the peak value M_s than for the series topology. Also, the parallel topology is simpler to apply considering that it has less parameters to compute. The performance of the method for the PMR controller has been analysed regarding harmonic disturbance rejection in terms of the percent of total harmonic distortion in the output. It was shown, as expected, that the method accomplished satisfactory results in cases for which most of the harmonic modes of the disturbance is present in the dynamics of the PMR controller.

In future works, the performance of the method can be assessed for the implementation with actual systems. Compliance of the output signals to performance standards can be analysed and documented. Different processes, disturbance and reference signals can be used to evaluate the obtained performance. The proposed method can be thoroughly compared with other approaches for the tuning of resonant controllers in terms of computational effort, overall performance and concerns such as saturation of control signal.

REFERENCES

ABU-RUB, H.; MALINOWSKI, M.; AL-HADDAD, K. **Power electronics for renewable energy systems, transportation and industrial applications**. [S.l.]: John Wiley & Sons, 2014.

ÅSTRÖM, K. J.; HÄGGLUND, T. Revisiting the Ziegler–Nichols step response method for PID control. **Journal of process control**, [S.l.], v. 14, n. 6, p. 635–650, 2004.

ASTRÖM, K.; MURRAY, R. **Feedback Systems**: an introduction for scientists and engineers. [S.l.]: Princeton University Press, 2010.

BAO, C. *et al.* Step-by-step controller design for LCL-type grid-connected inverter with capacitor–current-feedback active-damping. **IEEE Transactions on Power Electronics**, [S.l.], v. 29, n. 3, p. 1239–1253, 2013.

BAZANELLA, A. S.; PEREIRA, L. F. A.; PARRAGA, A. A New Method for PID Tuning Including Plants Without Ultimate Frequency. **IEEE Transactions on Control Systems Technology**, [S.l.], v. 25, n. 2, p. 637–644, March 2017.

BENGTSSON, G. Output regulation and internal models – A frequency domain approach. **Automatica**, [S.l.], v. 13, n. 4, p. 333–345, 1977.

DAS, S. K.; POTA, H. R.; PETERSEN, I. R. Resonant controller design for a piezoelectric tube scanner: a mixed negative-imaginary and small-gain approach. **IEEE Transactions on Control Systems Technology**, [S.l.], v. 22, n. 5, p. 1899–1906, 2014.

FAIRBAIRN, M. W.; MOHEIMANI, S. R. A switched gain resonant controller to minimize image artifacts in intermittent contact mode atomic force microscopy. **IEEE transactions on nanotechnology**, [S.l.], v. 11, n. 6, p. 1126–1134, 2012.

FAROOQ, H.; ZHOU, C.; FARRAG, M. E. Analyzing the harmonic distortion in a distribution system caused by the non-linear residential loads. **International Journal of Smart Grid and Clean Energy**, [S.l.], v. 2, n. 1, p. 46–51, 2013.

FRANCIS, B. A.; WONHAM, W. M. The internal model principle of control theory. **Automatica**, [S.l.], v. 12, n. 5, p. 457–465, 1976.

FUKUDA, S.; YODA, T. A novel current-tracking method for active filters based on a sinusoidal internal model [for PWM invertors]. **IEEE Transactions on Industry Applications**, [S.l.], v. 37, n. 3, p. 888–895, 2001.

GRADY, W. M.; SANTOSO, S. Understanding power system harmonics. **IEEE Power Engineering Review**, [S.l.], v. 21, n. 11, p. 8–11, 2001.

HALIM, D.; MOHEIMANI, S. R. Spatial resonant control of flexible structures-application to a piezoelectric laminate beam. **IEEE transactions on control systems technology**, [S.l.], v. 9, n. 1, p. 37–53, 2001.

IEEE. **Std 519-1992, IEEE Recommended Practices and Requirements for Harmonic Control in Electrical Power Systems**. 1992. n. 519-1992.

LASCU, C. *et al.* Frequency response analysis of current controllers for selective harmonic compensation in active power filters. **IEEE Transactions on Industrial Electronics**, [S.l.], v. 56, n. 2, p. 337–347, 2008.

LING, J. *et al.* A robust resonant controller for high-speed scanning of nanopositioners: design and implementation. **IEEE Transactions on Control Systems Technology**, [S.l.], v. 28, n. 3, p. 1116–1123, 2019.

LORENZINI, C.; PEREIRA, L. F. A.; BAZANELLA, A. S. A Generalized Forced Oscillation Method for Tuning Proportional-Resonant Controllers. **IEEE Transactions on Control Systems Technology**, [S.l.], v. 28, n. 3, p. 1108–1115, 2020.

LORENZINI, C. *et al.* Resonant–repetitive controller with phase correction applied to uninterruptible power supplies. **Control Engineering Practice**, [S.l.], v. 77, p. 118–126, 2018.

LORENZINI, C. *et al.* Single-phase uninterruptible power supply control: a model-free proportional-multi-resonant method. **IEEE Transactions on Industrial Electronics**, [S.l.], p. 1–1, 2021.

MAHMOOD, I. A.; MOHEIMANI, S. R.; BHIKKAJI, B. Precise tip positioning of a flexible manipulator using resonant control. **IEEE/ASME Transactions on Mechatronics**, [S.l.], v. 13, n. 2, p. 180–186, 2008.

MESSNER, W. C. *et al.* Lead and lag compensators with complex poles and zeros design formulas for modeling and loop shaping. **IEEE Control Systems Magazine**, [S.l.], v. 27, n. 1, p. 44–54, 2007.

MOHEIMANI, S. R.; VAUTIER, B. J. Resonant control of structural vibration using charge-driven piezoelectric actuators. **IEEE Transactions on control systems technology**, [S.l.], v. 13, n. 6, p. 1021–1035, 2005.

MORARI, M.; ZAFIRIOU, M.; ZAFIRIOU, E. **Robust Process Control**. [S.l.]: Prentice Hall, 1989.

MOSSMANN, B. H.; PEREIRA, L. F. A.; GOMES DA SILVA JR, J. M. Síntese de parâmetros de controladores Proporcionais-Ressonantes através do método da resposta em frequência. *In*: XIV SIMPÓSIO BRASILEIRO DE AUTOMAÇÃO INTELIGENTE, 2019. **Anais [...]** [S.l.: s.n.], 2019.

MOSSMANN, B. H.; PEREIRA, L. F. A.; GOMES DA SILVA JR, J. M. Tuning of Proportional-Resonant Controllers Combined with Phase-Lead Compensators Based on the Frequency Response. **Journal of Control, Automation and Electrical Systems**, [S.l.], p. 1–17, 2021.

NEJABATKHAH, F.; LI, Y. W. Overview of power management strategies of hybrid AC/DC microgrid. **IEEE Transactions on Power Electronics**, [S.l.], v. 30, n. 12, p. 7072–7089, 2014.

NGUYEN, K. L. *et al.* Robustness of a resonant controller for a multiphase induction heating system. **IEEE Transactions on Industry Applications**, [S.l.], v. 51, n. 1, p. 73–81, 2014.

OPPENHEIM, A.; WILLSKY, A.; NAWAB, S. **Signals and Systems**. [S.l.]: Prentice Hall, 1997. (Prentice-Hall signal processing series).

PEREIRA, L. F. A.; BAZANELLA, A. S. Tuning rules for Proportional Resonant controllers. **IEEE Transactions on Control Systems Technology**, [S.l.], v. 23, n. 5, p. 2010–2017, 2015.

PEREIRA, L. F. A. *et al.* Multiple resonant controllers for Uninterruptible Power Supplies: a systematic robust control design approach. **IEEE Transactions on Industrial Electronics**, [S.l.], v. 61, n. 3, p. 1528–1538, 2014.

RODRÍGUEZ, J. R. *et al.* PWM regenerative rectifiers: state of the art. **IEEE Transactions on Industrial Electronics**, [S.l.], v. 52, n. 1, p. 5–22, 2005.

SALEHIFAR, M. *et al.* Observer-based open transistor fault diagnosis and fault-tolerant control of five-phase permanent magnet motor drive for application in electric vehicles. **IET Power Electronics**, [S.l.], v. 8, n. 1, p. 76–87, 2014.

SATO, Y. *et al.* A new control strategy for voltage-type PWM rectifiers to realize zero steady-state control error in input current. **IEEE Transactions on Industry Applications**, [S.l.], v. 34, n. 3, p. 480–486, 1998.

SETH, A. K.; SINGH, M. Resonant controller of single-stage off-board EV charger in G2V and V2G modes. **IET Power Electronics**, [S.l.], v. 13, n. 5, p. 1086–1092, 2020.

SHEN, G. *et al.* A new feedback method for PR current control of LCL-filter-based grid-connected inverter. **IEEE Transactions on Industrial Electronics**, [S.l.], v. 57, n. 6, p. 2033–2041, 2010.

SU, Z. *et al.* Improving operational performance of magnetically suspended flywheel with PM-biased magnetic bearings using adaptive resonant controller and nonlinear compensation method. **IEEE Transactions on Magnetics**, [S.l.], v. 52, n. 7, p. 1–4, 2016.

TEODORESCU, R. *et al.* Proportional-resonant controllers and filters for grid-connected voltage-source converters. **IEE Proceedings – Electric Power Applications**, [S.l.], v. 153, n. 5, p. 750–762, 2006.

TIMBUS, A. *et al.* Evaluation of current controllers for distributed power generation systems. **IEEE Transactions on Power Electronics**, [S.l.], v. 24, n. 3, p. 654–664, 2009.

WU, W. *et al.* A new design method for the passive damped LCL and LLCL filter-based single-phase grid-tied inverter. **IEEE Transactions on Industrial Electronics**, [S.l.], v. 60, n. 10, p. 4339–4350, 2012.

YEPES, A. G. *et al.* Effects of discretization methods on the performance of resonant controllers. **IEEE Transactions on Power Electronics**, [S.l.], v. 25, n. 7, p. 1692–1712, 2010.

APPENDIX A ADDITIONAL SIMULATION RESULTS

A.1 More Examples for the PR Controller

Tables 32 to 37 summarise the results achieved for different ratios between ω_r and ω_u for processes $G_1(s)$, $G_2(s)$ and $G_3(s)$. Tables 38 to 43 summarise the results achieved for different ratios between ω_r and ω_{-20dB} for processes $G_4(s)$, $G_5(s)$ and $G_6(s)$. These tables present the obtained values for settling time n_s, maximum percent overshoot $M_{O_\%}$, peak of sensitivity function M_s, phase margin PM and gain margin GM of the controlled system, as well as the phase of process $G(j\omega)$ at frequency ω_r. All simulation tests produced a stable response, despite the considerably higher settling time for frequencies ω_r close to the ultimate frequency ω_u.

Table 32 – Tuning parameters and performance indicators for the closed-loop system of $G_1(s)$ with $n = 4$ and different values of ω_r.

ω_r	k_p	k_{r_1}	n_s	$M_{O_\%}$	M_s	GM	PM	$\angle G(j\omega_r)$
$0.1\omega_u$	0.20	0.14	2.24	0%	1.19	$18.7dB$	$95.1°$	$-23°$
$0.25\omega_u$	0.19	0.34	2.35	1.72%	1.37	$15.8dB$	$51.8°$	$-56.2°$
$0.5\omega_u$	0.17	0.11	11.21	3.64%	1.41	$18.5dB$	$47.2°$	$-106°$
$0.75\omega_u$	0.12	0.01	46.56	20.51%	2.11	$19.9dB$	$28.7°$	$-148°$
$0.9\omega_u$	0.06	0.01	> 50	59.6%	5.79	$19.5dB$	$9.96°$	$-169°$

Table 33 – Tuning parameters and performance indicators for the closed-loop system of $G_1(s)$ with $n = 5$ and different values of ω_r.

ω_r	k_p	k_{r_1}	n_s	$M_{O_\%}$	M_s	GM	PM	$\angle G(j\omega_r)$
$0.1\omega_u$	0.14	0.1	3.20	0%	1.15	$19.0dB$	$95.8°$	$-28°$
$0.25\omega_u$	0.14	0.25	3.34	0.74%	1.25	$16.8dB$	$58°$	$-51.6°$
$0.5\omega_u$	0.12	0.1	13.2	3.42%	1.37	$18.5dB$	$48.5°$	$-100°$
$0.75\omega_u$	0.09	0.005	44.22	15.21%	1.85	$19.9dB$	$33.2°$	$-143°$
$0.9\omega_u$	0.05	0.006	> 50	54.16%	4.91	$19.5dB$	$11.8°$	$-166°$

Table 34 – Tuning parameters and performance indicators for the closed-loop system of $G_2(s)$ with $T = 0.5$ and different values of ω_r.

ω_r	k_p	k_{r_1}	n_s	$M_{O_\%}$	M_s	GM	PM	$\angle G(j\omega_r)$
$0.1\omega_u$	0.27	0.36	1.73	0%	1.23	$18.2dB$	$93.4°$	$-25.2°$
$0.25\omega_u$	0.26	0.9	1.80	3.12%	1.52	$14.4dB$	$46.2°$	$-60.2°$
$0.5\omega_u$	0.23	0.22	9.22	3.32%	1.44	$18.5dB$	$46.7°$	$-111°$
$0.75\omega_u$	0.17	0.02	48.82	26.08%	2.39	$19.8dB$	$24.9°$	$-151°$
$0.9\omega_u$	0.09	0.02	> 50	65.68%	7.12	$19.3dB$	$8.09°$	$-170°$

Table 35 – Tuning parameters and performance indicators for the closed-loop system of $G_2(s)$ with $T = 1$ and different values of ω_r.

ω_r	k_p	k_{r_1}	n_s	$M_{O_\%}$	M_s	GM	PM	$\angle G(j\omega_r)$
$0.1\omega_u$	0.24	0.21	1.79	0%	1.24	$18dB$	$98.3°$	$-21.4°$
$0.25\omega_u$	0.23	0.53	1.83	0.48%	1.49	$14dB$	$51.7°$	$-53.9°$
$0.5\omega_u$	0.21	0.16	8.63	3.55%	1.48	$18dB$	$45.7°$	$-108°$
$0.75\omega_u$	0.15	0.01	47.8	26.82%	2.44	$19.7dB$	$24.5°$	$-151°$
$0.9\omega_u$	0.08	0.01	> 50	66.6%	7.29	$19.2dB$	$7.82°$	$-171°$

Table 36 – Tuning parameters and performance indicators for the closed-loop system of $G_3(s)$ with $\alpha = 0.9$ and different values of ω_r.

ω_r	k_p	k_{r_1}	n_s	$M_{O_\%}$	M_s	GM	PM	$\angle G(j\omega_r)$
$0.1\omega_u$	0.20	0.16	2.23	0%	1.19	$18.6dB$	$96°$	$-23°$
$0.25\omega_u$	0.20	0.40	2.34	1.79%	1.38	$15.7dB$	$51.4°$	$-56.5°$
$0.5\omega_u$	0.17	0.13	11.18	3.76%	1.42	$18.5dB$	$46.9°$	$-106°$
$0.75\omega_u$	0.12	0.008	46.52	20.67%	2.12	$19.8dB$	$28.6°$	$-148°$
$0.9\omega_u$	0.07	0.009	> 50	59.51%	5.77	$19.5dB$	$9.99°$	$-167°$

Table 37 – Tuning parameters and performance indicators for the closed-loop system of $G_3(s)$ with $\alpha = 5$ and different values of ω_r.

ω_r	k_p	k_{r_1}	n_s	$M_{O_\%}$	M_s	GM	PM	$\angle G(j\omega_r)$
$0.1\omega_u$	1.50	0.01	0.56	6.38%	1.61	$17.5dB$	$45.8°$	$-64°$
$0.25\omega_u$	1.46	0.005	1.92	0.08%	1.54	$18.9dB$	$45.6°$	$-107°$
$0.5\omega_u$	1.29	3.90×10^{-4}	12.28	15.87%	1.95	$19.9dB$	$31.7°$	$-143°$
$0.75\omega_u$	0.92	5.85×10^{-4}	> 50	51.69%	4.5	$19.7dB$	$12.9°$	$-165°$
$0.9\omega_u$	0.48	7.02×10^{-4}	> 50	81.33%	13.95	$18.8dB$	$4.1°$	$-175°$

Table 38 – Tuning parameters and performance indicators for the closed-loop system of $G_4(s)$ with $\alpha = 0.9$ and different values of ω_r.

ω_r	k_p	k_{r_1}	n_s	$M_{O_\%}$	M_s	GM	PM	$\angle G(j\omega_r)$
$0.1\omega_{-20dB}$	0.70	1.23	0.94	0%	1	∞	$77.9°$	$-45°$
$0.25\omega_{-20dB}$	1.35	2.02	1.40	0.38%	1	∞	$69.7°$	$-68.2°$
$0.5\omega_{-20dB}$	2.56	2.78	1.53	0.10%	1	∞	$70.6°$	$-78.7°$
$0.75\omega_{-20dB}$	3.79	3.62	1.92	0.04%	1	∞	$70.8°$	$-82.4°$
ω_{-20dB}	5	4.5	1.95	0.03%	1	∞	$70.8°$	$-84.3°$

Table 39 – Tuning parameters and performance indicators for the closed-loop system of $G_4(s)$ with $\alpha = 5$ and different values of ω_r.

ω_r	k_p	k_{r_1}	n_s	$M_{O_\%}$	M_s	GM	PM	$\angle G(j\omega_r)$
$0.1\omega_{-20dB}$	0.70	6.87	0.94	0%	1	∞	77.9°	$-45°$
$0.25\omega_{-20dB}$	1.35	11.27	1.40	0.38%	1	∞	69.7°	$-68.2°$
$0.5\omega_{-20dB}$	2.56	15.44	1.53	0.10%	1	∞	70.6°	$-78.7°$
$0.75\omega_{-20dB}$	3.79	20.11	1.92	0.04%	1	∞	70.8°	$-82.4°$
ω_{-20dB}	5	25	1.95	0.03%	1	∞	70.8°	$-84.3°$

Table 40 – Tuning parameters and performance indicators for the closed-loop system of $G_5(s)$ with $\alpha = 0.9$ and different values of ω_r.

ω_r	k_p	k_{r_1}	n_s	$M_{O_\%}$	M_s	GM	PM	$\angle G(j\omega_r)$
$0.1\omega_{-20dB}$	0.54	0.39	0.76	0%	1.21	∞	77.7°	$-33.4°$
$0.25\omega_{-20dB}$	0.78	0.53	1.01	0.06%	1.42	∞	50°	$-73.7°$
$0.5\omega_{-20dB}$	1.62	0.23	1.46	0.68%	1.57	∞	42.9°	$-112°$
$0.75\omega_{-20dB}$	3.01	0.02	2.57	6.99%	1.78	∞	36.5°	$-132°$
ω_{-20dB}	5	0.02	3.64	19.05%	2.21	∞	27.8°	$-143°$

Table 41 – Tuning parameters and performance indicators for the closed-loop system of $G_5(s)$ with $\alpha = 5$ and different values of ω_r.

ω_r	k_p	k_{r_1}	n_s	$M_{O_\%}$	M_s	GM	PM	$\angle G(j\omega_r)$
$0.1\omega_{-20dB}$	0.59	0.85	0.70	0%	1.14	∞	76.5°	$-39.1°$
$0.25\omega_{-20dB}$	0.96	1.11	1.41	0.05%	1.26	∞	56.6°	$-74.3°$
$0.5\omega_{-20dB}$	1.92	0.76	1.56	0%	1.42	∞	48.7°	$-104°$
$0.75\omega_{-20dB}$	3.27	0.37	2.02	1.30%	1.80	∞	42.7°	$-121°$
ω_{-20dB}	5	0.05	2.53	6.12%	1.75	∞	37.3°	$-132°$

Table 42 – Tuning parameters and performance indicators for the closed-loop system of $G_6(s)$ with $\alpha = 0.5$ and different values of ω_r.

ω_r	k_p	k_{r_1}	n_s	$M_{O_\%}$	M_s	GM	PM	$\angle G(j\omega_r)$
$0.1\omega_{-20dB}$	0.48	0.44	1.23	0.08%	1.58	∞	58.2°	$-20°$
$0.25\omega_{-20dB}$	0.44	0.76	2.57	20.04%	2.46	∞	26.3°	$-67.4°$
$0.5\omega_{-20dB}$	1.14	0.01	4.04	14.25%	2.03	∞	31.2°	$-135°$
$0.75\omega_{-20dB}$	2.72	0.02	6.31	36.81%	3.14	∞	18.9°	$-153°$
ω_{-20dB}	5	0.03	7.89	51.96%	4.30	∞	13.6°	$-161°$

Table 43 – Tuning parameters and performance indicators for the closed-loop system of $G_6(s)$ with $\alpha = 0.9$ and different values of ω_r.

ω_r	k_p	k_{r_1}	n_s	$M_{O_\%}$	M_s	GM	PM	$\angle G(j\omega_r)$
$0.1\omega_{-20dB}$	0.53	0.42	0.77	0%	1.24	∞	77.6°	−31.3°
$0.25\omega_{-20dB}$	0.72	0.59	0.96	0.96%	1.49	∞	46.7°	−73°
$0.5\omega_{-20dB}$	1.54	0.19	2.02	1.47%	1.62	∞	41.5°	−116°
$0.75\omega_{-20dB}$	2.98	0.02	2.57	10.98%	1.92	∞	33.1°	−136°
ω_{-20dB}	5	0.03	3.92	24.17%	2.44	∞	25°	−147°

A.2 More Examples for the PR+Lead Compensator

Tables 44 to 49 summarise the results achieved for different ratios between ω_r and ω_u for processes $G_1(s)$, $G_2(s)$ and $G_3(s)$. Tables 50 and 51 summarise the results achieved for different ratios between ω_r and ω_{-20dB} for process $G_6(s)$. These tables present the obtained values for settling time n_s, maximum percent overshoot $M_{O_\%}$, peak of sensitivity function M_s, phase margin PM and gain margin GM of the final controlled system, as well as the original phase margin of process $G(j\omega)$ at the frequency of interest. All simulation tests produced a stable response.

Table 44 – Tuning parameters and performance indicators for the closed-loop system of $G_1(s)$ with $n = 4$ and different values of ω_r for PR+lead compensator.

ω_r	k_p	k_{r_1}	n_s	$M_{O_\%}$	M_s	GM	PM	$\angle G(j\omega_r)$
$0.5\omega_u$	1.31	0.69	2.68	3.35%	1.56	$13.9dB$	45.2°	−106°
$0.75\omega_u$	1.21	0.26	8.71	2.89%	1.40	$17.7dB$	48.4°	−148°
$0.9\omega_u$	1.12	0.14	13.59	4.31%	1.45	$18.7dB$	45.8°	−169°
ω_u	1.04	0.04	17.12	4.33%	1.43	$19.6dB$	46.3°	−180°

Table 45 – Tuning parameters and performance indicators for the closed-loop system of $G_1(s)$ with $n = 5$ and different values of ω_r for PR+lead compensator.

ω_r	k_p	k_{r_1}	n_s	$M_{O_\%}$	M_s	GM	PM	$\angle G(j\omega_r)$
$0.5\omega_u$	0.72	0.50	4.29	0.91%	1.34	$15.1dB$	54.5°	−100°
$0.75\omega_u$	0.65	0.23	12.65	3.40%	1.37	$17.6dB$	48.5°	−143°
$0.9\omega_u$	0.59	0.11	19.17	3.92%	1.40	$18.7dB$	47.5°	−166°
ω_u	0.53	0.03	25.12	4.81%	1.43	$19.5dB$	46°	−180°

Table 46 – Tuning parameters and performance indicators for the closed-loop system of $G_2(s)$ with $T = 0.5$ and different values of ω_r for PR+lead compensator.

ω_r	k_p	k_{r_1}	n_s	$M_{O_\%}$	M_s	GM	PM	$\angle G(j\omega_r)$
$0.5\omega_u$	3.47	1.40	1.34	7.32%	1.92	$13.4dB$	$38.1°$	$-111°$
$0.75\omega_u$	3.33	0.61	3.22	3.17%	1.63	$17.3dB$	$42.7°$	$-151°$
$0.9\omega_u$	3.20	0.31	5.58	5.10%	1.61	$18.6dB$	$42°$	$-170°$
ω_u	3.10	0.11	7.14	5.74%	1.60	$19.5dB$	$42°$	$-180°$

Table 47 – Tuning parameters and performance indicators for the closed-loop system of $G_2(s)$ with $T = 1$ and different values of ω_r for PR+lead compensator.

ω_r	k_p	k_{r_1}	n_s	$M_{O_\%}$	M_s	GM	PM	$\angle G(j\omega_r)$
$0.5\omega_u$	3.17	0.83	1.61	9.83%	1.98	$13.5dB$	$36.3°$	$-108°$
$0.75\omega_u$	3.04	0.36	3.12	3.97%	1.65	$17.4dB$	$41.8°$	$-151°$
$0.9\omega_u$	2.94	0.17	5.14	4.85%	1.60	$18.8dB$	$42.4°$	$-171°$
ω_u	2.85	0.07	7.03	5.72%	1.60	$19.5dB$	$41.9°$	$-180°$

Table 48 – Tuning parameters and performance indicators for the closed-loop system of $G_3(s)$ with $\alpha = 0.9$ and different values of ω_r for PR+lead compensator.

ω_r	k_p	k_{r_1}	n_s	$M_{O_\%}$	M_s	GM	PM	$\angle G(j\omega_r)$
$0.5\omega_u$	1.32	0.80	2.68	3.49%	1.57	$13.9dB$	$45°$	$-106°$
$0.75\omega_u$	1.22	0.32	8.69	3.34%	1.41	$17.6dB$	$47.4°$	$-148°$
$0.9\omega_u$	1.13	0.16	13.17	4.28%	1.45	$18.7dB$	$45.9°$	$-167°$
ω_u	1.06	0.05	17.13	4.73%	1.46	$19.6dB$	$45.5°$	$-180°$

Table 49 – Tuning parameters and performance indicators for the closed-loop system of $G_3(s)$ with $\alpha = 5$ and different values of ω_r for PR+lead compensator.

ω_r	k_p	k_{r_1}	n_s	$M_{O_\%}$	M_s	GM	PM	$\angle G(j\omega_r)$
$0.5\omega_u$	17.13	0.016	2.47	0.14%	1.33	$18.9dB$	54.2°	$-143°$
$0.75\omega_u$	16.60	0.012	4.71	1.63%	1.39	$19.1dB$	48.7°	$-165°$
$0.9\omega_u$	16.16	0.007	6.24	2.60%	1.43	$19.4dB$	47°	$-175°$
ω_u	15.81	0.004	7.68	3.44%	1.46	$19.7dB$	45.9°	$-180°$

Table 50 – Tuning parameters and performance indicators for the closed-loop system of $G_6(s)$ with $\alpha = 0.5$ and different values of ω_r for PR+lead compensator.

ω_r	k_p	k_{r_1}	n_s	$M_{O_\%}$	M_s	GM	PM	$\angle G(j\omega_r)$
$0.1\omega_{-20dB}$	4.51	0.45	1.40	0.39%	1.08	∞	84.6°	$-20°$
$0.25\omega_{-20dB}$	3.46	1.11	0.96	0.30%	1.23	∞	56.6°	$-67.4°$
$0.5\omega_{-20dB}$	6.22	0.76	1.83	0.73%	1.17	∞	57.9°	$-135°$
$0.75\omega_{-20dB}$	10.94	0.70	1.91	0.11%	1.21	∞	57.3°	$-153°$
ω_{-20dB}	15.81	0.72	1.91	0.02%	1.27	∞	54.4°	$-161°$

Table 51 – Tuning parameters and performance indicators for the closed-loop system of $G_6(s)$ with $\alpha = 0.9$ and different values of ω_r for PR+lead compensator.

ω_r	k_p	k_{r_1}	n_s	$M_{O_\%}$	M_s	GM	PM	$\angle G(j\omega_r)$
$0.5\omega_{-20dB}$	8.30	1.43	1.23	0.54%	1.17	∞	59.9°	$-116°$
$0.75\omega_{-20dB}$	11.86	1.27	1.50	0.05%	1.20	∞	59.1°	$-136°$
ω_{-20dB}	15.81	1.19	1.56	0%	1.24	∞	56.8°	$-147°$

A.3 More Examples for the Parallel Topology of the PMR Controller

Tables 52 to 57 summarise the results achieved for processes $G_1(s)$, $G_2(s)$ and $G_3(s)$ with reference signal $r(t)$ subject to disturbance $d(t)$ composed by harmonic components odd multiples of the fundamental frequency ω_r up to N. Tables 58 to 63 summarise the results achieved for processes $G_4(s)$, $G_5(s)$ and $G_6(s)$. The tables present the obtained values for settling time n_s, maximum percent overshoot $M_{O_\%}$, peak of sensitivity function M_s, phase margin PM and gain margin GM of the final controlled system. All simulation tests produced a stable response.

Table 52 – Tuning parameters and performance indicators for the closed-loop system of $G_1(s)$ with $n = 4$ and odd multiples of ω_r up to N for PMR controller.

ω_r	N	k_{pmr}	$k_{r_{11}}$	n_s	$M_{O_\%}$	M_s	GM	PM
$0.40\ rad/s$	3	0.66	0.54	10.53	4.82%	2.38	$16.2dB$	25.1°
$0.24\ rad/s$	5	0.68	0.33	6.59	0.07%	2.31	$15.6dB$	26.1°
$0.17\ rad/s$	7	0.68	0.23	6.67	0.01%	2.29	$14.3dB$	26.4°
$0.13\ rad/s$	9	0.68	0.18	7.73	0.58%	2.28	$13.1dB$	26.6°
$0.11\ rad/s$	11	0.68	0.15	9.76	1.96%	2.29	$11.9dB$	26.5°

Table 53 – Tuning parameters and performance indicators for the closed-loop system of $G_1(s)$ with $n = 5$ and odd multiples of ω_r up to N for PMR controller.

ω_r	N	k_{pmr}	$k_{r_{11}}$	n_s	$M_{O_\%}$	M_s	GM	PM
$0.28\ rad/s$	3	0.37	0.38	14.84	4.51%	2.31	$16.0dB$	26.3°
$0.17\ rad/s$	5	0.38	0.23	10.24	0%	2.26	$15.2dB$	26.8°
$0.12\ rad/s$	7	0.38	0.16	11.71	0.04%	2.22	$13.9dB$	27.4°
$0.09\ rad/s$	9	0.38	0.13	14.24	1.01%	2.27	$12.6dB$	26.7°
$0.08\ rad/s$	11	0.38	0.10	17.81	3.00%	2.27	$11.4dB$	26.8°

Table 54 – Tuning parameters and performance indicators for the closed-loop system of $G_2(s)$ with $T = 0.5$ and odd multiples of ω_r up to N for PMR controller.

ω_r	N	k_{pmr}	$k_{r_{11}}$	n_s	$M_{O_{\%}}$	M_s	GM	PM
$1.09\ rad/s$	3	1.75	1.50	5.19	4.68%	2.49	$16.3dB$	24.2°
$0.65\ rad/s$	5	1.77	0.90	2.80	0.15%	2.37	$16.2dB$	25.6°
$0.47\ rad/s$	7	1.78	0.64	2.70	0.09%	2.35	$15.1dB$	25.9°
$0.36\ rad/s$	9	1.78	0.50	3.73	1.20%	2.37	$13.9dB$	25.9°
$0.30\ rad/s$	11	1.79	0.41	5.13	2.94%	2.42	$12.7dB$	25.5°

Table 55 – Tuning parameters and performance indicators for the closed-loop system of $G_2(s)$ with $T = 1$ and odd multiples of ω_r up to N for PMR controller.

ω_r	N	k_{pmr}	$k_{r_{11}}$	n_s	$M_{O_{\%}}$	M_s	GM	PM
$0.65\ rad/s$	3	1.60	0.90	5.19	4.62%	2.47	$16.4dB$	24.3°
$0.39\ rad/s$	5	1.62	0.54	2.82	0.18%	2.36	$16.3dB$	25.7°
$0.28\ rad/s$	7	1.62	0.38	3.20	0.34%	2.33	$15.2dB$	26.1°
$0.22\ rad/s$	9	1.63	0.30	4.30	2.47%	2.36	$14.0dB$	25.9°
$0.18\ rad/s$	11	1.63	0.24	6.76	5.80%	2.54	$12.8dB$	25.7°

Table 56 – Tuning parameters and performance indicators for the closed-loop system of $G_3(s)$ with $\alpha = 0.9$ and odd multiples of ω_r up to N for PMR controller.

ω_r	N	k_{pmr}	$k_{r_{11}}$	n_s	$M_{O_\%}$	M_s	GM	PM
$0.46\ rad/s$	3	0.67	0.64	10.36	4.68%	2.33	$16.4dB$	25.8°
$0.28\ rad/s$	5	0.69	0.38	6.12	0.06%	2.28	$15.7dB$	26.6°
$0.20\ rad/s$	7	0.69	0.27	6.67	0.01%	2.23	$14.5dB$	27.1°
$0.15\ rad/s$	9	0.69	0.21	7.72	0.57%	2.23	$13.2dB$	27.2°
$0.13\ rad/s$	11	0.69	0.17	9.27	1.94%	2.24	$12.0dB$	27.1°

Table 57 – Tuning parameters and performance indicators for the closed-loop system of $G_3(s)$ with $\alpha = 5$ and odd multiples of ω_r up to N for PMR controller.

ω_r	N	k_{pmr}	$k_{r_{11}}$	n_s	$M_{O_\%}$	M_s	GM	PM
$0.042\ rad/s$	3	8.59	0.016	5.85	2.67%	2.15	$19.9dB$	28°
$0.025\ rad/s$	5	8.70	0.017	2.92	1.52%	2.16	$17.6dB$	28°
$0.018\ rad/s$	7	8.73	0.017	1.94	1.58%	2.16	$15.8dB$	27.9°
$0.014\ rad/s$	9	8.75	0.019	1.45	9.14%	2.20	$14.3dB$	27.6°
$0.012\ rad/s$	11	8.75	0.016	1.38	7.82%	2.20	$13.1dB$	27.8°

Table 58 – Tuning parameters and performance indicators for the closed-loop system of $G_4(s)$ with $\alpha = 0.9$ and odd multiples of ω_r up to N for PMR controller.

ω_r	N	k_{pmr}	$k_{r_{11}}$	n_s	$M_{O_{\%}}$	M_s	GM	PM
$3.00\ rad/s$	3	0.87	2.22	3.68	3.02%	1.08	∞	89.1°
$1.80\ rad/s$	5	0.56	1.56	3.13	2.80%	1.07	∞	90.3°
$1.28\ rad/s$	7	0.44	1.11	3.01	0.79%	1.08	∞	90.8°
$1.00\ rad/s$	9	0.37	0.86	3.03	0%	1.09	∞	91°
$0.82\ rad/s$	11	0.34	0.71	3.04	0%	1.11	∞	91.1°

Table 59 – Tuning parameters and performance indicators for the closed-loop system of $G_4(s)$ with $\alpha = 5$ and odd multiples of ω_r up to N for PMR controller.

ω_r	N	k_{pmr}	$k_{r_{11}}$	n_s	$M_{O_{\%}}$	M_s	GM	PM
$16.67\ rad/s$	3	0.87	12.35	3.68	3.03%	1.08	∞	89.1°
$10\ rad/s$	5	0.56	8.66	3.13	2.80%	1.07	∞	90.3°
$7.14\ rad/s$	7	0.44	6.19	3.01	0.79%	1.08	∞	90.8°
$5.56\ rad/s$	9	0.37	4.81	3.03	0%	1.09	∞	91°
$4.55\ rad/s$	11	0.34	3.94	3.04	0%	1.11	∞	91.1°

Table 60 – Tuning parameters and performance indicators for the closed-loop system of $G_5(s)$ with $\alpha = 0.9$ and odd multiples of ω_r up to N for PMR controller.

ω_r	N	k_{pmr}	$k_{r_{11}}$	n_s	$M_{O_{\%}}$	M_s	GM	PM
$4.90\ rad/s$	3	14.06	1.04	5.55	3.86%	2.02	∞	29.7°
$2.94\ rad/s$	5	8.18	1.28	5.03	3.64%	2.00	∞	30°
$2.10\ rad/s$	7	5.93	1.34	4.53	3.24%	1.99	∞	30.2°
$1.63\ rad/s$	9	4.87	1.41	4.02	3.02%	1.99	∞	30.2°
$1.34\ rad/s$	11	4.20	1.16	3.52	0.33%	1.98	∞	30.3°

Table 61 – Tuning parameters and performance indicators for the closed-loop system of $G_5(s)$ with $\alpha = 5$ and odd multiples of ω_r up to N for PMR controller.

ω_r	N	k_{pmr}	$k_{r_{11}}$	n_s	$M_{O_{\%}}$	M_s	GM	PM
$11.83\ rad/s$	3	14.55	3.01	5.08	3.98%	2.03	∞	29.7°
$7.10\ rad/s$	5	8.77	3.81	4.54	3.49%	2.01	∞	30°
$5.07\ rad/s$	7	6.89	4.39	3.55	4.53%	2.00	∞	30.1°
$3.94\ rad/s$	9	5.86	3.42	3.03	0.18%	1.98	∞	30.3°
$3.23\ rad/s$	11	5.28	2.79	2.98	0.35%	1.98	∞	30.4°

Table 62 – Tuning parameters and performance indicators for the closed-loop system of $G_6(s)$ with $\alpha = 0.5$ and odd multiples of ω_r up to N for PMR controller.

ω_r	N	k_{pmr}	$k_{r_{11}}$	n_s	$M_{O_{\%}}$	M_s	GM	PM
$4.83\ rad/s$	3	13.12	0.65	5.55	3.75%	2.02	∞	29.8°
$2.90\ rad/s$	5	6.88	0.71	5.54	3.07%	2.00	∞	30°
$2.07\ rad/s$	7	4.34	0.70	5.54	2.84%	1.99	∞	30.1°
$1.61\ rad/s$	9	3.08	0.78	5.53	3.58%	1.99	∞	30.2°
$1.32\ rad/s$	11	2.36	0.94	4.54	5.03%	1.99	∞	30.2°

Table 63 – Tuning parameters and performance indicators for the closed-loop system of $G_6(s)$ with $\alpha = 0.9$ and odd multiples of ω_r up to N for PMR controller.

ω_r	N	k_{pmr}	$k_{r_{11}}$	n_s	$M_{O_{\%}}$	M_s	GM	PM
$5.13\ rad/s$	3	14.06	0.99	5.54	3.71%	2.03	∞	29.6°
$3.08\ rad/s$	5	8.00	1.20	5.04	3.35%	2.01	∞	29.9°
$2.20\ rad/s$	7	5.73	1.27	4.54	3.04%	2.00	∞	30°
$1.71\ rad/s$	9	4.55	1.37	4.03	3.17%	1.99	∞	30.1°
$1.40\ rad/s$	11	3.87	1.21	3.53	0.88%	1.99	∞	30.2°

A.4 More Examples for the Disturbance Rejection with PMR controller

Tables 64 to 69 summarise the results achieved for different orders of the PMR controller. For each process, The fundamental frequency ω_r is selected such that the phase of the pre-compensated system is equal to $-145°$ at the 11^{th} harmonic frequency. These tables present the obtained values for settling time n_s, maximum percent overshoot $M_{O_\%}$ and percent of total harmonic distortion $THD_\%$ of the final controlled system.

Table 64 – Performance indicators for the closed-loop system of $G_1(s)$ with $n = 4$ and different orders of the PMR controller subject to disturbance $d(t)$

N	k_{pmr}	$k_{r_{11}}$	n_s	$M_{O_\%}$	M_s	GM	PM	$THD_\%$
1	0.69	0.09	–	38.04%	1.08	25.5dB	117°	24.49%
3	0.69	0.09	–	17.22%	1.83	22dB	139°	12.08%
5	0.69	0.09	–	5.90%	1.84	19.2dB	106°	4.90%
7	0.69	0.09	12.56	1.38%	1.84	16.9dB	75.2°	1.34%
9	0.69	0.09	9.71	0.78%	1.83	14.6dB	48.8°	0.30%
11	0.69	0.09	9.72	0.94%	2.27	12dB	26.7°	0%

Table 65 – Performance indicators for the closed-loop system of $G_1(s)$ with $n = 5$ and different orders of the PMR controller subject to disturbance $d(t)$

N	k_{pmr}	$k_{r_{11}}$	n_s	$M_{O_\%}$	M_s	GM	PM	$THD_\%$
1	0.38	0.07	–	44.94%	1.07	25.6dB	117°	15.36%
3	0.38	0.07	–	22.18%	2.13	22dB	148°	6.40%
5	0.38	0.07	–	8.46%	2.12	19.3dB	118°	2.38%
7	0.38	0.07	–	2.50%	2.12	16.9dB	84.9°	0.63%
9	0.38	0.07	18.78	1.35%	2.11	14.4dB	54.3°	0.14%
11	0.38	0.07	17.27	1.49%	2.25	11.5dB	27°	0%

Table 66 – Performance indicators for the closed-loop system of $G_2(s)$ with $T = 0.5$ and different orders of the PMR controller subject to disturbance $d(t)$

N	k_{pmr}	$k_{r_{11}}$	n_s	$M_{O_{\%}}$	M_s	GM	PM	$THD_{\%}$
1	1.79	0.41	–	29.34%	1.15	25.1dB	121°	19.14%
3	1.79	0.41	–	12.72%	1.81	21.7dB	123°	8.78%
5	1.79	0.41	–	4.27%	1.80	19.1dB	84.4°	3.48%
7	1.79	0.41	5.56	1.20%	1.79	16.9dB	57.9°	0.96%
9	1.79	0.41	4.70	1.08%	1.78	14.9dB	39.6°	0.22%
11	1.79	0.41	4.53	1.24%	2.39	12.9dB	25.8°	0%

Table 67 – Performance indicators for the closed-loop system of $G_2(s)$ with $T = 1$ and different orders of the PMR controller subject to disturbance $d(t)$

N	k_{pmr}	$k_{r_{11}}$	n_s	$M_{O_{\%}}$	M_s	GM	PM	$THD_{\%}$
1	1.63	0.15	–	33.92%	1.15	25.1dB	125°	21.76%
3	1.63	0.15	–	16.18%	2.15	21.8dB	124°	10.17%
5	1.63	0.15	–	6.29%	2.14	19.2dB	81.2°	4.01%
7	1.63	0.15	6.67	3.62%	2.13	17dB	56.4°	1.10%
9	1.63	0.15	5.78	2.39%	2.11	15dB	39.4°	0.25%
11	1.63	0.15	5.61	2.54%	2.36	13dB	26.3°	0%

Table 68 – Performance indicators for the closed-loop system of $G_3(s)$ with $\alpha = 0.9$ and different orders of the PMR controller subject to disturbance $d(t)$

N	k_{pmr}	$k_{r_{11}}$	n_s	$M_{O_{\%}}$	M_s	GM	PM	$THD_{\%}$
1	0.70	0.11	–	37.82%	1.08	$25.5dB$	117°	24.38%
3	0.70	0.11	–	17.07%	1.82	$22dB$	139°	12%
5	0.70	0.11	–	5.82%	1.83	$19.3dB$	106°	4.86%
7	0.70	0.11	12.55	1.34%	1.83	$16.9dB$	75.4°	1.33%
9	0.70	0.11	9.70	0.76%	1.82	$14.7dB$	49.2°	0.30%
11	0.70	0.11	9.24	0.92%	2.24	$12.1dB$	27.3°	0%

Table 69 – Performance indicators for the closed-loop system of $G_3(s)$ with $\alpha = 5$ and different orders of the PMR controller subject to disturbance $d(t)$

N	k_{pmr}	$k_{r_{11}}$	n_s	$M_{O_{\%}}$	M_s	GM	PM	$THD_{\%}$
1	8.76	0.01	–	6.73%	1.13	$25.3dB$	78.9°	5.08%
3	8.76	0.01	–	6.39%	1.18	$21.9dB$	79.4°	1.75%
5	8.76	0.01	1.52	7.80%	1.28	$19.3dB$	64.8°	0.60%
7	8.76	0.01	1.51	7.55%	1.42	$17.1dB$	51.1°	0.15%
9	8.76	0.01	1.50	6.91%	1.68	$15.1dB$	38.7°	0.03%
11	8.76	0.01	1.48	6.82%	2.22	$13.2dB$	27.6°	0%